UNIVERSIDADE FEDERAL DO PARANÁ

BRUNO DUFAU MATTOS

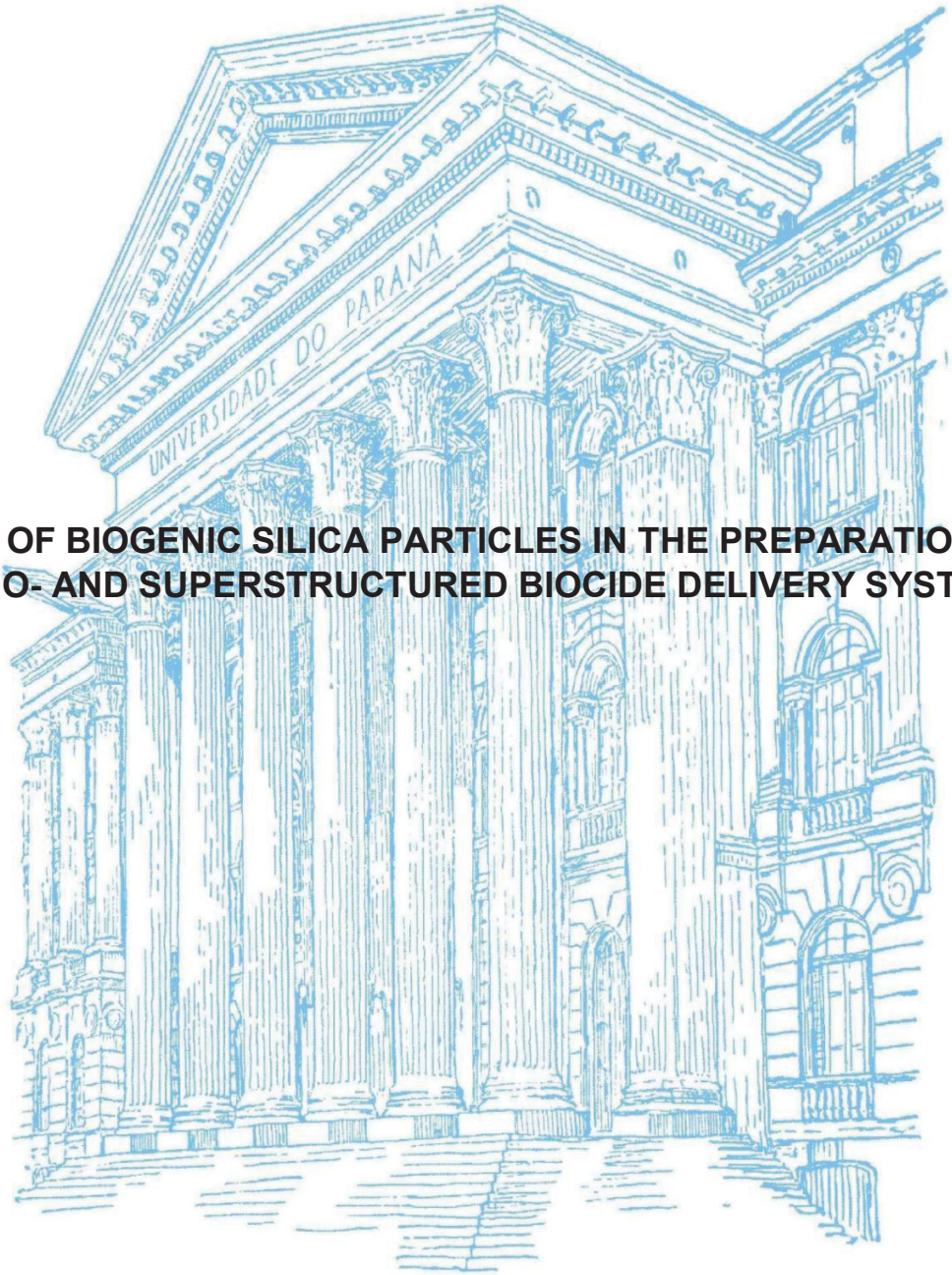

USE OF BIOGENIC SILICA PARTICLES IN THE PREPARATION OF NANO- AND SUPERSTRUCTURED BIOCIDE DELIVERY SYSTEMS

CURITIBA

2018

BRUNO DUFAU MATTOS

USE OF BIOGENIC SILICA PARTICLES IN THE PREPARATION OF NANO- AND SUPERSTRUCTURED BIOCIDE DELIVERY SYSTEMS

Final version of the thesis presented to the Postgraduate Program in Materials Engineering and Science, Universidade Federal do Paraná, Exact Sciences Sector as a requirement to obtain the Doctor degree in Materials Engineering and Science.

Supervisor: Prof. Dr. Washington L. E. Magalhães

CURITIBA

2018

M444u Mattos, Bruno Dufau
Use of biogenic silica particles in the preparation of nano- and superstructured biocide delivery systems / Bruno Dufau Mattos. – Curitiba, 2018.
150 f. : il. color. ; 30 cm.

Tese - Universidade Federal do Paraná, Setor de Tecnologia, Programa de Pós-Graduação em Engenharia e Ciências dos Materiais, 2018.

Orientador: Washington L. E Magalhães.

https://doi.org/10.1016/j.jconrel.2017.07.025

https://doi.org/10.1007/s12649-017-9993-y

1. Bioeconomina. 2. Nanotecnologia. 3. Química verde. I. Universidade Federal do Paraná. II. Magalhães, Washington L. E. III. Título.

CDD: 620.11

MINISTÉRIO DA EDUCAÇÃO
SETOR CIÊNCIAS EXATAS
UNIVERSIDADE FEDERAL DO PARANÁ
PRÓ-REITORIA DE PESQUISA E PÓS-GRADUAÇÃO
PROGRAMA DE PÓS-GRADUAÇÃO ENGENHARIA E CIÊNCIA DOS MATERIAIS

TERMO DE APROVAÇÃO

Os membros da Banca Examinadora designada pelo Colegiado do Programa de Pós-Graduação em ENGENHARIA E CIÊNCIA DOS MATERIAIS da Universidade Federal do Paraná foram convocados para realizar a arguição da tese de Doutorado de **BRUNO DUFAU MATTOS** intitulada: **USE OF BIOGENIC SILICA PARTICLES IN THE PREPARATION OF NANO AND SUPERSTRUCTURED BIOCIDE DELIVERY SYSTEMS**, após terem inquirido o aluno e realizado a avaliação do trabalho, são de parecer pela sua aprovação no rito de defesa.

A outorga do título de doutor está sujeita à homologação pelo colegiado, ao atendimento de todas as indicações e correções solicitadas pela banca e ao pleno atendimento das demandas regimentais do Programa de Pós-Graduação.

CURITIBA, 22 de Fevereiro de 2018.

WASHINGTON LUIZ ESTEVES MAGALHÃES
Presidente da Banca Examinadora

CARLOS TSUO YAMAMOTO
Avaliador Interno

MARCO AURÉLIO DA SILVA CARVALHO FILHO
Avaliador Externo

CLAUDIA ELIANA BRUNO MARINO
Avaliador Interno

RENATO GRILLO
Avaliador Externo

ACKNOWLEDGEMENTS

I would like to thank the following agencies and institutions that had contributed funding this work:

To CAPES (Coordenação de Aperfeiçoamento de Pessoal de Nível Superior) and Fundação Araucária for supporting this work through the provision of a 4-year scholarship.

To Embrapa (Empresa Brasileira de Pesquisa Agropecuária) for providing me free access to laboratories and facilities. Also, for providing me any material that I needed to carry out my research.

To the PDSE program (Programa Doutorado Sanduíche no Exterior) from CAPES for financing a 6-months exchange period at Aalto University.

To Aalto University (Finland) for giving me free access to facilities and providing me materials that were necessary in my research work abroad.

To the Programa de Pós Graduação em Engenharia e Ciência dos Materias (PIPE) of the Universidade Federal do Paraná, where I had the opportunity to carry out my doctoral studies.

Besides, there have been many people who have walked alongside me during the last four years. They have guided me, placed opportunities in front of me, and showed me the doors that might be useful to open. I would like to properly thank each and every one of them:

I would like to express my sincere gratitude to my supervisor Dr. Washington L. E. Magalhães for the continuous support of my doctoral study and related research. For his friendship. For his unstinting support and constructive critique. For his instigating and motivation in the search by the new and different.

My sincere thanks also goes to Prof. Dr. Luiz P. Ramos, Prof. Dr. Wido H. Schreiner and Profª. Drª. Graciela I. B. de Muñiz, who provided me precious discussion, and who gave access to the laboratory and research facilities.

I am grateful to Prof. PhD. Orlando J. Rojas, who hosted me during my exchange at Aalto University, as a member of his group (BiCMat, Bio-based Colloids and Materials). For his insightful comments and encouragement, but also for valuable discussions which incited me to widen my research from various perspectives.

I thank all my labmates and friends from Embrapa, specially André L. Missio, Mailson de Matos, Pedro H. G. de Cademartori, Tiélidi A. de Lima, Francine C. Claro, Edson A. Lima, Cristiane Helm, Simone Sopchaki, Elizabeth R. Câmara, Fabricio A. Hansel, Dayanne Mendes and Marcelo Lazzarotto for their continuous support and friendship.

I thank all my fellows from BiCMat, especially Dr. Blaise L. Tardy and Luiz G. G. Greca who made me feel like home in Finland and became very good friends. Their support and friendship were essential for getting me one of the best times in my life.

Last but not the least, I would like to thank my family:

To my mother Telma and sister Karina for supporting me every time I needed. For their understanding. For their love.

To my beloved wife, Tainise V. Lourençon, to whom this thesis is dedicated, for her unending support, tireless care, and unconditional love. For being more than anything for me.

ABSTRACT

Biocides are crucial molecules for the protection of several biosystems; however, residual toxins have been found in food, soil and ground water. Looking for safer biosystems, on-demand release strategies have been investigated aiming at the replacement of the traditional biocides. Properties such as tailored and controlled release are paramount in the development of sustainable biocide delivery systems (BDS). Firstly, BDS which are designed to deter or control harmful organisms that damage agricultural crops, forests and forest products, were reviewed. The review considers the most important BDS vehicles or carriers, their synthesis, the environmental impact of their constituents and interactions with the active components together with the factors that affect their rates of release such as environmental factors and interaction of BDS with the crops or forest products. During the literature review, it was observed an interesting opportunity for the use of biogenic silica particles as carriers for BDS. Typically, the isolation of biogenic silica from biomasses is a low profitable process as usually *ca.* 80% of the biomass is wasted; however, herein a biorefinery platform was developed to consecutively isolate medicinal compounds, carbohydrate derivates and silica particles from horsetail biomass (*Equisetum arvense*). The self-similar nano-organized architecture, responsible for a specific surface area of *ca.* 350 $m^2 \cdot g^{-1}$, of the obtained biogenic silica particles is a special structure that could be used in the design of biocide delivery systems. Their high surface area and pore access are essential to achieve high biocide payload. Thymol, a natural compound extracted from plants, was used as a model biocide. The high surface area accessibility of the carrier allowed the development of an efficient, low energy loading strategy, reaching significant dynamic loadings of up to 100 $mg \cdot g^{-1}$. The release rate and responsiveness of the biogenic silica-based BDS were tuned by manipulating the interfaces, using either the native hydroxyl surfaces of the carrier or systems modified with amines or carboxylic acids in high density. The impact of the carrier-biocide interactions on the release rate as a function of pH, ionic strength and temperature was thoroughly evaluated. The amine and carboxyl functionalization strategy led to three-fold decrease in the release rate, while higher responsiveness against important agro-industrial variables. Key to our discoveries, nanostructuring thymol in the biogenic silica endowed systems with controlled, responsive release promoting remarkable, high and localized biocidal activity. The nanosize of this BDS turns it into a very special system to protect, for instance, wood-based materials. Lastly, a superstructuring approach was applied to design carriers with significantly larger sizes aiming at a less problematic and easier-to-handle delivery system for crop protection. Biogenic silica particles and cellulose nanofibrils were assembled into millimetric scaled porous supraparticles, via confined capillary force action. The obtained supraparticles presented biocide delivery patterns comparable with nanoparticles, lower mobility in soil and higher UV protection.

Keywords: bioeconomy, nanotechnology, self-assembly, controlled release, soft-chemistry.

RESUMO

Biocidas são moléculas cruciais para a proteção de diversos biosistemas; entretanto, toxinas residuais vêm sendo encontradas no solo, água e alimentos. Estratégias de proteção biocida baseadas em sistemas de ação sob demanda vêm sendo investigadas para a substituição de sistemas biocidas tradicionais. Propriedades como liberação controlada e modificada tornaram-se primordiais para o desenvolvimento de sistemas biocidas sustentáveis. Neste trabalho, é apresentada uma revisão de literatura de sistemas biocidas projetados para deter ou controlar organismos danosos à colheitas, florestas e produtos florestais. A revisão inicialmente apresentada discuti os suportes e veículos mais importantes no desenvolvimento de biocidas de liberação controlada, sua síntese, impacto ambiental de seus constituintes, e interações dos ingredientes ativos em paralelo à fatores que afetam sua performance. Quando revisando a literatura recente, observou-se a oportunidade para o uso de sílica biogênica como um suporte interessante para a concepção de biocidas. Tipicamente, a extração de sílica de biomassas é um processo de baixo rendimento econômico uma vez que aproximadamente 80% da biomassa é desperdiçada; entretanto, neste trabalho foi desenvolvida uma plataforma de biorrefinaria para isolar consecutivamente compostos medicinais, derivados de carboidratos, e partículas de sílica de cavalinha (*Equisetum arvense*). Observou-se que as partículas de sílica biogênica apresentam uma estrutura hierarquicamente nano-organizada em agregados fractais, resultando em uma área específica de superfície de *ca.* 350 $m^2 \cdot g^{-1}$. Esta estrutura é especial para atingir alta carga de biocida, uma vez que agregados fractais apresentam alta acessibilidade de área. Neste estudo utilizou-se timol, um composto também extraído de plantas, como biocida modelo. A partir da escolha de sílica biogênica como suporte, foi possível desenvolver de um processo eficiente e de baixa energia, capaz de atingir carregamentos dinâmicos de biocida de até 100 $mg \cdot g^{-1}$. A taxa de liberação e a responsividade do sistema biocida puderam ser ajustadas utilizando manipulações da interface entre suporte e biocida, o qual foi conduzido por meio da funcionalização do suporte com aminas ou ácidos carboxílicos em alta densidade. O efeito das interações de interface na taxa de liberação foi investigado em função de pH, força iônica e temperatura. A estratégia de funcionalização resultou em decréscimo significativo na taxa de liberação, enquanto que houve aumento na responsividade do sistema às variáveis estudadas. A escala nanométrica de tal sistema o torna apto para ser aplicado por exemplo na proteção de produtos de madeira. Por último, utilizou-se uma abordagem de supraestruturação para projetar sistemas com tamanho significativamente maior, menos problemáticos e de mais fácil manuseio para a aplicação na proteção de colheitas. Sílica biogênica foi combinada com nanofibrilas de celulose para formar suprapartículas porosas milimétricas, via método ação capilar em espaço confinado. As suprapartículas obtidas apresentaram perfis de liberação comparáveis aos sistemas nanométricos, enquanto que menor mobilidade em solo e maior proteção contra fotodegradação.

Palavras-chave: bioeconomina, nanotecnologia, auto-montagem, liberação controlada, química verde.

LIST OF FIGURES

CHAPTER I

CHAPTER II

CHAPTER III

CHAPTER IV

SUPPLEMENTARY MATERIAL

LIST OF TABLES

LIST OF SYMBOLS, ACRONYMS AND ABBREVIATIONS

[H+]: Acid concentration
APTES: 3-aminopropyltriethoxysilane
BET: Brunauer–Emmett–Teller
BDS: Biocide delivery system
CRS: Controlled Release Society
CT: Calcination temperature
DCOIT: 4,5-dichloro-2-octyl-4-isothiazolin-3-one
dH_2O: Distilled water
DMF: Dimethylformamide
DTA: Differential-thermal analysis
EDS: Energy dispersive spectroscopy
EU: European Union
FEG-SEM: Field emission gun scanning electron microscopy
FTIR: Fourier-transformed infrared
HHV: High heating value
HPLC: High performance liquid chromatography
HT: Hydrolysis temperature
IEP: Isoelectric point
IUPAC: International Union of Pure and Applied Chemistry
LDH: Layered doubled hydroxide
MBT: 2-mercaptobenzothiazole
MCM: Mobil Composition of Matter
NBE: Neem bark extract
NREL: National Renewable Energy Laboratory
O/W: Oil in water
Rf: Retention factor
SHPI: Sodium hypophosphite monohydrate
SSA: Specific surface area
SP: Supraparticle
t: Time
TEM: Transmission electron Microscopy
TEOS: 2-mercaptobenzothiazole
TGA: Thermogravimetric analysis
THY: Thymol
TLC: Thin layer chromatography
U$: United States Dollar
UV-Vis: Ultraviolet-Visible
VSSA: Volume-specific surface area
WI: Whiteness index
XPS: X-Ray photoelectron spectroscopy

TABLE OF CONTENTS

CHAPTER I

GENERAL ASPECTS

I.1 GENERAL INTRODUCTION

Biocides have been widely applied to decrease crop losses to pests, and to improve the service life of biodegradable materials (LAMICHHANE et al., 2015; MAGALHÃES et al., 2012; MAXMEN, 2013; PARISI et al., 2014). A wide range of organic compounds is commonly used for biocidal purposes such as the azoles, carbamates, pyrethroids, cupric, aromatics and halogenated heterocycle compounds. Despite the high efficacy of these organic biocides in controlling pests, there is a concern related to their potential as contaminant of cultivable soil and water. It became a problem due their water leachability and soil mobility (HALL et al., 2015; KATAGI, 2013), which could be considered as the main factors for their bioaccumulation. The uptake of biocides by the soil has lead to acute and chronic hazards to human health and environmental (CHANG et al., 2016; TSABOULA et al., 2016).

An increased biocide efficiency is needed in order to reduce toxic risks derived from their use. To avoid higher initial dosages or repeated applications, there have been many attempts to control the release rate of biocides by loading or encapsulating them in nano/micrometric carriers (MATTOS et al., 2017a). In the last years, delivery systems were developed using several materials as carriers, depending of the targeted application. Herein, silica-based materials were chosen as they are thermally, dimensionally and chemically stable. In traditional drug delivery, nanostructured mesoporous silica particles are becoming the *de facto*, state-of-the-art delivery system due to their biocompatibility, high loading capacity and extensive morphological variety (MALEKI et al., 2017; SLOWING et al., 2008; WANG et al., 2010). Although hierarchical pore size distributions have been demonstrated with mesoporous silica (KUANG; BREZESINSKI; SMARSLY, 2004), the principle of self-similarity does not most naturally arise in the typical bottom-up synthesis routes, which involve the use of templating agents to spatially regulate the sol-gel reaction, in which tuning the pore architecture requires the control of process variables at the preparation step (WU; MOU; LIN, 2013). On the other hand, as will be discussed here, biomass-derived silica particles (biogenic silica) are consisting of a fractal-like architecture of 8-10 nm subunits hierarchically organized into agglomerates with sizes ranging from 100 nm to 4 μm, depending on the treatment

applied for dispersion (LIU et al., 2013; MATTOS et al., 2017a). Fractal patterns and hierarchical systems abound nature in response to a wide variety of transport process (MANDELBROT, 1983; TURCOTTE, 1997). In *e.g.* chromatography (MARTENS et al., 2011) and heterogeneous catalysis (HARTMANN, 2004; VANTOMME et al., 2007) the importance of hierarchical architectures has been favorably recognized. In fractal aggregates, the cluster morphology results from competing stochastic and energetic processes (LAZZARI et al., 2016; MEAKIN, 1987; NICOLÁS-CARLOCK; CARRILLO-ESTRADA; DOSSETTI, 2017), which can result in structures spanning across a wide range of length scales (LIU; HEINSON; CHAKRABARTY, 2017). This design paradigm herein explored offers an alternative hierarchical approach with a wide range of possible applications outside of payload delivery vehicles. The fractal aggregate strategy consequently lends a different pore topology. Whereas the connectivity between adjacent pores is irregular in templated porous materials, the pore network of fractal aggregates is fully connected in the mesopore level due to sphere packing constrictions. This has implications to release kinetics as it can be enhanced by high pore connectivity and small pore tortuosity (ANDERSSON et al., 2004; ARMATAS, 2006; QU et al., 2006; STRØMME et al., 2009). A fully interconnected mesopore architecture forming a system-wide percolating pore structure can contribute to a small tortuosity up to the nanoparticle surface level, which could facilitate the preparation of highly accessible high surface area materials. Thus, it is understandable that biogenic silica is an excellent opportunity to explore fractal architectures as carriers in delivery science where high biocide payload and intensified carrier-biocide interactions can be achieved due the high surface area accessibility of fractal aggregates. When compared to mesoporous silica, $BSiO_2$ present opportune morphology, identical surface chemistry, besides lower price and environmental impact.

The most significant contribution of this thesis stands on the design and preparation of biocide delivery systems based on biogenic silica as carrier. The information obtained and discussed in this work may contribute to the improvement of the sustainability in the agro-indutrial sector, for both traditional and upcoming technologies and processes. This work was separated into chapters to promote a pleasant reading rate and a satisfactory understanding of the whole concept of sustainability toward developing

greener biocide delivery systems. **CHAPTER I** brings a comprehensive review of breakthrough ideas on biocide delivery systems. Since biogenic silica was chosen as carrier due its uncountable advantages over other materials, a biorefinery platform for the isolation of biogenic silica particles from horsetail biomass was developed and discussed in the **CHAPTER II**. In **CHAPTER III** and **CHAPTER IV** biocide delivery systems were designed, synthesized, characterized and discussed. In the first, self-similar nano-organized biogenic silica particles were used in the preparation of a nanoscaled biocide delivery system, in which the release rate and responsiveness of the biocide could be controlled by manipulating the biocide-carrier interface. In the last, a suprastructuring strategy, that has been recognized in many fields of science, was applied to design biocide delivery systems with significantly larger sizes aiming at a less problematic and easier-to-handle delivery system for crop protection.

I.2 HYPOTHESIS AND OBJECTIVES

I.2.1 HYPOTHESIS

“Biogenic silica could be used as a cheaper and greener nanostructured carrier in the synthesis of biocide delivery systems”.

I.2.2 MAIN OBJECTIVE

This work aimed to design and synthesize nano and superstructured biocide delivery systems by using biogenic silica as carrier and thymol as a model biocide.

I.2.3 SPECIFIC OBJECTIVES

- Isolate nanostructured biogenic silica particles from *Equisetum arvense* (horsetail) biomass using a biorefinery platform;
- modify the surface of the biogenic silica using simple, one-pot routes;
- develop strategies for efficiently load thymol into the biogenic silica;
- prepare biocide delivery systems with tunable and responsive biocidal properties;
- obtain biocide delivery systems from the nano to the millimetric scales;
- measure the release of the loaded biocides into water as a function of important agro-industrial variables.

I.3 LITERATURE REVIEW

I.3.1 APPLICATIONS OF NANOSTRUCTURED SYSTEMS FOR CROPS AND WOOD MATERIALS PROTECTION

Derived from research focusing on the development of drug delivery systems (DDS) in the biomedical field, controlled release formulations have recently attracted interest in the protection of agricultural crops and wood materials. This is owing to the fact that living environments and agrochemical-free food production has become a predominant concern (CRUTE, 2012; OSBORN, 2012; ROBERTS; LEIBOVITCH, 2011). For biomedical applications, DDS have been developed continuously over the past 70 years. However, the number of new, successful clinical applications has slowed down since associated requirements have become more stringent, specialized and sophisticated (PARK, 2016; YUN; LEE; PARK, 2015). Consequently, some of the vast knowledge accumulated in this area is being transferred and adapted in agricultural release systems. Here, the use of environmentally friendly and low toxicity compounds for crop protection, for example in biocide delivery systems (BDS), is a considerably less constraining field of application when compared with DDS. It can be expected that transfer of knowledge to this area will only increase in the future. Nevertheless, although less stringent for technical applications of BDS, soil properties together with climatic conditions need to be considered as they can significantly affect release properties or potential long term hazardous effects of BDS. For instance, these environment-associated factors have been observed to play an important role in the degradation and stability of pesticides when applied to crops (BURROWS et al., 2002; KATAGI, 2004). Additionally, answers to the many challenges pertaining the development of new agrochemicals (LAMBERTH et al., 2013) may exploit synergies with novel BDS that can have a particularly large socio-economic impact, highly interrelated to human health and to the development of a sustainable bioeconomy.

Interest in the formulation of BDS arises because traditional methods of biocide-based protection in the agriculture fields usually imply high-volume application of active molecules at high initial dosages (and often require repeated use). Furthermore, delivery

is often uncontrolled, which results in short-time biocidal protection and increased bioaccumulation. In fact, excessive toxins concentration in ground and surface water has led to acute health problems and water purification costs (MUKHOPADHYAY, 2014). In this context, the preparation and application of engineered nanoparticles for controlled release of biocides, *i.e.* "nano-agriculture", represent an effective answer that, among others, may involve 'on-demand' modes of action. In turn, BDS may take advantage of efficient methods that minimize or completely avoid repeated application of agrochemicals, which impact positively any effects related to environmental pollution and food poisoning. A representative example of efforts in this area includes the European program Horizon 2020, the biggest EU Research and Innovation effort ever, with nearly €80 billion funds available over 7 years (2014 to 2020). Horizon 2020 addresses the most important challenges in nanotechnologies to achieve health and wellbeing, efficient energy, food, sustainable agriculture, forestry, water and the future bioeconomy (PARAK; NEL; WEISS, 2015). In sum, there is no doubt that the objectives of BDS will benefit from new developments in agricultural nanotechnologies.

In agricultural applications, nano- and micro-particulate biocides, including those that display nanometric features (*i.e.,* nanostructured), are some of the most promising ones for achieving sustainability, high payload and high efficiency. This is in part due to the functions that emerge in nanometric materials, usually associated to their high surface area, which have been applied to impart new physical, mechanical, electrical/electronic, catalytic, and optical properties (CHEN; MAO, 2007; GUO; HU; WAN, 2008; RAI; YADAV; GADE, 2009; ZENG et al., 2014). For example, high surface area, superstructures associated with nano-organized architectures offer a mean to increase the density of the active sites in order to improve levels of detection, reactivity and selectivity (APPELL; JACKSON, 2013). While less evident, many possibilities exist for the application of nanotechnologies in agriculture, silviculture and wood protection. Among these, the most impactful applications include crop protection and efforts to improve plantation yields, water management, early diagnostics, plant breeding and the isolation of nanomaterials from plants (PARISI; VIGANI; RODRÍGUEZ-CEREZO, 2014).

Despite of the remarkable advantages of nanotechnology in the agricultural sector, the few efforts that exist have not been as prominent as in other industrial sectors. The

biggest obstacle that has prevented a wider adoption is the high initial investments, which is encountered with a demand for materials in large scales. Indeed, from the onset of their application, most nanotechnology products need to display a clear positive impact while being economically viable (PARISI; VIGANI; RODRÍGUEZ-CEREZO, 2014). The use of nanotechnology may be a solution to the increased food needs (for example, grains and others), given the growing worldwide consumption and the pressure to achieve high yields (MAXMEN, 2013). In this scenario, food demand is expected to double in the following decades (FOLEY et al., 2011). However, limits in cropland expansion implies that future strategies will likely focus in improving agricultural operations. For example, this can be achieved by drastically reducing the crop losses to pests via efficient and prolonged exposure to safe biocide (OERKE, 2006). In addition, nanostructured controlled release biocides can bring benefits at large scales in silviculture and in wood protection and preservation (DING et al., 2011; SORENSEN et al., 2010). This is especially the case if they offer alternatives that are safe and meet the requirements and regulations that are in place, which limit or forbid the application of some otherwise traditional systems. In this context, popular wood preservatives have included creosote, pentachlorophenol, and waterborne chromate copper arsenate. (CAO; JIANG, 2014). Among biggest incentives to replace highly-toxic chemical preservatives one can include the risk of contamination of inhabited areas and associated negative effects to human health (MERCER; FROSTICK, 2014). A solution to address these issues includes the utilization of organic biocides. However, they may be either too soluble (SORENSEN et al., 2010), promoting high soil and water contamination or, otherwise, poorly soluble, which often entails a lower bioavailability (GE et al., 2012). Thus, a better strategy is that of controlled release, for example, in fertilizers to improve cereal production (AZEEM et al., 2014; NAZ; SULAIMAN, 2016). Their development closely matches that of BDS since the technologies are developed in parallel for a common goal. This has recently been reviewed by Naz and Sulaiman (2016), and Azeem et al. (2014).

Here, the use of sustainable biocides and carriers as means of protection from harmful organisms is presented. The most significant and recent breakthroughs reported in the literature in relation to controlled release of fungicides, herbicides, and insecticides, with focus on biocidal activity are discussed (FIGURE I.1). These systems have changed

conceptually over the years, introducing new carriers, biocides and methods of preparation. The fundamental thermodynamics driving the delivery of biocides through complex carrier-biocide-environment interactions are firstly expanded. Following, there is a discussion on how the architecture and morphology of carrier materials affect the release profile of biocides, in parallel the parameters affecting their performance in given applications are also considered. Then the scope is broadened for biocide delivery systems and recent developments are highlighted for BDS designed and synthesized bottom-up, from renewable or mineral resources. Finally, the presented reports are critically discussed and putted in perspective in order to bring forward important necessary considerations for future BDS developments.

FIGURE I.1 – SCHEMATIC REPRESENTATION OF THE INCORPORATION OF BIOCIDES (1) THAT ARE INTEGRATED WITH CARRIERS (2) IN DELIVERY SYSTEMS DISPLAYING A NUMBER OF INTERACTION (K_{XY}) RELEVANT TO CROP AND WOOD PROTECTION (3)

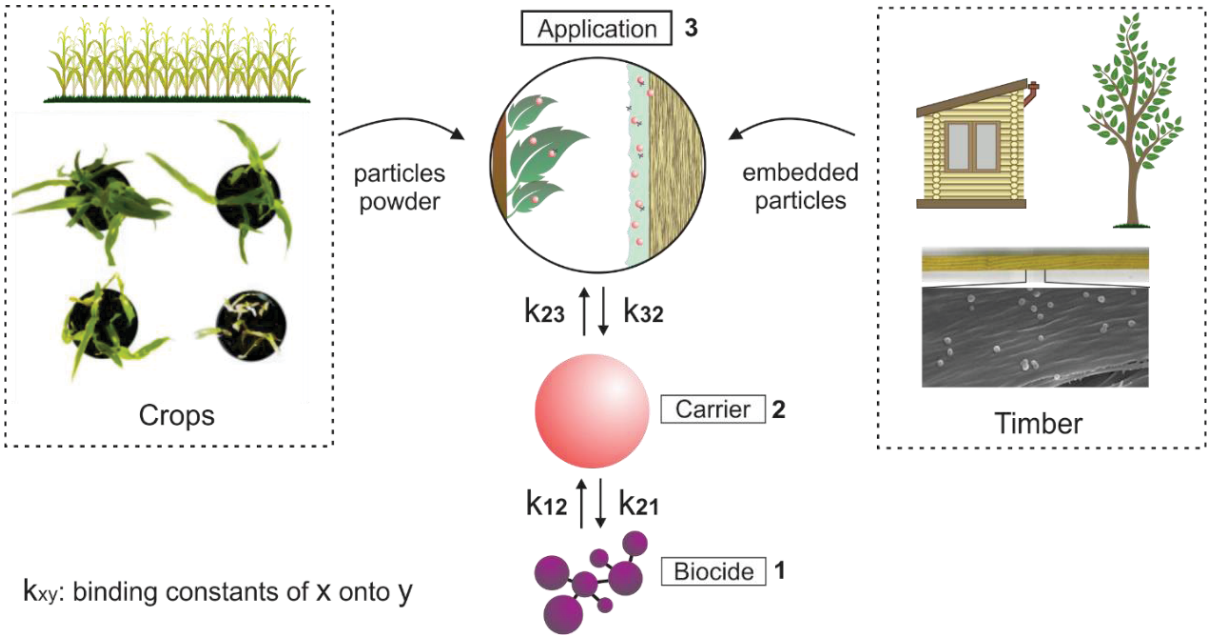

SOURCE: the author (2018). The figure is adapted and redrawn from references (DING et al., 2011) and (GRILLO et al., 2014).

I.3.2 CARRIER-BIOCIDE-WATER INTERACTIONS IN CONTROLLED RELEASE SYSTEMS

Fundamentally, controlled release systems involve competitive interactions between the carrier or vehicle, the biocide and the environment to which it will be released (FIGURE I.1). Controlling the associated balances is key in the design of sustainable biocides delivery systems. In this section, the thermodynamics of underlying interactions between biocide substrates and target surfaces were briefly introduced. The solubility in controlled release systems are often described under the theories of Hansen (1967) and Hildebrand and Scott (1964), recently adapted by Zhang and Cresswell (2016). Here, the Gibbs free energy (ΔG_r) gives a fundamental relationship that governs the interaction between the biocide, the carrier and the microenvironment. More specifically, ΔG_r relates to the biocide dissolution enthalpy (ΔH_r) and entropy (ΔS_r), at a given temperature (T):

$$\Delta G_r = \Delta H_r - T\,\Delta S_r \qquad \text{Equation 1}$$

For a controlled release system consisting of a biocide *b*, a solvent/environment that is usually water *w* and a support or carrier *c*, the relevant enthalpy and entropy components of Equation 1 include:

$$\Delta H_r = \Delta H_{bb} + \Delta H_{bw} + \Delta H_{bc} + \Delta H_{wc} + \Delta H_{cc} \qquad \text{Equation 2}$$

$$\Delta S_r = \Delta S_{bb} + \Delta S_{bw} + \Delta S_{bc} + \Delta S_{wc} + \Delta S_{cc} \qquad \text{Equation 3}$$

where ΔH_{bb} is the enthalpy of a biocide's cohesive energy, related to the disruption of the crystal lattice into individual molecules; ΔH_{bw} is the energy related to the interaction between biocide molecules and water; ΔH_{bc} is the carrier-biocide interaction energy; ΔH_{wc} is the energy between the carrier and the surrounding water, and ΔH_{cc} is the enthalpy of the carrier that is represented by possible phase changes, if applicable. Their corresponding entropies are ΔS_{bb}, ΔS_{bw}, ΔS_{bc}, ΔS_{wc} and ΔS_{cc}. Classical dissolution models do not consider the enthalpic and entropic contributions of the carrier, namely, carrier-biocide, carrier-carrier, and carrier-water. In such cases, only ΔH_{bb} and ΔH_{bw} (and

related entropies) drive the dissolution of the molecule. For water-soluble systems, ΔH_r is normally not a significant component because the required energy to promote the dissolution is almost null; meanwhile, the contribution of the entropy change (ΔS_r) is generally large because the system achieves very fast an irreversible state; thus $\Delta G_r < 0$. In contrast, the biocide cohesive energy (ΔH_{bb}) is high for poorly water-soluble molecules, which means that dissolution occurs only after transfer of a given external energy. Before complete dissolution, the entropy related to biocide-biocide interaction (ΔS_{bb}) and biocide-water interaction (ΔS_{bw}) are negligible, which together with the large value of ΔH_s, leads to $\Delta G_s > 0$. Thus, dissolution and delivery of poorly soluble compounds in water is not a thermodynamically spontaneous process.

For dissolution from controlled release systems, it can be assumed that the active molecule is adsorbed at a pseudo-molecular level onto the surfaces of the carrier, and no (or very low) energy is needed to overcome the cohesive energy of the substance ($\Delta H_{bb} = 0$). After adsorption, dissolution is considered completed, so $\Delta S_{bb} = 0$. This implies a high probability of release of a given, poorly soluble molecule from the support and the dissolution is thermodynamically spontaneous ($\Delta G_r < 0$). This is because the largest portion of energy involved in the dissolution is required to separate individual molecules from their crystal phase. In addition, considering a non-soluble carrier support, there will be no changes in enthalpy and entropy related to carrier-carrier interactions (ΔH_{cc} and ΔS_{cc} are null).

Up to this point, it is not possible to express quantitatively the enthalpy and entropy of these controlled release systems; however, qualitative understanding can be gained on the release of a substance when driven by the carrier-biocide-water competition, as follow:

$$\Delta G_r = (\Delta H_{bw} + \Delta H_{bc} + \Delta H_{wc}) - T\,(\Delta S_{bw} + \Delta S_{bc} + \Delta S_{wc}) \qquad \text{Equation 4}$$

Since the only variables that can be controlled are the carrier-biocide and carrier-water interactions, efforts aiming at reducing the spontaneity of the dissolution make use of systems that display a high chemical affinity between the carrier and the biocide. Siepmann and Siepmann (2008) pointed out that the carrier-biocide interactions play a

dominant role in the release mechanism. For instance, compared to molecules that interact with the support by H-bonds, molecules covalently bound require more energy for dissolution or release (FIGURE I.2). Alternatively, one can operate on the carrier-water interactions, for example, by modifying the surface chemical groups of the carrier material. In fact, the functionalization of the carrier material is the most commonly applied approach to change the interactions between carrier, biocide and water (CHANG et al., 2010; HONGMIN et al., 2016; HU; TANG; CHU, 2014; JIA et al., 2015; WANI et al., 2012; YANG et al., 2014). Overall, material selection is critical for providing the best balance of interactions with the carrier (PASETA et al., 2016). Considering these strategies, it is possible not only to work on the carrier-biocide interactions but also on those between the carrier and water.

FIGURE I.2 – BIOCIDE DISSOLUTION PROFILES (A) OF PURE NEEM BARK EXTRACT, AND AFTER PHYSICALLY ADSORBED (B) OR COVALENTLY CROSS-LINKED INTO BIOGENIC SILICA CARRIER (C)

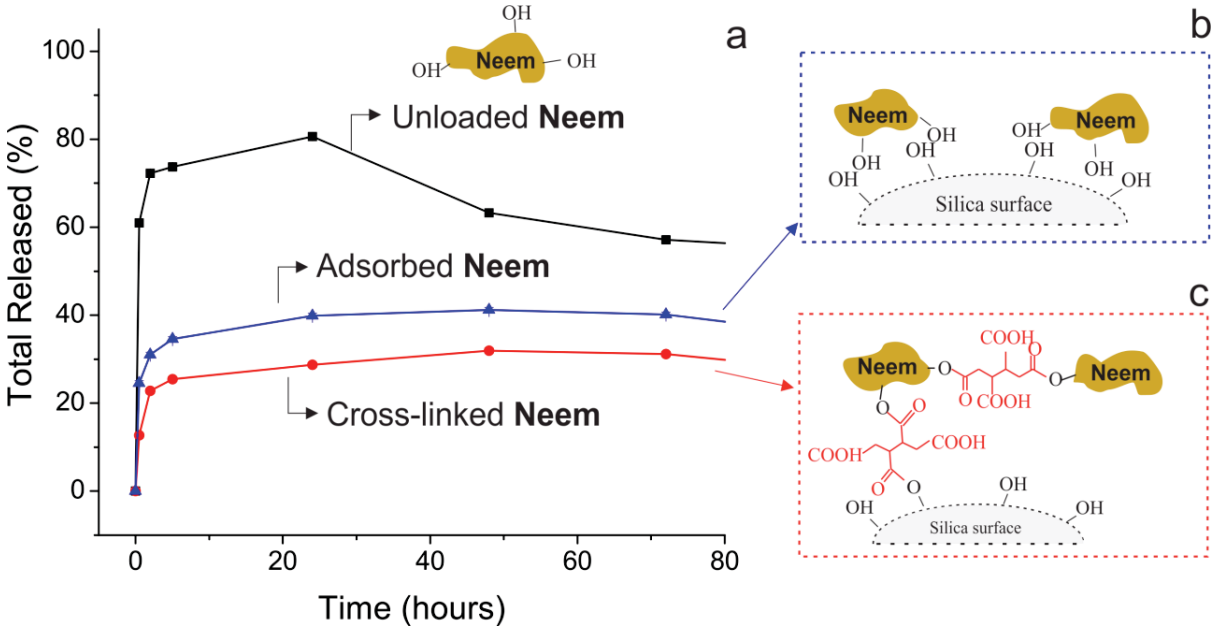

SOURCE: the author (2018). The figure is adapted and redrawn with copyright permission from reference (MATTOS et al., 2017d).

I.3.2 CARRIER MATERIAL, ARCHITECTURE AND SHAPE FOR BIOCIDE DELIVERY SYSTEMS

According to Siepmann and Siepmann (2012), the different types of mass-transport mechanisms involved in the control of substance release are mostly associated to the architecture of the support material. Many nano-structured morphologies are of interest toward the preparation of controlled release systems, such as aerogels, mesoporous structures, tubules, fractal-like microstructures, platelets and a range of spheroids (FIGURE I.3a**)**. Consideration should be given to reservoirs with constant and variable activity of the biocide that is present in the different release models. For instance, there is a vast difference between the release of a given substance from “core-shell” or “matrix” systems. In the first one, the active molecule and the barrier material (controlling the release rate) are physically separated, which leads to a lag-time effect in the release profile, due to the diffusion of the substance through the shell (FIGURE I.3b). On the other hand, in matrix systems the substance and the release rate controlling material are homogeneously distributed, which promotes an initial burst delivery due to the fact that the substance is readily available in the outer layers of the system (FIGURE I.3c).

The supporting architectures for controlled release of biocides can be categorized as slabs, cylinders or spheres. Among the slab-shaped supports, films (BÖTTCHER et al., 1999) and lamellae structures (CHEN et al., 2013; WANG et al., 2015; ZHENG et al., 2013) are common. The cylindrical supports often include nanotubes (ABDULLAYEV et al., 2009; LVOV; ABDULLAYEV, 2013) and nanofibers (LIAO et al., 2005; LUONG-VAN et al., 2006; WANG et al., 2007). The spherical shapes are the most common supports for controlled release; they most often comprise microporous/mesoporous inorganic particles (CHEN et al., 2011; DAS et al., 2009; GHOSH; JIJIL; DEVI, 2012; JOSHI et al., 2011; KAPOOR; HEGDE; BHATTACHARYYA, 2009; MAS et al., 2014; TANG et al., 2013; WANYIKA, 2013), polymeric capsules (ASRAR et al., 2004; CABRAL; KATAOKA, 2014; LIU; LAKS; HEIDEN, 2002a; PERLATTI et al., 2013; ROY et al., 2014) and carbohydrate beads (JEROBIN et al., 2012; KUMAR et al., 2014; SINGH; SHARMA; GUPTA, 2009).

FIGURE I.3 – DIFFERENT ARCHITECTURE OF MATERIALS (A) AND TYPES OF BIOCIDE DISPERSION INSIDE THE CARRIER THAT RESULT IN GIVEN BIOCIDE RELEASE PROFILES (B,C)

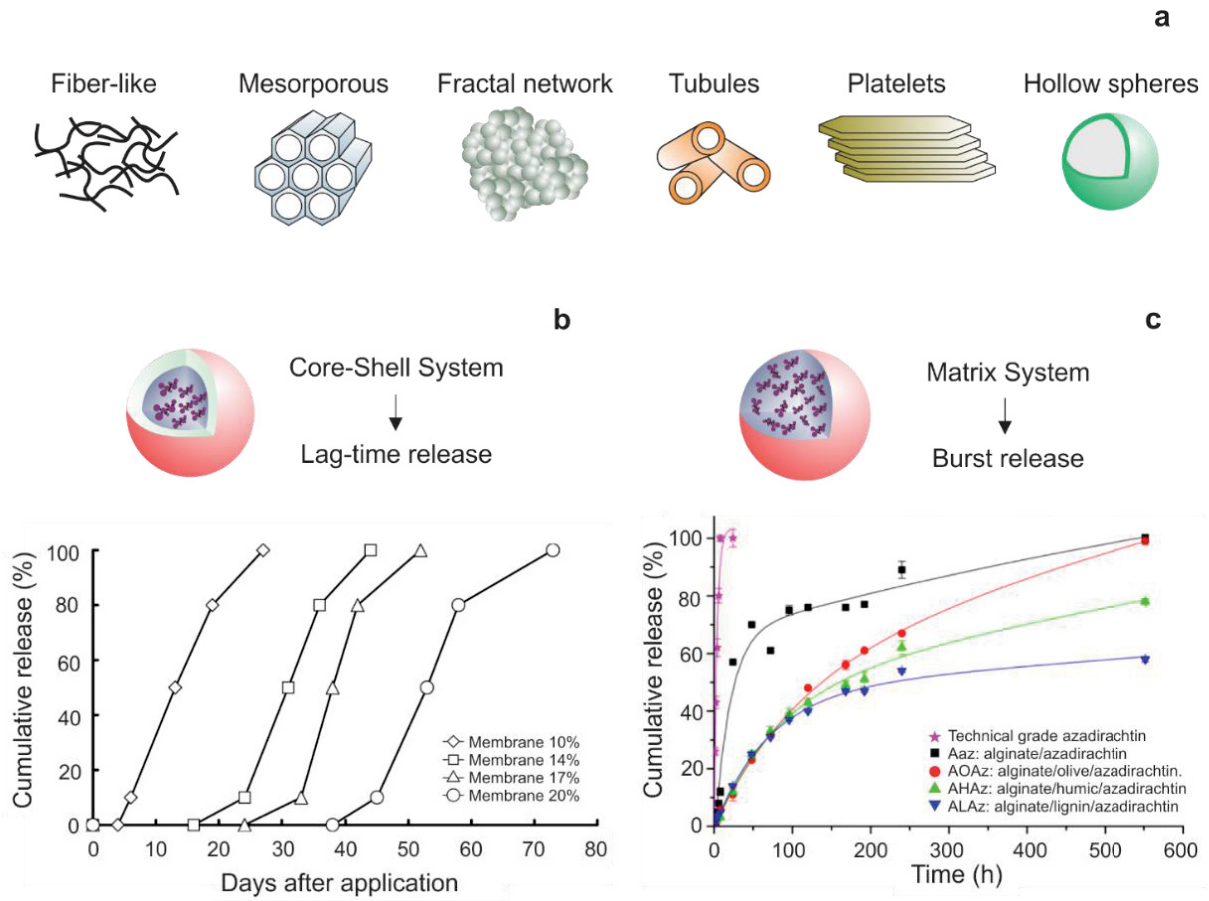

SOURCE: the author (2018). The figure is adapted and redrawn with copyright permission from references (KIMOTO; TAKAHASHI; INUBUSHI, 2007) and.(FLORES-CÉSPEDES et al., 2015).

The materials used as support or carrier can be derived from natural resources or synthesized by bottom-up routes (FIGURE I.4). For instance, nature provides materials such as cellulose, lignin, chitin, alginates and starch that are highlighted for their sustainability and biodegradability. Also, biogenic silica, halloysite and layered double hydroxides can be obtained from natural resources but they are not biodegradable (ALI; RAJENDRAN; JOSHI, 2011; LVOV et al., 2008; MATTOS; ROJAS; MAGALHÃES, 2016; ROY et al., 2014; SINGH; SHARMA; GUPTA, 2009; WANG et al., 2007; ZHENG et al., 2013). These nature-derived materials have a high potential as supports for controlled release systems. Among the bottom-up systems, carbon nanotubes, polymers, mesoporous alumina and mesoporous/hollow silica have been reported (DAS et al., 2009; JAMSA et al., 2013; KAPOOR; HEGDE; BHATTACHARYYA, 2009; LIU; LAKS; HEIDEN,

2002a; PERLATTI et al., 2013; WANG et al., 2015; ZHU et al., 2014). All of the above-mentioned materials are suitable for the construction of controlled release systems; however, they would be less expensive if obtained by a simple means of fabrication (*i.e.*, self-assembly and sol-gel processes) or by using directly natural resources (LVOV et al., 2008). Importantly, and intimately linked to the nature of the system, it has been pointed out that many concurrent phenomena are involved in the release profile, depending on the associated physical-chemical properties of the material (SIEPMANN; SIEPMANN, 2008). Involved mechanisms include wetting of the surface, water penetration, phase transitions, chemical interactions, pore closing or opening due to swelling, creation of cracks and changes in geometry. These are very important considerations for a proper selection of the material, for example, as a support for controlling the release of a given crop protection agent.

I.3.3 GREEN CARRIERS IN BIOCIDE DELIVERY SYSTEMS

Green approaches to design and synthesize BDS have been mainly carried out by using natural and renewable materials as carriers, for example, for crop protection (FIGURE I.4). TABLE I.1 includes carriers and delivery systems based on renewable and non-renewable resources. In this section, the most common carrier systems based on biopolymers (biobased or biodegradable) as well as inorganics obtained from natural resources are discussed.

Efforts related to “green” systems began with lignin as a matrix to control the release of biocides (TABLE I.1). Lignin-based biocide carriers has been already reported two decades ago (COTTERILL; WILKINS, 1996; DELLICOLLI; CHARLESTON, 1977; FERNANDEZ-PEREZ; GONZALEZ-PRADAS; URENA-AMATE, 1998; ZHAO; WILKINS; ILKINS, 2003) but only a small number of reports have been published since then. However, many advances in the preparation of both nano and micro particles of lignin with different chemical features have been developed (AGO et al., 2017; RICHTER et al., 2016), increasing the potential of lignin as a carrier for sustainable biocide delivery systems. According to Dellicolli (DELLICOLLI; CHARLESTON, 1977), the aromatic nature of lignin makes it excellent protective matrix for related biocides, which may be

sensitive to degradative processes triggered by sunlight. Besides, it has been emphasized that the antioxidant properties of lignin could help to enhance the stability of chemically unstable pesticides, which is the case of several non-persistent agents that are still in use. The procedure used to prepare the controlled release system is quite simple and results in granules of lignin loaded with biocides. The general approach involves mixing dry lignin powder with saturated biocide solutions, followed by drying and granulation. The lignin-biocide formulations have been noted to be effective in keeping the microorganisms under control even after seven weeks (DELLICOLLI; CHARLESTON, 1977).

Other work using lignin as a carrier include significant modifications. Some systems, for example, added a melting step during the granulation of the lignin-biocide mixture (COTTERILL; WILKINS, 1996; FERNANDEZ-PEREZ; GONZALEZ-PRADAS; URENA-AMATE, 1998; ZHAO; WILKINS; ILKINS, 2003). The T_{50}, the time required to release 50% of the biocide, varied from 2.4 to 11.2 days in the case of fluometuron herbicide. The variation in the release rate of the biocide was attributed to the proportion of low molecular weight, more water-soluble lignin in the granules. Thus, it is possible to tune the release properties of the biocide formulation by using different fractions of water-soluble lignin.

In a recent report, granulation was used to prepare hybrid coated granules of lignin, with the biocide (chloridazon), ethyl cellulose and poly(ethylene glycol) (PEG) (FERNÁNDEZ-PÉREZ et al., 2011). The controlled release formulation was prepared in two steps. First, granules were formulated by mixing lignin, PEG and chloridazon (wt.% ratios of 65:20:15) at 200 °C, followed by cooling and grounding. Then, solutions of ethyl cellulose were sprayed onto the granules in different amounts to create shell of different thicknesses. At optimized conditions, the lignin-based granules achieved full biocide release after 800 h.

A breakthrough approach for lignin-based biocides was accomplished by using the nanoprecipitation technique to prepare spheres containing an entrapped biocide (YEARLA; PADMASREE, 2016). In this process, lignin was co-precipitated with Diuron biocide into a non-solvent under vigorous stirring to form a nano-suspension. As

entrapment took place within the spheres, the biocide profiles showed very slow release, achieving 80% total release after 120 days.

FIGURE I.4 – DIVERSITY OF MATERIALS AND RELATED STRUCTURES SUITABLE FOR APPLICATION IN THE PREPARATION OF CONTROLLED RELEASE BIOCIDES

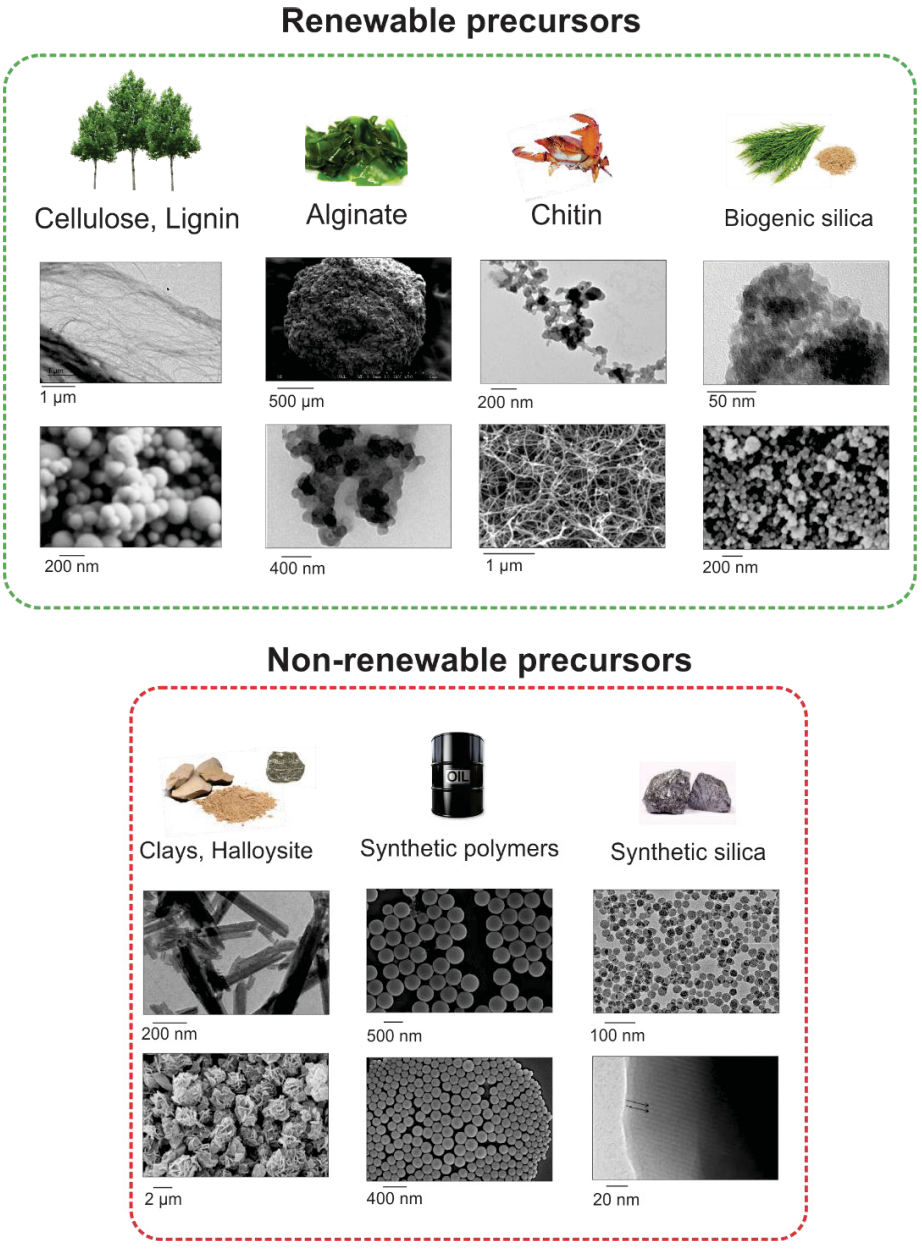

SOURCE: the author (2018). The figure is adapted and redrawn with copyright permission from references (ABDULLAYEV et al., 2009; AGO et al., 2017; CHAUHAN et al., 2016; CHEN et al., 2013, 2011; FLORES-CÉSPEDES et al., 2015; HORNIG et al., 2009; KUMAR et al., 2014; LIU et al., 2016; MATTOS; MAGALHÃES, 2016; RIDGWAY; GANE; SCHOELKOPF, 2004; YI et al., 2015).

Lignin was also used together with cellulose to prepare chemically cross-linked hydrogels for controlled release of natural polyphenolics (CIOLACU et al., 2012). Alkali-dissolved cellulose was mixed with different amounts of lignin and fixed with an epichloridrin cross-linker under vigorous stirring. Finally, the dried hydrogel (powder form) was immersed in hydro-alcoholic, polyphenolic solution and let to swell for a day for incorporation of the polyphenols into the matrix. After drying, the resultant material released 15-25% of the loaded polyphenolics after 10 h. Similarly, poly(acrylamide) and methylcellulose hydrogels loaded with N, N′-dimethyl-4,4′-bipyridinium dichloride (or Paraquat, a commonly used herbicide) were prepared (AOUADA et al., 2010). The herbicide release from these hydrogels achieved plateau after 10 days.

The chemical heterogeneity of lignin can be identified as the largest hurdle for its utilization as a biocide carrier, since it will directly affect the interaction with the BDS and with the environment. However, very significant advances on lignin's purification and separation have been advanced in recent years (LIANG et al., 2016; LOURENÇON et al., 2015; WEINWURM et al., 2016); in turn, such purified or isolated fractions enable the preparation of more consistent carriers.

Cellulose and cellulose esters have been applied as a carrier material for controlled release of biocides (MILOVANOVIC et al., 2016). This includes cellulose acetate beads containing a biocide (natural monoterpene phenols, thymol). The incorporation of thymol in the cellulose matrix was carried out by supercritical impregnation at 10 MPa and 35 °C. This system resulted in thymol payload release over 4000 minutes. Microcrystalline cellulose was employed in the preparation of cross-linked membranes to protect biopesticides (auxins, rotenone, chlorogenic acid) against UV light and to control their release (PANG et al., 2016). First, the cellulose was dissolved in DMAc/LiCl, and a cross-linker solution (containing toluene diisocyanate as modifier, and 4,4-dihydroxy benzophenone as catalyst) was prepared. Then, different ratios of these solutions were prepared and exposed to air followed by drying. The permeation of the biopesticides through the membrane was evaluated by using a transdermal diffusion device. Cellulose nanofibrils (CNF) were recently used together with biogenic silica to prepare inorganic/organic nanocomposites for sustained release of tebuconazole biocide (MATTOS; MAGALHÃES, 2016). The work was based on the adsorption of tebuconazole

onto silica, followed by blending the loaded nanoparticles with cellulose nanofibrils. Tebuconazole adsorbed on silica and was released slower than the neat biocide; however, the release rate was even slower in the presence of CNF. After 15 days of immersion, 95 % of the pure biocide was released, compared with 30–45% when incorporated as a CNF nanocomposite.

The affinity of cellulose for water enhances the release profiles of cellulose-based BDS. However, the mechanical integrity of such cellulose-based BDS can be compromised by water uptake. This can be addressed by utilizing cellulosic nanostructures, including nanocrystals and nanofibrils (the latter from pure cellulose or from lignocellulose) since they have shown promise in overcoming the effects associated with water. For instance, all-cellulose composites with good levels of mechanical resistance (MAGALHÃES; CAO; LUCIA, 2009) can be achieved toward BDS. Alternatively, different degrees of hydrophobization could be applied (TARDY et al., 2017) in order to limit cellulose interaction with surrounding water, leading to a better maintenance of the mechanical integrity and, potentially, of the release profile.

Several options exist for inorganic carriers obtained from natural resources. Biogenic silica nanoparticles derived from *Equisetum arvense* biomass were used as a carrier of an eco-friendly biocide comprising of a neem bark extract cross-linked with polycarboxylic acids (MATTOS et al., 2017d). Self-assembly in a one-pot procedure was designed to prepare such systems. A suspension containing silica nanoparticles, neem bark oil, cross-linker (1,2,3,4-butanetetracarboxylic acid) and a catalyst was prepared and let to react for 2 h. The obtained biocides delivered 60-75% of the active molecules after 30 days. Another approach to prepare controlled release biocides was presented in which clays and polysaccharides were combined into beads (SINGH et al., 2009). The polysaccharides included starch and alginate, while the clays were kaolin and bentonite. The principle of the bead formation relied on the ability of the sodium alginate to readily cross-link after contact with an ionic solution (usually $CaCl_2$). The bead formation was triggered by dispersing given amounts of the polysaccharides, clays and thiram biocide in hot water, and then stirring the suspension to form a homogenous mixture. This mixture was further added drop-wise into a 0.1 M $CaCl_2$ solution, forming the beads. They were washed and dried at low temperature. The entrapment of the biocide into the beads was

97% efficient and the presence of the clay in the bead formulation slightly retarded the release of thiram, which tended to decrease with increasing the clay content.

Sodium alginate nanoparticles were formulated by the emulsion cross-linking technique (KUMAR et al., 2014). In this procedure, water-in-oil (W/O) emulsions were prepared via ultra-sonication of an aqueous dispersion comprising sodium alginate, imidacloprid pesticide and dioctyl sodium sulfosuccinate as surfactant and with methylene chloride as the oil phase. A water-in-oil-in-water (W/O/W) double emulsion was emulsified into an aqueous polyvinyl alcohol (PVA) solution. The nanoparticles were crosslinked by addition of a saturated solution of calcium chloride. The resultant nanoparticles (diameter ranging from 70 to 350 nm) displayed a 99% efficiency in pesticide entrapment, depending upon the formulation variables. The smallest particles yielded the lowest entrapment efficiency (< 50%). Evaluations in the field, confirmed that the pesticide-loaded nanoformulations were more effective and presented a lower toxicity compared to the pure pesticide.

The botanical pesticide azadirachtin was encapsulated in alginate-based granules to obtain controlled release formulations (FLORES-CÉSPEDES et al., 2015). Lignin, humic acid and olive pomace biosorbents were incorporated in the formulation (sodium alginate – azadirachtin - water) to improve the entrapment efficiency of the biocide. In fact, the practical azadirachtin loading in the bead doubled after adding approximately 5 wt.% of the biosorbents in the formulation. Furthermore, the biosorbent played an important role in decreasing the biocide release (especially during the first 250 h) and in increasing its photostability.

Starch, chitosan and cyclodextrin have been widely investigated both in pure form or combined with synthetic polymers (CAMPOS et al., 2014). Amphiphilic self-assembled chitosan-grafted-poly(methyl methacrylate) nanoparticles containing up to 28 wt.% of the fungicide tebuconazole were synthesized (DING et al., 2011). Nanoparticle formation occurred by micellar growth polymerization, and the hydrophilic/hydrophobic character was controlled by addition of 2-hydroxyethyl methacrylate. The tebuconazole-loaded nanoparticles were impregnated into pinewood to achieve target retentions of 0.2, 0.4 and 0.8 kg tebuconazole/m³, and then submitted to release and soil jar decay tests. The loaded biocide released out from wood three times slower than the neat biocide;

nevertheless, the wood treated with both neat and encapsulated biocides presented the same decay resistance.

Starch-based hydrogels containing carbendazim biocide were reported (BAI et al., 2015). First, carbendazim-loaded starch-grafted-(acrylic acid-co-methyl methacrylate) beads were synthesized by dissolving carbendazim in acrylic acid and introducing them in a flask containing methyl methacrylate, catalyst and water and gradually heated to 70 °C. Then, gelatinized starch was added to the system to form the beads. In order to form the hydrogel, the obtained beads were blended with a fresh mixture containing acrylic acid, acrylamide, potassium peroxydisulfate, N,N-methylenebisacrylamide, water and starch paste. The hydrogel released carbendazim during 400 h at a constant rate, whereby the slowest and complete release of biocide occurred in acid pH.

Biodegradable synthetic polymers have been used as green approaches for biocide delivery systems (BOYANDIN et al., 2016; MEYER et al., 2015). Pellets of poly(3-hydroxybutyrate) mixed with birch sawdust, poly(ε-caprolactone) and/or poly(ethylene glycol), were prepared by cold pressing the components at different ratios together with metribuzim biocide (BOYANDIN et al., 2016). The release of biocide from the pellet was different, depending on the pellet composition but, in general, 16-38% of the biocide was released after 35 days. The pellet prepared with poly(ethylene glycol) displayed the fastest release due to its high water solubility. Also, poly(lactic-co-glycolic acid) nano-dispensers were created using an emulsion-solvent evaporation method for delivery of imidacloprid (MEYER et al., 2015). With this system, acceptable levels of protection were achieved, for at least 10 days. In this device, the high exposed surface area of biocide allowed a 200-fold dosage reduction of the active ingredient when compared with the current commercial formulation.

I.3.4 BIOCIDE DELIVERY SYSTEMS PREPARED FROM SYNTHETIC MATERIALS OR NON-RENEWABLE RESOURCES

Besides biodegradable carriers, the synthetic materials and mineral resources such as polymers, clays and metal oxides (FIGURE I.4), have been widely investigated to prepare BDS formulations. Although these materials are synthetic, which may be a drawback, their ability to control the release rate of biocides make them appealing as

carriers. Any suitable strategy for their utilization should consider recyclability and biodegradability, particularly for crop applications. These carriers are included in TABLE I.1. BDS prepared with these supports have drawn attention especially for protection of forest products since wood and its expected extended service life are easily affected by microorganisms such as fungi. Studies related to BDS using synthetic nanostructured supports have been reported before 2000. These earlier efforts, mainly financed by the United States Department of Agriculture (USDA), discussed the synthesis of wood preservatives by incorporating tebuconazole and chlorothalonil into poly(vinylpyridine) and poly(vinylpyridine-co-styrene) nanoparticles (median particle diameters of 100–250 nm) (LIU; LAKS; HEIDEN, 2002a, 2002b, 2002c). O/W emulsions were used to synthesize particles containing the biocide via internal phase separation. This process requires proper selection of the volatile solvent, the barrier-forming polymer, the oil (which needs to be a poor solvent for the barrier polymer) and the biocide (that needs to be soluble in the oil phase). The proposed polymeric capsules containing biocides improved, over 10-fold, the resistance of birch wood to white-rot attack, with a very low biocide loading required (0.1 to 0.8 $kg \cdot m^{-3}$).

In parallel to these developments, biocide delivery systems were considered for use with different substrates such as polymer foil, paper or wood (BÖTTCHER et al., 1999). BDS formulated in this manner involved, for example, the entrapment of sorbic, benzoic or boric acid inside silica xerogel conjugated with small amounts of hydroxypropylcellulose (0.1 to 2.0 wt%) (BÖTTCHER et al., 1999). The obtained liquid phases were coated on cellite foils and wood surfaces, by solidification of the cast suspension upon solvent evaporation. The release of the entrapped biocides from the sol-gel films ranged from ca. 39 to 98% after 24 h, depending on the hydroxypropylcellulose content, biocide-to-silica ratio and film thickness. These systems were found to be effective in hindering the growth of bacterial and fungal colonies. Accordingly, the greatest advantage of these films was that the biocides were only liberated in the presence of moisture, making them “on-demand” release systems. A great number of efforts have been carried out based on similar principles as those discussed thus far (ANDERSSON TROJER et al., 2015; BERGEK et al., 2014; HANDA; FANT; NYDÉN, 2006; ICONOMOPOULOU et al., 2005; JAMSA et al., 2013; KITAMURA;

FUJIMOTO, 2003; PELTO et al., 2014; SORENSEN et al., 2010; YANG et al., 2009). The main distinction for each controlled release system is related to the various combinations matrix material, biocide and the solvents.

Among clays, halloysite ($Al_2Si_2O_5(OH)_4$) could be considered as one of the most promising tubule-shaped material for carrier applications. Contrary to most tubule-shaped materials used as nano/micro containers, halloysite is an economically viable clay carrier that can be mined from deposits. Depending on its origins, its size varies from 500-1000 nm in length and 15-100 nm in internal diameter (LVOV et al., 2008). Halloysite present remarkable advantages over synthetic tubule-shaped materials, making them suitable as nanocontainers for a wide range of small molecules, including biocides (ABDULLAYEV et al., 2009; LVOV et al., 2008; SCARFATO et al., 2016; SHCHUKIN et al., 2008). Halloysite nanotubes were loaded with iodobutylpropyl carbonate (IBPC) to design a biocidal paint. In this process, halloysite tubules were mixed as a dry powder with a saturated IPBC (iodopropynyl butylcarbamate) solution, exposed to high vacuum, and then dried to eliminate the solvent and to entrap the biocide. The biocide was released from the nanocontainer following a Peppas kinetic model (power law, n = 0.6), which took over 50-fold longer compared to that from the unloaded biocide (LVOV; PRICE, 2007). Moreover, the incorporation of these biocide-loaded halloysite coatings could be aided by the SiO_2 surface chemistry, allowing for a range of surface treatments (LVOV et al., 2008). Finally, a halloysite nanotube-based support suitable for biocide activity in construction materials was developed by impregnating the halloysite nanotubes via vacuum-assisted processes with a commercial biocide (Biotin T) (SCARFATO et al., 2016). The potential of the nanobiocide to reduce the bioreceptivity of the structural building components over two years was demonstrated.

Besides halloysite, other clays have been used as supports for prolonged biocide activities. this includes a controlled release herbicide system based on intercalated atrazine salts onto montmorillonite (MMT) clay platelets (AKELAH; REHAB; EL-GAMAL, 2008). The intercalation process was carried out by swelling MMT in distilled water, and then an ethanolic solution of atrazine hydrochloride salt was added slowly to the swollen MMT at 80 °C. The mixture was kept under stirring overnight, then cooled, filtered off,

washed, and dried under vacuum. A two-fold decrease of the solubility rate of the herbicide was determined– the release rate was even lower in acidic pH.

The entrapment of commercial biocides (Wocosen, Fungaflor and Bethoguard) in a sodium-intercalated montmorillonite (commercialized as Nanofil 116) was also reported (EVERSDIJK et al., 2012). The basic idea was to assemble pillared platelets by swelling the exfoliated clay layers with a surfactant solution. For the entrapment of the biocides into the clay platelets, the biocides were dissolved in THF, clay material was added into this solution, and then the mixture was stirred overnight. Afterwards, the solvent was evaporated, resulting in a pillared material with the biocide entrapped between the layers. These systems were incorporated in gypsum for prolonged protection of building materials. Using an artificial rain test, the authors proved that the free biocides were leached out from the gypsum matrix after seven days, compared to 42 days if entrapped in the clay material.

Intercalated sodium paeonolsilate in a Zn_2Al layered double hydroxide (LDH) matrix resulted in controlled release of antifouling agents (SUN et al., 2016). The LDH-intercalated biocide was synthesized by an ion-exchange method: sodium-based biocide was dissolved in an aqueous solution (pH 7.5), and then Zn_2Al-NO_3 precursor was added, in which the amounts of each one was based on their ion-exchange capacity. The mixture was kept under stirring at 70 °C and N_2 atmosphere for 48 h, and then the precipitate was centrifuged, washed and dried. The release of the intercalated biocide was twice as slow (surface release lasting a longer time) compared to that from pristine biocide, which resulted in a lower density of *Ulva* spores attached on the coating.

Alumina nanoparticles were also used as carriers in the preparation of BDS for wood protection (MATTOS; MAGALHÃES, 2017). The biocide system was prepared by loading alumina nanoparticles with carbendazim through surfactant-assisted ball milling. The obtained BDS released up to 76% of biocide after 600 h. In addition, pinewood impregnated with a biocide retention of only 0.4 $kg \cdot m^{-3}$ showed a 10-fold improvement in decay resistance.

Several researchers have studied silica nanostructures as carriers of bioactive molecules: they are thermally and chemically inert and present negligible swelling in aqueous media. Until now, mesoporous silica have been the most common nanostructure

in controlled release formulations (CHEN et al., 2011; JANATOVA et al., 2015; KAPOOR; HEGDE; BHATTACHARYYA, 2009; POPAT et al., 2012a; QIAN et al., 2013; WANYIKA, 2013; YI et al., 2015). Biocides such as imidacloprid, tebuconazole, metalaxyl, pyoluteorin have been loaded into mesoporous silica. In related work, the loading procedure consisted in the addition of silica nanoparticles in a solution saturated with the biocide, under stirring, followed by centrifugation and drying (freeze-drying in some cases). The biocides loaded by this procedure were fully released from silica in a time interval between 50 h and 30 days, depending of specific surface area and on the biocide concentration in the silica support.

Functionalized mesoporous silica nanoparticles with short-chain gatekeepers were designed to control the release of salicylic acid, according to the redox changes in the release media (YI et al., 2015). After the synthesis of a typical mesoporous silica (MCM-41), a cationic surfactant (CTBA) can be kept inside the mesoporous structure (no calcination is applied). The CTBA attached to the internal surface of silica walls, made it possible to graft thiol groups (-SH) at the entrance of mesopores. Then a mixture of absolute ethanol and hydrochloric acid removed the CTBA template. Following, the thiol-capped silica was loaded with salicylic acid through free diffusion. Finally, dodecyl disulfide was added to the mixture to react with -SH groups on the entrance of mesopores and to assemble the gatekeepers. These functionalized nanoparticles were found to be stimuli-responsive to glutathione in the release media. In this case, the glutathione could interact with the decanethiol gatekeepers allowing the release of the active molecules.

Besides mesoporous silica, silica nanostructures have been applied as support for biocides. For instance, 2-mercaptobenzothiazole (MBT) and 4,5-dichloro-2-octyl-4-isothiazolin-3-one (DCOIT) were incorporated in silica nanocapsules for protective coatings (MAIA et al., 2015). The synthesis of the loaded nanocapsules was carried out by the oil-in-water emulsion method, in which the biocides were dissolved in the oil phase and the silica precursor was tetraethyl orthosilicate (TEOS). The obtained biocide-loaded nanocapsules presented a diameter of 300 nm, compared to 126 nm for the capsules without biocide. Both capsules showed micro-porosity (pore width < 2 nm), which helped to prolong the release of the bioactive molecules.

Biocompatible silica nanocapsules containing the insecticide fipronil were designed as BDS to act against subterranean termites (WIBOWO et al., 2014). The nano-formulation was prepared by dissolving fipronil in oil (mixture of decanoyl- and octanoyl glycerides) and then emulsifying it via sonication in the presence of a peptide surfactant – in this process the pH was maintained neutral with a buffer solution. Following, tetraethyl orthosilicate (TEOS) was added as silica precursor for the system to form a silica shell encasing the nanoemulsion core. The polar, cationic arginine and lysine residues from the peptide induced the hydrolysis of TEOS at the oil/water interface. By controlling the amount of silica precursor and its condensation time, it was possible to obtain shells with different thickness (8 to 44 nm). After 144 h immersion, the nanocapsules released 15-40% of total encapsulated insecticide; as expected, thicker shells released with a slower kinetics. *In vivo* treatment tests using these systems against worker termites showed that the time interval between the application of the biocide and the termite mortality could be adjusted, depending on the silica-shell thickness.

Silica could also be covalently cross-linked with biocides in order to prepare conjugated nanospheres (DING et al., 2014). Related systems have been prepared via reaction between biocide kasugamycin, 3-aminopropyltriethoxysilane (APTES) and TEOS. The diameter of the obtained conjugated nanospheres varied between 85 and 185 nm, depending on the preparation conditions (pH, volume of water, stirring rate). Near neutral pH, intermediate stirring rates and small volume of water added resulted in smaller diameters. The stability to light of the biocide conjugated with silica was five times higher than that of the pure biocide, while its release from silica occurred during 20 weeks. Small particles, acidic pH and high temperatures increased the release rate of the biocide.

TABLE I.1 – CARRIERS REPORTED FOR THE SYNTHESIS OF CONTROLLED RELEASE BIOCIDES. THE TABLE INCLUDES CO-MATERIALS AND METHODS FOR BDS SYNTHESIS

Carrier Material	Co-materials	Biocides	Method	References
Alginate	Chitosan, PVA, Olive pomace, humic acid, lignin, bentonite	Paraquat, acetamiprid, imidacloprid, azadirachtin, carbofuran	Bead formation via cross-linking ionic gelation, polyelectrolyte complexation, W/O/W emulsion cross-linking	a
Chitin	Sodium tripolyphosphate, alginate, PMMA	Paraquat, hexaconazole, tebuconazole	Ionic gelation, self-assembly	b
Kraft and Organosolv lignin	PEG, ethyl cellulose, plasticizers	Dimethyl amine, diuron, chloroxuron, fluometuron, metoxuron, imidacloprid, chloridazon, metribuzin	Granulation, melt granulation followed by spray coating, nanoprecipitation in co-solvent	c
Cellulose	Lignin, cross-linkers	Polyphenols extracts, thymol, capsaicin, rotenone	Hydrogel formation by chemical cross-linking, supercritical impregnation	d
Other polysaccharides: Pectin, Starch	PVA, alginate, kaolin, bentonite, acrylic acid, MMA,	metsulfuron-methyl, thiram, carbendazim	Nanoencapsulation by W/O/W emulsion, bead forming by ionic gelation, hydrogel solution polymerization	e
Biodegradable synthetic polymers: PCL, PHB, PLA	PEG, PCL, wood	Essential oils, imidacloprid, metribuzin	Emulsion solvent evaporation, mechanical palletization	f
Biogenic silica	Cellulose nanofibrils, poly carboxylic acids	Neem bark extract, tebuconazole	Inorganic-organic nanocomposite preparation, biocide cross-linking	g
Minerals: MMT and halloysite	Surfactants	Atrazine, IPBC, propiconazole, imazalil, bethoxazin	Cationic exchanging, loading by incubation in biocide saturated solution	h
Synthetic polymers: AA, MA, EA, St, LDPE, PVP, PEG, PEI, PMMA	Bentonite, several cross-linkers, PCL	Bifenthrin, imidacloprid, garlic acid, tebuconazole, chlorothalonil, sodium benzoate, OIT	Extrusion followed by coating, melt-dispersion, internal phase separation, interfacial polyaddition, emulsion solvent evaporation	i
Synthetic silica: mesoporous, hollow, nonporous	Hydroxypropyl cellulose, block copolymers, SurSi peptide	Benzoic acid, sorbic acid, boric acid, IPBC, pyoluteorin, imidacloprid, tebuconazole, metalaxyl, fipronil, MBT, DCOIT	Sol-gel films, self-assembly, highly ordered monolith carrier preparation followed by incubation, miniemulsion, gatekeeping	j

Key: PVA: poly(vinyl alcohol); PEG: poly(ethylene glycol); PCL: poly(caprolactone); PHB: poly(hydroxybutyrate); PLA: poly(lactic acid); MMA: methyl methacrylate; AA: acrylic acid; MA: methacrylic acid; EA: ethyl acrylate; St: styrene; LDPE: low-density poly(ethylene); PEI: poly(ethylenimine); PMMA: poly(methyl methacrylate); MMT: montmorillonite; OIT: 2-n-Octyl-4-Isothiazolin-3-One; IPBC: Iodopropynyl butylcarbamate; DCOIT: Dichloro-2-octyl-2H-isothiazol-3-one; MBT: 2-mercaptobenzothiazole.

[a] (FERNÁNDEZ-PÉREZ et al., 1999; FLORES-CÉSPEDES et al., 2015; KUMAR et al., 2014, 2015; SILVA et al., 2011)
[b] (DING et al., 2011; GRILLO et al., 2014, 2015)
[c] (CHOWDHURY, 2014; COTTERILL; WILKINS, 1996; DELLICOLLI; CHARLESTON, 1977; FERNÁNDEZ-PÉREZ et al., 2011, 2015; FERNANDEZ-PEREZ; GONZALEZ-PRADAS; URENA-AMATE, 1998; YEARLA; PADMASREE, 2016; ZHAO; WILKINS; ILKINS, 2003)
[d] (CIOLACU et al., 2012; MARTINI et al., 2014; MILOVANOVIC et al., 2016; PANG et al., 2016)
[e] (BAI et al., 2015; CAMPOS et al., 2014; KUMAR et al., 2017; SINGH et al., 2009)
[f] (MEYER et al., 2015; PINTO et al., 2016)
[g] (MATTOS et al., 2017; MATTOS; MAGALHÃES, 2016)
[h] (AKELAH; REHAB; EL-GAMAL, 2008; EVERSDIJK et al., 2012; LVOV et al., 2008)
[i] (BERGEK et al., 2014; JAMSA et al., 2013; KIMOTO; TAKAHASHI; INUBUSHI, 2007; LIU; LAKS; HEIDEN, 2002a, 2002c, 2003; PELTO et al., 2014; PETOSA et al., 2017; YANG et al., 2009)
[j] (BÖTTCHER et al., 1999; CHEN et al., 2011; MAIA et al., 2015; POPAT et al., 2012; QIAN et al., 2013; SORENSEN et al., 2010; WANYIKA, 2013; WIBOWO et al., 2014)

I.3.5 PROSPECTS AND CONSIDERATIONS IN BIOCIDE DELIVERY SYSTEMS

As highlighted in this review, the loading or encapsulation of biocides in carriers has become a remarkable strategy to gain efficient control on biocides in terms of their loading and rate of delivery. It is expected that in the near future the controlled release of biocides will turn into key tools to improve cropland productivity and protection with minimum or no impact to the environment, health and well-being. Through effective pest control management, it will be possible to achieve more efficient protection while using lower amounts of biocidal molecules. The materials and biocides available are expected to offer solutions that are generic and flexible in their applications but will make use of local resources.

Biocide delivery systems will become closer to the field as deep insights are gained in relation to the effect of climate (*e.g.* sunlight, precipitation, temperature), soil composition (*e.g.* minerals, organic matter, pH), texture (*e.g.* sand, clay) and plants' surface. It will be necessary to understand how BDS behave under different, potentially harsh, climate conditions, *e.g.,* BDS applied in tropical or subtropical environments. Some recently published work considers these aspects, including environmental changes as triggers for release (AKELAH; REHAB; EL-GAMAL, 2008; CHEN et al., 2011; EVERSDIJK et al., 2012; KUMAR et al., 2014; QIAN et al., 2013; YI et al., 2015). This also underlines the need to benchmark experiments at different scales, as with wood protection (GREAVES et al., 2015). Realistic release conditions for various climates or soil types are necessary for a better understanding of BDS performance at large scale. After initial *in vitro* tests, greenhouse experiments and small-scale field-testing must be considered before an experimental BDS can reach the market. Besides, the current regulations about the toxicity of pesticides are well consolidated (UNITED STATES ENVIRONMENTAL PROTECTION AGENCY, 2017), and could be used as a ground to assess BDS toxicity evaluation once they have been formulated with regulated biocides.

Another burgeoning trend in the design BDS is the development of new responsive systems, able to deliver active substances after changes in pH, temperature or salinity. Such approaches will draw inspiration from the interesting but perhaps not directly

translatable findings in drug delivery. The responsive systems could enhance and revolutionize agriculture and silviculture as well as wood protection.

While this review did not address the nature of pesticides, a major revolution is expected in response to opposition and regulatory restrictions; so that options are adopted that are not harmful to humans, non-target species, and the environment. Here, bio-based products are gaining popularity and are growing in the biocide markets. Their integration with conventional and new carriers needs to be addressed. For this, consideration to factors that maintain their advantages is required, including slowing the development of resistance, reducing chemical residues, and minimizing the chemical load to the environment. Preparation, storage and delivery equipment was not discussed in this review but they deserve much attention in view of the type of carrier and active components present in emerging biocide delivery systems.

CHAPTER II

BIOREFINERY PLATFORM TOWARD DEVELOPING A MORE SUSTAINABLE PROCESS FOR THE ISOLATION OF SILICA NANOPARTICLES FROM BIOMASS

II.1 INTRODUCTION

There are many species of silicon accumulating plants but their extraction yields differs greatly due to differences in the biochemical pathway of silicon uptake by the roots (MA; YAMAJI, 2006). These plants include grasses such as maize, wheat and rice, or plants from genus *Equisetum* (HOLZHUTER et al., 2003; LAW; EXLEY, 2011; MA; YAMAJI, 2006). Nowadays, using biorefinery concepts, rice husks are the most exploited biomass for the production of silica (SiO_2) particles (GU et al., 2013; UMEDA et al., 2007; ZHANG et al., 2010). Silica deposits in plant materials are usually up to 20% of their dry mass, depending on the variety and on the edaphoclimatic conditions used for growth. Despite the high silica content of these plants, the profitability is impaired for just silica production. In this context, some smart strategies have been used to produce other high-value products in parallel with silica particles. Some good examples are the co-production of xylose (ZHANG et al., 2010), activated carbon (LIU et al., 2012), ethanol and organosolv lignin (ZHANG et al., 2015).

The extraction of silica particles from *Equisetum arvense* (horsetail) is interesting due to the possibility of simultaneously producing a hydro alcoholic extract with several medicinal properties (DO MONTE et al., 2004; DOS SANTOS et al., 2005; OH et al., 2004). Also, over 70% of the horsetail biomass is composed of carbohydrates that can be converted to liquid fuels, organic acids, biopolymers and other green chemicals by fermentation, as well as to furan compounds such as furfural and 5-hydroximethylfurfural through dehydration of pentoses and hexoses (GANDINI; LACERDA, 2015). Silica deposits are observed in all parts of *E. arvense* (LAW; EXLEY, 2011). Holzhuter et al. (2003) showed that most of the silica is deposited as a thin layer (from nano to micrometers) onto the internal surface of the plant cell wall. Other alkali and alkaline earth elements such as Mg, K and Ca were also found in the mineral deposits of horsetail. The silica layers consist of dense particles sizing 25-40 nm and other porous structures formed by agglomeration of 8 nm spheres whose porosity is probably due to the presence and distribution of organic compounds. These layers can be disassembled to obtain particles for many purposes.

Micro- and sub-micrometric silica powders have a range of interesting applications such as in concrete, rubber and ceramics as reinforcing agents, fillers in composites and blends, and materials for heat isolation and photoelectric devices. On the other hand, nanostructured silica with high specific surface area and extremely high porosity can be applied in specific high-value market niches as photo catalysts, adsorbents, drug delivery materials, corrosion inhibitors and inorganic supports for many other purposes (PODE, 2016; PRADO et al, 2011; SIDDIQUE, 2011; WIBOWO et al., 2014). Considering the many fields in which silica nanoparticles could be applied, it is of general interest the development of a sustainable process to produce high-quality silica from renewable sources. The consecutive obtainment of medicinal extracts and carbohydrate derivatives together with silica nano-, microparticles could be a good way to improve the profitability of the silica production from plant biomass. In this chapter, the conditions in which valuable extractives with medicinal properties, carbohydrate derivatives and silica nanoparticles could be obtained from horsetail biomass were investigated.

II.2 MATERIAL AND METHODS

II.2.1 START MATERIAL AND BIOREFINERY PROCEDURE

Equisetum arvense (horsetail) was harvested from the experimental farm of Embrapa Florestas (Colombo-PR, Brazil). Stems and branches were cut into small pieces (10-40 mesh), washed and oven-dried at 60±2 ºC until constant mass. The biorefinery process was carried out in three main sequential steps: hydro alcoholic extraction, acid hydrolysis and calcination (FIGURE II.1).

FIGURE II.1 – BIOREFINERY SCHEME APPLIED FOR THE COPRODUCTION OF HYDRO-ALCOHOLIC EXTRACTS, CARBOHYDRATES DERIVATIVES AND SILICA NANOPARTICLES FROM *E. ARVENSE*

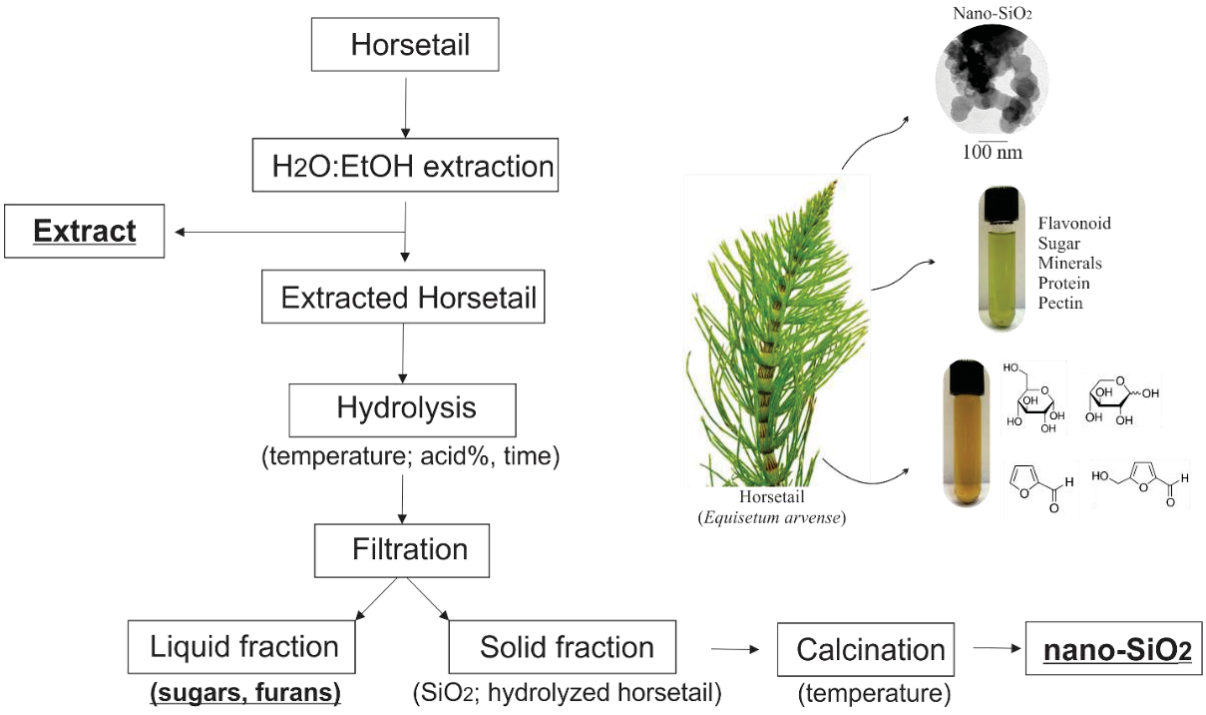

SOURCE: the author (2018).

The hydro alcoholic extraction was performed to remove low molar mass polar compounds from the horsetail biomass. The extract was obtained by immersing washed horsetail biomass in 1:1 (v/v) H_2O:EtOH at a fixed solid:liquid ratio of 1:10. After 24 h, the hydro alcoholic extract was filtered and the remaining horsetail stems were oven-dried at 103±2 ºC until constant mass.

The hydrolysis step using diluted sulfuric acid or water (auto-hydrolysis) was applied to leach out the alkali and alkaline earth metal impurities and to partially hydrolyze the hemicellulose components of the horsetail biomass. The pre-extracted horsetail (2 g) was suspended in the hydrolysis solution (20 mL) at a fixed solid:liquid ratio of 1:10, and placed in a small reactor (30 mL) to be heated at different temperatures and times according to the statistical design that is described in TABLES II.1 and II.2. The hydrolysate was filtered; the solids were washed until pH 7 with distilled water and dried at 103±2 ºC until constant mass, while the liquid fraction was kept for chromatographic analysis (see below for details). The hydrolysis yield was obtained using the following equation:

$$\text{Hydrolysis yield (\%)} = \frac{Mr - Ms}{Mr} \times 100$$

where Mr is the oven-dried mass of the raw horsetail (g) and Ms is the oven-dried mass of the pre-extracted horsetail biomass (solid fraction).

The calcination step was performed by transferring 1 g of the solids in a porcelain crucible and placing it in a pre-heated electric muffle furnace for 1 h.

II.2.2 STATISTICAL DESIGN AND ANALYSIS OF VARIANCE APPLIED TO THE OPTIMIZATION OF THE BIOREFINERY PROCESS

The main factors affecting the silica properties are the temperature, time and acid concentration used for hydrolysis as well as the calcination temperature (GU et al., 2013). Also, these same factors except the calcination temperature are very influential for the production of soluble sugars (BAMUFLEH et al., 2013). Thus, an orthogonal $L_9 (3)^4$ test was designed to investigate the main factors affecting this biorefining process (TABLE II.1) and to reduce the number of experiments (TABLE II.2) that were required for process optimization. Each experiment was carried out in three replicates.

ANOVA was carried out to identify the most significant factors affecting the response variables. Then, the estimated coefficients were used to create multiple linear regression models to evaluate the quantitative effect of each factor on the reaction response.

TABLE II. 1 **–** FACTORS AND LEVELS PROPOSED FOR OPTIMIZING THE BIOREFINING PROCESS OF THE HORSETAIL BIOMASS

Factors (F)	Unit	Abbreviation	Levels (l)		
			1	2	3
Hydrolysis temperature	ºC	HT	120	140	160
Hydrolysis time	h	t	1	2	4
Sulfuric acid concentration	wt.%	$[H^+]$	0	2	4
Calcination temperature	ºC	CT	550	650	750

TABLE II. 2 – $L_9(3)^4$ EXPERIMENTAL DESIGN USING THE FACTORS AND LEVELS PROPOSED IN TABLE II.1

Experiment	Factors (F)*			
	HT (°C)	t (h)	$[H^+]$ (%)	CT (°C)
EXP1	1	1	1	1
EXP2	1	2	2	2
EXP3	1	3	3	3
EXP4	2	1	3	2
EXP5	2	2	1	3
EXP6	2	3	2	1
EXP7	3	1	2	3
EXP8	3	2	3	1
EXP9	3	3	1	2

* Legend according to TABLE II.1.

II.2.3 CHARACTERIZATION OF THE RAW AND PRE-EXTRACTED HORSETAIL BIOMASSES AND THE PRODUCTS RESULTING FROM HYDROLYSIS

The raw and pre-extracted horsetail biomasses were characterized by quantifying their ethanol/toluene extractive, acid soluble lignin, acid insoluble lignin, ash, monomeric carbohydrates, as well as their total protein content. In addition, biomass acid hydrolysates were analyzed by high performance liquid chromatography (HPLC) for their

contents in sugars and furan compounds and the corresponding solid fractions were characterized for their energy content and thermal properties.

The biomass preparation and further quantification of ethanol/toluene extractives, acid insoluble lignin and acid soluble lignin followed the analytical procedures proposed by the National Renewable Energy Laboratory (NREL, Golden, CO, USA) (HAMES et al., 2004; SLUITER et al., 2004, 2010, 2012). Elemental analysis of raw and pre-extracted horsetail biomasses was carried out in Elementar Vario Macro Cube CHNS analyzer and their protein content was estimated using the total nitrogen conversion factor proposed by Merrill and Watt (1973).

Sugar and furan compounds were quantified in biomass acid hydrolysates by HPLC using a Shimadzu LC20AD workstation and an Aminex HPX-87H column that was protected by a Cation-H^+ guard column. Analyses were performed at 65 °C with 5 mmol·L^{-1} H_2SO_4 as the mobile phase and a flow rate of 0.6 mL·min^{-1}. Detection was carried out by refractive index and quantification was performed by external calibration using standard solutions of cellobiose, glucose, xylose, 5-HMF and furfural.

The ash content was quantified by using the TAPPI T211 method while the ash metal oxide composition was evaluated by energy dispersive X-ray spectrometry using a Shimadzu EDX-720 spectrometer

The energy content and thermal properties of the solid fractions derived from acid hydrolysis were evaluated by measuring their high heating value (HHV) in an adiabatic calorimeter IKA® (model C5000) and by thermogravimetric analysis (TGA). TGA experiments were performed in a DTG-60 equipment (Shimadzu) using a N_2 atmosphere with a gas flow of 20 mL·min^{-1}. The temperature range was between 25 and 600 ºC with a heating rate of 10 ºC·min^{-1}.

II.2.4 CHARACTERIZATION OF THE BIOGENIC SILICA NANOPARTICLES

The whiteness index (WI) of biogenic silica was performed using the ASTM E313−15 (2015) method in a Konica Minolta CM-5 spectrophotometer. Metal oxides were quantified by energy dispersive X-ray spectrometry using a Shimadzu EDX-720 spectrometer. Organic matter was estimated by mass loss after calcination at 1100 °C for

2 h. The specific surface area ($m^2 \cdot g^{-1}$) was calculated using the Brunauer–Emmett–Teller (BET) multipoint model in the linear relative pressure range (P/P_0) of 0.05 to 0.35; the equipment used in these measurements was the Quantachrome NOVA 1200e analyzer. The morphologic features of the biogenic silica were studied using a field emission gun scanning electron microscope (FEG-SEM) FEI Quanta 450 and a transmission electron microscope JEOL, model JEM-1200 EXII.

II.3 RESULTS AND DISCUSSION

II.3.1 EVALUATION OF THE HYDRO ALCOHOLIC EXTRACTION

The hydro alcoholic extraction of *E. arvense* yielded 20.2%. The ethanol/toluene extractives, pectin, protein and ash contents of the horsetail biomass decreased after hydro alcoholic extraction while both acid insoluble and acid soluble lignin increased (TABLE II.3). The acid insoluble lignin was corrected by its ash content because most if not all silica present in the horsetail biomass remained in the lignin after acid hydrolysis. The decrease in sugar and extractive contents suggests that some flavonoid glycosides were extracted from the horsetail biomass. In fact, as showed elsewhere (DO MONTE et al., 2004; DOS SANTOS et al., 2005; ONISZCZUK et al., 2014), the hydro alcoholic extracts of *E. arvense* contain phenolic acids, flavonoids, flavonoids glycoside, sterols minerals, and minerals that are responsible for their antinociceptive, antioxidant, anti-inflammatory, hepatoprotective, sedative and anticonvulsive properties.

TABLE II. 3 – CHEMICAL COMPOSITION OF THE RAW MATERIAL BEFORE AND AFTER HYDRO ALCOHOLIC EXTRACTION

Quantification	Horsetail	Extracted horsetail
Overall chemical composition (wt.%)		
Ethanol/toluene extractives	6.33 (0.16)	3.07 (0.01)
Acid insoluble lignin	11.49 (0.45)	13.46 (0.56)
Acid soluble lignin	0.80 (0.01)	0.89 (0.04)
Anhydrous glucose	20.59 (0.09)	18.70 (0.05)
Anhydrous xylose	15.30 (0.31)	15.02 (0.08)
Pectin	8.29 (0.32)	7.38 (0.99)
Protein	24.21 (0.29)	19.25 (0.23)
Ash	18.21 (0.10)	16.70 (0.02)
Composition of ash (wt.%)		
SiO_2	53.14 (0.06)	72.83 (0.20)
K_2O	13.30 (0.05)	2.8 (0.10)
CaO	22.58 (0.17)	15.10 (0.08)
Al_2O_3	1.19 (0.02)	1.22 (0.06)
MgO	8.27 (0.20)	6.59 (0.41)
P_2O_5	0.79 (0.10)	0.98 (0.07)
Fe_2O_3	0.36 (0.01)	0.18 (0.01)
Loss at 1100 °C	9.60 (0.50)	9.25 (0.45)

Values in brackets are standard deviations;

Extraction proved to be effective for the removal of alkaline metal cations such as K^+ while Ca^{2+} and Mg^{2+} were also removed but in less amount (TABLE II.3). In fact, Chen et al. (2013) and Umeda et al. (2007) showed that water can remove large amounts of potassium from plant tissues; however, other metal cations such as calcium require acidification for its effective removal. TABLE II.3 shows that the hydro alcoholic extract from *E. arvense* is rich of K^+, Ca^{2+} and Mg^{2+} and the presence of these justifies the mineralizing activity of horsetail extract, likewise other medicinal plants such as chamomile, sage and peppermint (PYTLAKOWSKA et al., 2012).

II.3.2 EVALUATION OF THE PRODUCTS OBTAINED AFTER ACID HYDROLYSIS

Dilute sulfuric acid hydrolysis released higher yields of soluble sugars from horsetail (20-45%) compared to auto-hydrolysis (2-10%) (FIGURE II.2). Acid concentration and hydrolysis temperature promoted statistically significant changes in the hydrolysis yield (see the TABLE S1 for details) but the effect of the former was higher than that of the latter (TABLE II.5).

FIGURE II 2 – INTERACTION PLOT OF THE SIGNIFICANT FACTORS ([H+] AND HT) AFFECTING THE RESPONSES OF HYDROLYSIS YIELD

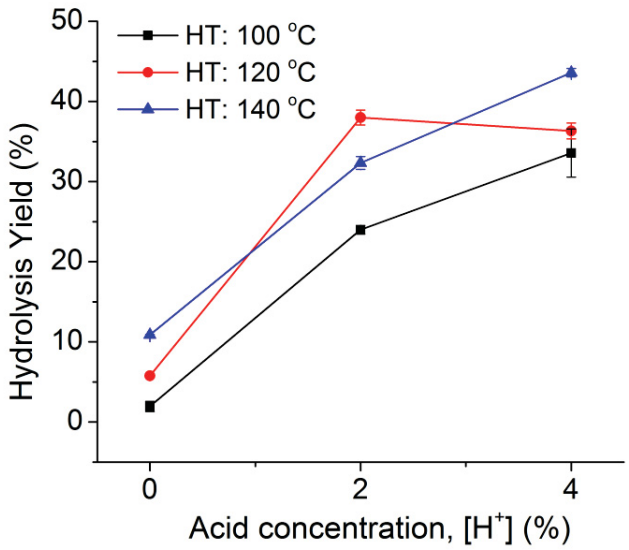

SOURCE: the author (2018).

For both auto-hydrolysis and diluted acid hydrolysis, the observed changes in biomass chemical composition were directly related to carbohydrate depolymerization and its subsequent extraction. The thermogravimetric curves (FIGURE II.3a) and their derivatives (FIGURE II.3b) showed two thermal events in the pyrolysis of treated horsetail (FIGURE II.3), which are associated to thermal degradation of polysaccharides (from 220 to 360 ºC) and lignin (from 400 to 530 ºC).

FIGURE II.3 – THERMOGRAVIMETRIC (a) AND DERIVATIVE THERMOGRAVIMETRIC (b) CURVES OF THE SOLID FRACTION FROM EXPERIMENTS WITH DIFFERENT HYDROLYSIS YIELD

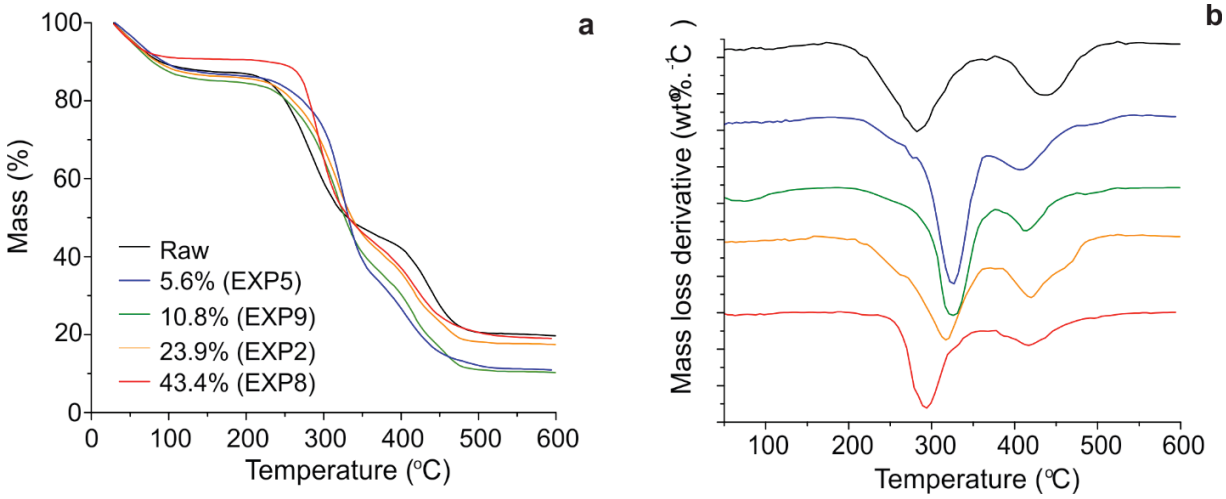

SOURCE: the author (2018).

After mild acid hydrolysis (EXP5 and EXP9), the event related to the thermal degradation of polysaccharides shifted from 285 to 330 ºC (FIGURE II.3b) and was probably due to the selective removal of hemicelluloses from the lignocellulosic matrix. In fact, hemicellulose removal usually increases the thermal stability of the biomass due the better structural properties of the remaining crystalline cellulose. However, at more drastic hydrolysis conditions (EXP2 and EXP8), the thermal degradation of polysaccharides peaked at 290 ºC (FIGURE II.3b) most likely due to the onset of cellulose degradation in parallel to hemicellulose removal. For all treated horsetail biomasses, the peak related to the thermal degradation of lignin shifted to lower temperatures (FIGURE II.3b) and this was probably due to the breakdown of acid-labile bonds in α-*O*-4 and β-*O*-4

substructures, causing a considerable decrease in the lignin average molecular mass. This effect was even more pronounced under mild dilute acid hydrolysis conditions, as observed in experiments 2 and 8 of FIGURE II.3. In general, the thermal degradation of isolated lignin occurs at temperatures lower than 400ºC (LOURENÇON et al., 2015) and this partially explains the thermal behavior of acid treated horsetail during the TG analysis.

Both HHV and ash contents were significantly affected by the acid concentration, whereas ash content was also affected by the hydrolysis temperature (TABLE S1). The filtered solids from auto-hydrolysis presented statistically lower ash content and HHV, compared to those derived from diluted acid treatments (FIGURE II.4). The HHV values of acid-treated horsetail were lower than that of other biomasses with biofuel potential such as miscanthus and sorghum fibers (up to 19 $MJ \cdot kg^{-1}$) (GODIN et al., 2013) and this was mainly due to its high ash content. Therefore, it seems that carbohydrate degradation during acid hydrolysis is detrimental to the energy capacity of the solid fraction. The ash content in the treated solids was mostly composed of SiO_2 (81-98%, FIGURE II.6) since acid hydrolysis promoted the selective leaching of alkali and alkaline earth metals. Both acid concentration and hydrolysis temperature had similar positive effects on the ash content of the resulting material. In addition, there was a large carbohydrate degradation at the more drastic acid hydrolysis conditions (reaching to 45%) but the acid leaching of metal impurities was not increased in the same order of magnitude

TABLE II. 4 – CONCENTRATION OF SUGARS AND FURAN COMPOUNDS OF THE LIQUID FRACTION FROM HYDROLYSIS

Experiment	Concentration ($g \cdot L^{-1}$)[a]				
	Cellobiose	Glucose	Xylose	5-HMF[c]	Furfural
EXP1	nd[b]	0.04 (0.01)	0.09 (0.01)	nd	nd
EXP2	0.05 (0.00)	0.43 (0.12)	2.80 (0.83)	0.02 (0.01)	0.01 (0.00)
EXP3	0.41 (0.02)	1.65 (0.05)	7.19 (0.30)	0.04 (0.00)	0.03 (0.00)
EXP4	0.19 (0.01)	2.97 (0.09)	11.83 (0.01)	0.12 (0.02)	0.13 (0.01)
EXP5	nd	0.28 (0.01)	0.39 (0.03)	nd	nd
EXP6	0.11 (0.03)	3.08 (0.04)	11.84 (0.14)	0.16 (0.01)	0.26 (0.01)
EXP7	0.04 (0.00)	3.23 (0.27)	12.07 (0.88)	0.31 (0.01)	0.51 (0.04)
EXP8	0.04 (0.02)	3.68 (1.91)	7.01 (0.86)	0.25 (0.08)	0.43 (0.14)
EXP9	0.02 (0.00)	0.29 (0.12)	0.36 (0.06)	0.01 (0.00)	0.01 (0.00)

[a] Values in brackets are standard deviations; [b] Below the detection limit of the HPLC method (nd = not detected); [c] 5-hydroxymethylfurfural.

FIGURE II.4 – INTERACTION PLOT OF THE SIGNIFICANT FACTORS AFFECTING THE HHV (a) AND THE ASH CONTENT (b) OF THE SOLID FRACTION, AS WELL AS THE CONCENTRATION OF TOTAL SUGARS (c) AND FURAN COMPOUNDS (d) IN THE LIQUID FRACTION DERIVED FROM ACID HYDROLYSIS

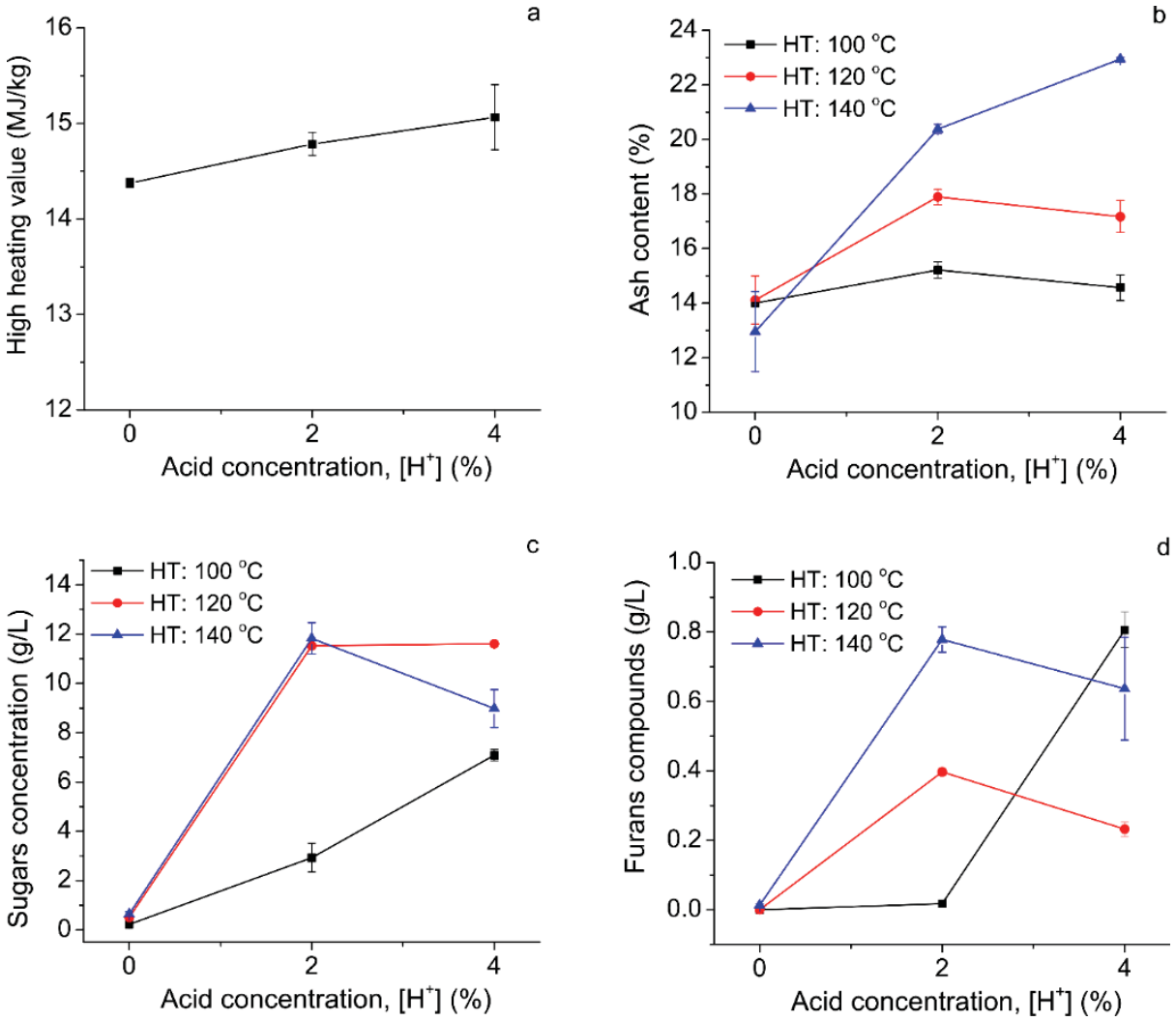

SOURCE: the author (2018).

Monomeric sugars and furan compounds mainly composed the horsetail biomass pretreatment liquor. Xylose was the main detectable sugar while furfural was observed at concentrations higher than those of 5-HMF (TABLE II.4). The concentration of sugars was significantly affected by acid concentration and hydrolysis temperature, while the effect of acid concentration was only significant for the accumulation of furan compounds

(TABLE S1 and S2). In general, the accumulation of furans was low compared to reports that are focused on the production of such carbohydrate derivatives from different types of biomass (BAMUFLEH et al., 2013; LÓPEZ et al., 2014; YEMIS; MAZZA, 2011). The low concentrations of both sugars and furan compounds were associated to the mild conditions applied for hydrolysis. However, at high HT and $[H^+]$ the total of sugars and furan compounds reached as much as 11 and 0.8 $g \cdot L^{-1}$ in the biomass acid hydrolysate, respectively (TABLE II.4 and FIGURE II.4).

TABLE II. 5 – MULTIPLE LINEAR REGRESSION MODELS AFTER HYDROLYSIS

Mathematical models [a]	R^2 [b]	Error [c]	p-value [d]
Yield (%) = -19.512 + 4.548 HT + 1.971 t + 15.814 $[H^+]$	0.87	5.49	<0.01
Sugars ($g \cdot L^{-1}$) = -4.893 + 1.867 HT - 0.731 t + 4.383 $[H^+]$	0.66	2.99	<0.01
Furans ($g \cdot L^{-1}$) = -0.504 + 0.101 HT + 0.034 t + 0.277 $[H^+]$	0.54	0.23	<0.01
HHV ($MJ \cdot kg^{-1}$) = 13.933 + 0.062 HT - 0.002 t + 0.344 $[H^+]$	0.68	0.21	<0.01
Ash (%) = 11.855 + 2.080 HT - 1.023 t + 2.269 $[H^+]$ - 0.963 CT	0.75	1.75	<0.01

[a] the input values and legends are according to the Table 1;
[b] Coefficient of determination;
[c] Standard error of the estimative (same unit of independent variable);
[d] Probability value.

The auto-hydrolysis at the applied range of temperature (100 – 140 ^oC) and time (1 – 4 h), resulted in the release of very low concentrations of all evaluated compounds in the pretreatment liquor and these were statistically lower compared with those obtained by acid hydrolysis (FIGURE II.4).

Regardless the statistically significance, the hydrolysis time had a negative effect on the total sugar concentration, HHV and ash content (TABLE II.5). On the other hand, both hydrolysis time and acid concentration had positive effects on the extent of acid hydrolysis while the calcination temperature had a negative effect on the ash content. By using the coefficients of the models, the most important factors affecting the hydrolysis were organized as [H+]>HT>t, which was similar to the results obtained for the total ash content of pretreated solids ([H+]>HT>t>CT).

II.3.3 MORPHOLOGICAL AND PHYSICOCHEMICAL PROPERTIES OF THE OBTAINED BIOGENIC SILICA NANOPARTICLES

Acid concentration was the only significant factor affecting the SiO_2 content in the ashes of acid-treated horsetail (TABLE S1). Auto hydrolysis experiments were not able to remove Ca and Mg from the biomass (FIGURE II.5b), resulting in ashes with statistically lower SiO_2 content compared to acid hydrolysis (FIGURE II.5a).

FIGURE II.5 – INTERACTION PLOT OF THE SIGNIFICANT FACTORS AFFECTING THE PURITY (a), AMOUNT OF METALLIC IMPURITIES (b), WHITENESS INDEX (c) AND SPECIFIC SURFACE AREA (d) OF THE OBTAINED BIOGENIC SILICA

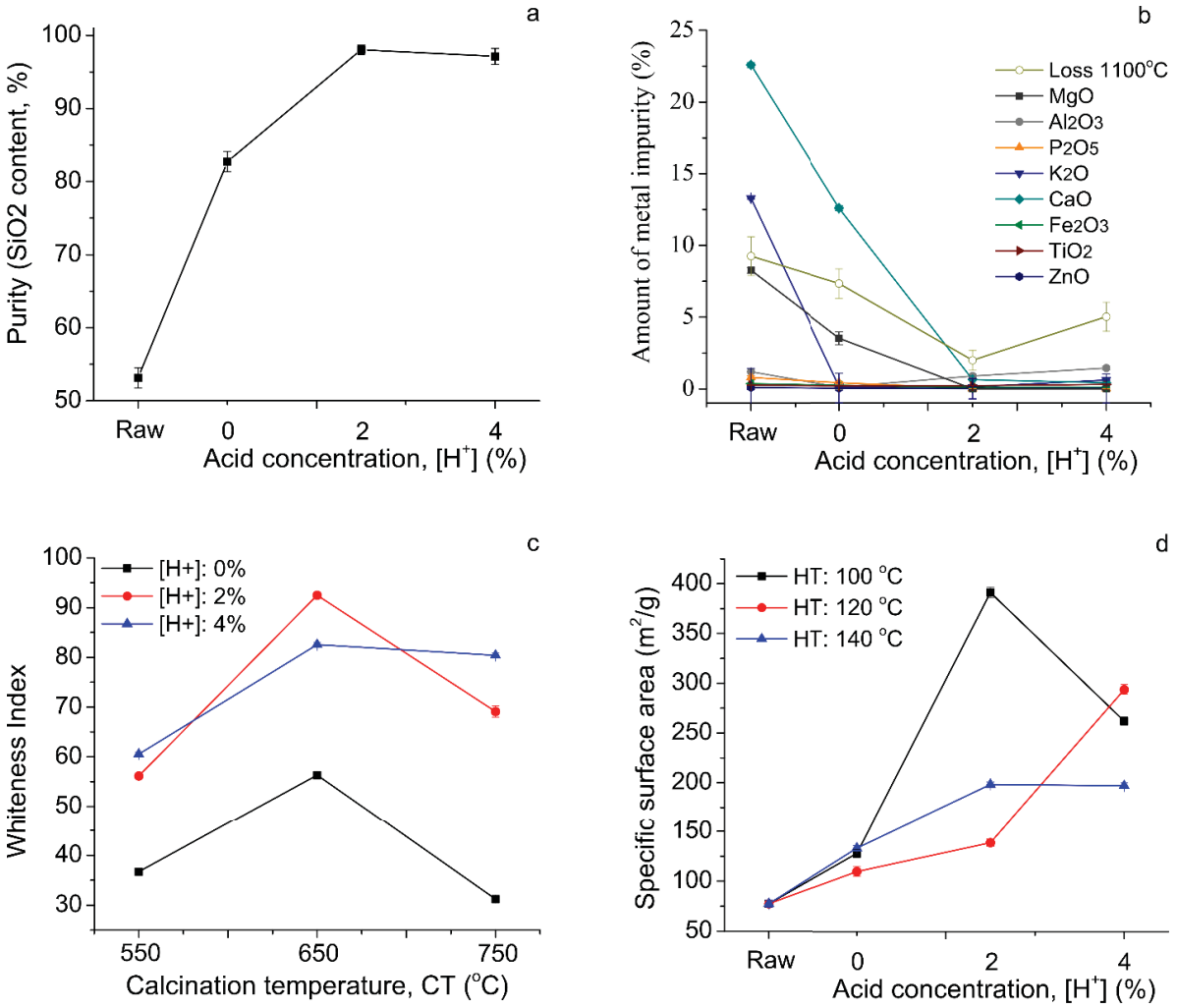

SOURCE: the author (2018).

However, by increasing the acid concentration from 2 to 4%, the metallic impurities did not change significantly (FIGURE II.5b). Other authors achieved the same levels of silica purity (over 96%) by performing acid treatments of rice husk ashes (ATHINARAYANAN et al., 2014).The removal of organic impurities followed a pattern similar to that of the inorganics. By increasing the acid concentration from 2 to 4%, higher amounts of organic matter remained in the horsetail ash composition (FIGURE II.5b). Thus, utilization of acid hydrolysis at high acid concentrations and temperatures inhibited the destruction of Si–C bonds, resulting in ashes containing a higher content of organic matter. Calcination temperature and acid concentration had both positive and statistically significant effects on the whiteness of horsetail ashes (TABLE S2) but the latter variable had a comparatively stronger effect (TABLE II.6).

TABLE II. 6 – MULTIPLE LINEAR REGRESSION MODELS FOR THE SILICA PROPERTIES

Mathematical models [a]	R^2 [b]	Error [c]	p-value [d]
Whiteness = 27.015 - 3.944 HT + 0.744 t + 16.550 $[H^+]$ + 4.555 CT	0.54	14.45	<0.01
SSA ($m^2 \cdot g^{-1}$) = 157.141 - 42.144 HT - 14.122 t + 63.144 $[H^+]$ + 17.494 CT	0.53	66.35	<0.01
Purity (%) = 75.869 - 0.081 HT + 1.038 t + 7.191 $[H^+]$ + 0.234 CT	0.70	4.27	<0.01

[a] the input values and legends of the factor are according to the Table 1;
[b] coefficient of determination;
[c] standard error of the estimative (same unit of independent variable);
[d] probability value.

Silica prepared by auto-hydrolysis presented statistically lower whiteness values compared to acid hydrolysis and this was due to its lower ability to remove the contaminating organic matter (FIGURE II.5c). Whiteness may be used as a rapid and cheap tool for process optimization because it is highly associated with both metallic and carbon impurities, and indirectly related to the surface area of the silica nanostructures. In general, the amount of impurities was inversely related to the average particle surface area (FIGURE II.5c and 5d). The specific surface area (SSA) of silica was positively affected by acid concentration but this was contrasted by the negative effect of the hydrolysis temperature (TABLE II.6). Besides, the presence of high metallic impurities and organic matter contents negatively affected the porosity of silica nanostructures. Silica with low metallic impurities showed SSA ranging from 144 to 393 $m^2 \cdot g^{-1}$ (FIGURE II.5d). Even with high contents of metallic and organic matter impurities, the silica

obtained by auto-hydrolysis showed SSA values high enough for its classification as a nanomaterial, which must have a volume-specific of the surface area greater than 60 m^2/cm^3 according to definition of Kreyling et al. (2010).

.

FIGURE II.6 – SEM (a) AND TEM (b) IMAGES OF THE SILICA PARTICLES OBTAINED FROM ACID-TREATED HORSETAIL

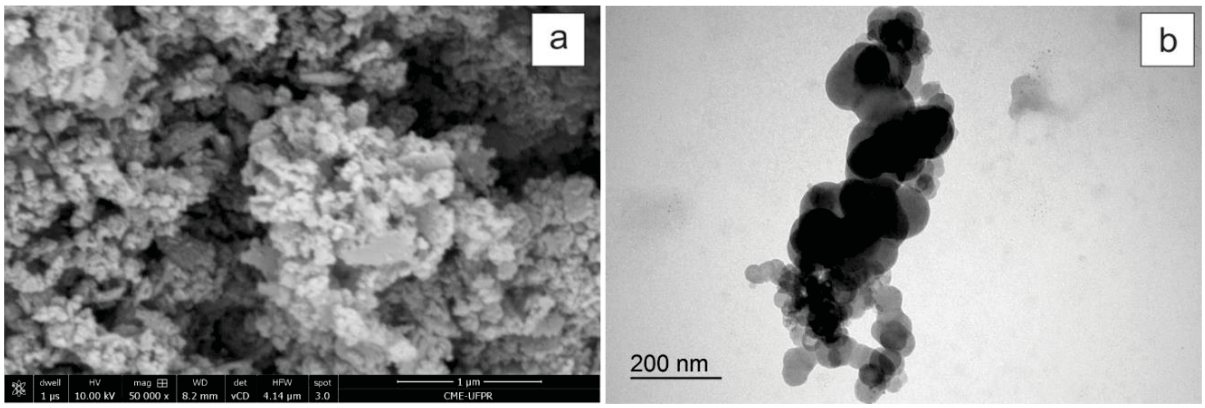

SOURCE: the author (2018).

The hydrolysis temperature had negative effect on all silica properties (TABLE II.6) while the calcination temperature had a positive effect. The range of calcination temperature from 550 to 750 ^oC can be considered small (GU et al., 2013) and its effect on SSA may have been overlapped by other highly significant factors. In fact, the coefficients of the SSA model were higher for acid concentration and hydrolysis temperature compared to that of the calcination temperature (TABLE II.6). Hence, the most important factors for the development of whiteness and SSA were $[H^+]$>HT>CT>t, whereas this order was $[H^+]$>t>CT>HT for the SiO_2 content of horsetail ashes (TABLE II.6).

At the optimized conditions for high surface area, purity and whiteness (HT of 2 h, [H+] of 2% and CT of 650 °C), most of silica particles behave as an agglomerate of irregular sphere-like nanoparticles (FIGURE II.6), which can be easily disaggregate via ultra-sonication or ball milling to form nanoparticles (MATTOS et al., 2016).

II.4 CONCLUSIONS

Equisetum arvense can be used as raw material for the production of biologically active low molar mass compounds, carbohydrate derivatives and silica nano- and microparticles. By doing so, the mass and energy balance of the biorefinery process for silica isolation from biomass can be greatly improved. Silica for high value-added products could be obtained by treating horsetail biomass with a 2% $w \cdot v^{-1}$ acid sulfuric aqueous solution at 100 ^{o}C for 1h, followed by calcination at 650 ^{o}C for 1h. In this case, the silica particles have surface area over 350 $m^2 \cdot g^{-1}$, and 98% of purity. However, at these hydrolysis conditions, the yield of co-products was low. If there is no need for high-quality silica, the amount of all co-products could be increased *ca*. ten times by increasing the hydrolysis temperature to 140 ^{o}C, and keeping the levels of the other variables. Silica particles with surface area ca. 170 $m^2 \cdot g^{-1}$, and same purity, are obtained in these conditions.

CHAPTER III

CONTROLLED BIOCIDE RELEASE FROM HIERARCHICALLY-STRUCTURED BIOGENIC SILICA: SURFACE CHEMISTRY TO TUNE RELEASE RATE AND RESPONSIVENESS

III.1 INTRODUCTION

Biocides are essential in agro-industrial applications to improve the yields in crop production and to extend the active life of biodegradable compositions (MATTOS et al., 2017a; NURUZZAMAN et al., 2016). Traditional methods of biocide-based protection often require high initial dosages or repeated applications; consequentially, they result in uncontrolled delivery and short protection time span. Additionally, this leads to excessive, potentially harmful, leaching of the biocide into soil and water. Their bioaccumulation brings hazardous consequences for human health, usually not shown but in the long term. Therefore, it is becoming paramount the development of biocide delivery systems (BDS) that offer controlled or triggered release. However, the development of new, effective, governmentally-approved and safe biocide molecules is a current and expensive challenge (LAMBERTH et al., 2013). A current paradigm is the development of BDS that minimize the concentration of toxins in soil, food and water while promoting long-term biocidal protection (MATTOS et al., 2017a). In this regard, we hypothesize that nanostructured BDS are a promising approach to achieve sustainability, high efficiency and high payload. Thus, engineering BDS at the nanometric scale is an effective answer to this need that requires control of the biocide-carrier interface interactions. Principal concerns in the development of efficient BDS include the environmental impact of the carrier, mechanical and chemical robustness to avoid unintended leaching into crops and, control of the loading and release rate for efficient biocidal effects (MATTOS et al., 2017a).

Synthetic silica nanoparticles have been widely investigated as carriers for delivery systems, both for pharmaceutical (SLOWING et al., 2008) and agrochemical applications (MATTOS et al., 2017a). These particles are particularly attractive for upcoming smart delivery, due to their high specific surface area (WU; MOU; LIN, 2013), engineerable surface chemistry (KOBLER; MÖLLER; BEIN, 2008), biological inertness to both flora and fauna (BRUNNER et al., 2006; LU et al., 2010) and thermal stability (KOBLER; MÖLLER; BEIN, 2008). However, the bottom-up synthetic processes to obtain silica nanoparticles are complex and use non-renewable precursors through a process that generates highly hazardous biproducts and toxic intermediate reactants such as

ferrosilicon (FeSi) and silicon tetrachloride ($SiCl_4$). Moreover, FeSi is responsible for a reasonable fraction of air pollution and cause severe health hazards around production sites (HOBBESLAND; KJUUS; THELLE, 1999; LANGÅRD; ANDERSEN; RAVNESTAD, 1990), while $SiCl_4$ is highly toxic (INDUSTRIES, 2010). We previously reported on biomass-derived silica particles (biogenic silica) that can be used as an affordable, ecofriendly and efficient alternative for BDS carriers (MATTOS et al., 2017d). Biogenic silica particles have a high surface area (up to 400 $m^2 \cdot g^{-1}$) and their surface chemistry is identical to the synthetic counterparts. Biogenic silica consists of a fractal-like network of 8-10 nm subunits hierarchically organized into agglomerates with sizes ranging from 100 nm to 4 µm, depending on the treatment applied for dispersion (CARMONA et al., 2013; LIU et al., 2013; MATTOS et al., 2017b). The facile surface modification of silica can be translated to that of biogenic silica structures as a mean to tune the dynamics of biocide release. Previously, this has been achieved in BDS, for instance, by gate keeping (YI et al., 2015) and near-infrared induced release (XU et al., 2017). However, these sophisticated approaches are costly and complicated for implementation, limiting their direct application as BDS. As Siepmann and Siepmann (2008) pointed out, the carrier/drug interface interaction plays a fundamental role in the drug release mechanism. Therefore, by promoting different carrier/biocide interface interactions through surface modifications, the release rates can be tuned. Furthermore, they can render BDS more responsive to external stimuli such as pH, temperature and ionic strength. Herein, through specific surface modifications of biogenic silica, we propose and develop a generic strategy to obtain “green” BDS with a tunable and responsive release. Such features are essential in order to minimize the amount of biocides delivered for efficient pest control as a function of soil or crop type as well as climatic conditions.

Thymol was used as a model biocide as it is one of the most interesting and highly investigated biopesticide (NURUZZAMAN et al., 2016). Thymol inhibits the proliferation of food fungi (ABBASZADEH et al., 2014), wood decay (MEDEIROS et al., 2016), mold (SEGVIĆ KLARIĆ et al., 2007), crop pests (THOMIDIS; FILOTHEOU, 2016), spoilage yeasts (CHAVAN; TUPE, 2014), mosquitoes and beetles (KORDALI et al., 2008; MARCHESE et al., 2016). Additionally, as it is sourced from plants belonging to the

Lamiaceae family, such as *Thymus* and *Origanum* species, its loading in biogenic silica would result in a fully biomass-derived BDS.

Thus, in this chapter, a framework was developed to modify the surface of the biogenic silica particles in order to promote different interface interactions with thymol. Additionally, as both carrier and biocide are sourced by plants, the biocide delivery system herein introduced can be considered a greener biocide system.

III.2 MATERIALS AND METHODS

III.2.1 MATERIALS AND CHEMICALS

Thymol (Thy), Maleic anhydride, 3-Aminopropyl-triethoxysilane (APTES), sodium chloride (NaCl), sodium hydroxide (NaOH), hydrochloric acid (HCl), calcium sulfate hemidrate, lysogeny, tryptone, yeast extract, agar, starch, casein, beef extracts and organic solvents were purchased from Sigma-Aldrich. Biogenic silica particles ($BSiO_2$) were isolated from *Equisetum arvense* (horsetail) as previously described.

III.2.2 DESIGN AND SYNTHESIS OF THE $BSIO_2$-THYMOL BDS

The $BSiO_2$ was amine-functionalized by using APTES (GESZKE-MORITZ; MORITZ, 2016): 1 g SiOH and APTES (4 mL) were placed in a flask containing 100 mL toluene. After ultrasonication (30 min), the dispersion was refluxed at *ca.* 110 °C for 6 h, and then subjected to centrifugation (5000 rpm, 10 min), sequential washing with toluene (3 x) and absolute ethanol (2 x), and drying at 103 °C. The obtained particles are thereafter referred to as "$SiNH_2$". Carboxyl-functionalized surface was achieved by subsequent amidation reaction of $SiNH_2$ particles using maleic anhydride (AN et al., 2007): 1 g $SINH_2$ and maleic anhydride-DMF solution (40 mL at 2 $mol \cdot L^{-1}$) were placed in a flask, ultrasonicated (30 min), and kept under stirring. After equilibrating for 24 h, the suspension was centrifuged (5000 rpm, 10 min), sequential washed with DMF (3 x) and absolute ethanol (2 x), and dried at 103 °C. The obtained particles are thereafter referred to as "SiCOOH".

The biocide-carrier-solvent affinities were investigated by using the thin layer chromatography (TLC) technique. The TLC plates preparation and experiments followed well-known procedures (SHERMA; FRIED, 1996). Unmodified and surface-functionalized $BSiO_2$ particles were used as the stationary phase. Organic solvents with different polarity were used as the mobile phase. The carrier-biocide interactions were compared by calculating the retention factor (Rf) of thymol on silica over solvent changes.

First, 200 mg of $BSiO_2$ was suspended in 10 mL n-hexane, submitted to indirect ultra-sonication for 30 min, and placed in a reciprocal shaker at 100 rpm and 25 °C. Then, under continuous mixing, 10 mL of thymol solution was added dropwise; the flask was sealed and left to equilibrate for 24 h. The thymol solutions were prepared in n-hexane at 1, 5, 10, 20 and 40 $g \cdot L^{-1}$ to optimize the loading procedure. The $BSiO_2$-thymol based BDS were recovered after centrifuging the suspension at 2000 rpm for 1 min and further drying it at 80 °C for 4 h.

III.2.3 ANALYTICAL AND MORPHOLOGICAL CHARACTERIZATION OF THE $BSIO_2$-THYMOL BDS

The biocide payload in BDS was assessed through an UV-adsorption calibration curve at 275 nm (FIGURE S1). The surface chemical features of the BDS were elucidated by X-ray photoelectron spectroscopy (XPS) using a VG Microtech ESCA 3000 spectrometer. The equipment operated at $3x10^{-10}$ mbar, with Mg Kα radiation as excitation source (photo energy at 1 253.6 eV). The C_{1s} binding energy was set at 285 eV to use as internal reference for compensating for surface charging effects. The functional chemical groups and chemical interactions of the BDS were investigated by using Fourier transform infrared spectroscopy (FTIR). FTIR spectra were acquired on a Bruker Tensor 37 FTIR unit, using KBr pellets, at a nominal resolution of 4 cm^{-1} (64 scans in the 4000 to 400 cm^{-1} wavenumber range were accumulated and averaged). Thermogravimetric (TGA) and differential thermal analysis (DTA) were applied to investigate the effect of the interface interactions on the thermal behavior of thymol. TGA and DTA experiments were carried out in a DTG-60 Shimadzu equipment using N_2 atmosphere with gas flow of 50 $mL \cdot min^{-1}$, temperature range from 25 to 200 °C, and a heating rate of 10 $°C \cdot min^{-1}$. Zeta potential of the starting $BSiO_2$ particles and the resultant BDS were examined over pH changes by using Zetasizer ZS NanoS90 (Malvern). The reported average results of the zeta potential were determined from at least five measurements. The pH was adjusted by the addition of 0.01 $mol \cdot L^{-1}$ HCl or NaOH aqueous solutions. The representative morphological features of typical $BSiO_2$ particles were studied by using a transmission electron microscope (TEM) JEOL, model JEM-1200

EXII, and a field-emission gun scanning electron microscope (FEG-SEM) FEI Quanta 450. Also, an optical microscope Leica ICC50 HD, operating in bright field, was used to observe the morphological features of the settling, larger, fraction of the silica particles.

III.2.4 BIOCIDE RELEASE PROFILES AND KINETICS

The biocide release profiles were investigated under various conditions in the release media. Specifically, three pH values (5, 7 and 9), electrolyte concentrations (NaCl, 0.5, 2.0 and 3.5% $w \cdot v^{-1}$) and temperatures (25, 35 and 45 °C) were evaluated. The pH of the release media was adjusted using the same procedure used for Zeta potential measurements. In a typical release experiment, filter paper envelopes (72 samples: 3 surfaces x 3 replicates x 8 time points) containing *ca.* 30 mg of BDS were placed in 1 L of dH_2O at given pH, salinity and temperature. This methodology was applied to precisely ensure the same release conditions for sample comparison. Then, the envelopes were removed at fixed time intervals, from 0 to 350 h, and the amount of the residual thymol in the BDS was extracted with ethanol and quantified via UV calibration curve. The release profile data were acquired using triplicates. The Elovich kinetic model (CHIEN; CLAYTON, 1980) led to the best fitting and allowed evaluation of the release rate as a function of a single kinetic parameter (*k*). The activation energy (AE) of the biocide delivery was calculated with the Arrhenius equation.

III.2.5 BIOLOGICAL ACTIVITY OF THE $BSIO_2$ PARTICLES SUPPORTING THYMOL

Suspensions at 20% solid content of each BDS, namely, SiOH@Thy, $SiNH_2$@Thy, and SiCOOH@Thy, were prepared for readily casting of 50 µL volume on a cleaned polystyrene plate. The resulting pellet was 10 mg in mass and *ca.* 5 mm in diameter. For the control samples, we considered an average thymol payload in the BDS of 100 $mg \cdot g^{-1}$. Thus, 1 µL of undissolved thymol oil was cast on a 5 mm filter paper disc. In addition, a physical mixture of undissolved thymol and SiOH particles was prepared. In this case, first the SiOH pellet was prepared as mentioned above and then 1 µL of thymol oil was cast on it.

The antibacterial effect of the BDS systems were tested using conventional agar diffusion experiments according to standardized Kirby-Bauer procedure (HUDZICKI, 2009), against gram-negative (*Escherichia coli*) and gram-positive (*Staphylococcus aureus*) bacteria. Both strains were first pre-cultured on lysogeny broth (LB) agar plate at 37 °C for 24 h containing 1% $w \cdot v^{-1}$ tryptone, 0.5% $w \cdot v^{-1}$ yeast extract, 1% $w \cdot v^{-1}$ NaCl and 1.5% $w \cdot v^{-1}$ agar at pH 7.4. Cells were then cultivated in LB medium by inoculating one colony from pre-cultured LB-agar plates at 37 °C for 14 h until the optical density at 600 nm reached 0.5 (*ca.* 150 million cell$\cdot mL^{-1}$). For the diffusion tests the preparation consisted of 4 mm-deep Mueller-Hinton agar plates in a 100 mm petri dish containing 1.7% agar, 0.15% $w \cdot v^{-1}$ starch, 1.75% $w \cdot v^{-1}$ casein hydrolysate and 0.2% $w \cdot v^{-1}$ beef extract at pH 7.4. To inoculate the cells on the Mueller-Hinton plates, sterile L-shaped polypropylene cell spreaders were dip into the inoculum container and excess liquid was allowed to drain. Cells were then inoculated on the surface of Muller-Hinton plates by streaking the cell spreader evenly over the entire surface of the plate. The lid of the Petri dish was left open for 5 min to allow the surface of the agar plate to dry before placing the BDS discs. Plates were cultured for 24 h at 35 °C before examination. Halo intensity ratios and distance between unaffected growth and samples were calculated using the ImageJ software and used for discussion (FIGURE S2).

III.3 RESULTS AND DISCUSSION

III.3.1 MORPHOLOGICAL FEATURES AND EVALUATION OF BIOCIDE LOADING EFFICIENCY AND PAYLOAD IN BIOGENIC SILICA

The deposits of silicon in the cell walls of horsetail plant are naturally nanostructured (HOLZHUTER; NARAYANAN; GERBER, 2003), and they can be deconstructed into particles, the biogenic silica (FIGURE III.1c). It has been shown that the top-down route for isolation of biogenic silica particles results in a polydisperse dispersion (MATTOS; ROJAS; MAGALHÃES, 2016). Such polydispersity of biogenic silica could be reduced by simple size fractionation, via sequential sedimentation. In this case, the biogenic silica can be separated into sedimenting fractions with particle sizes of *ca.* 10 µm, a significant fraction of particles < 5 µm, and a colloidal fraction with particles with a predominant diameter of *ca.* 200 nm (FIGURE S3). The larger particles had a sedimentation rate of *ca.* 1 h, which indicated that they did not contain dense clusters of silica but a rather porous structure that was homogeneously distributed.

Across the range of particles composing the as-obtained dispersion, the $BSiO_2$ particles formed nano-architectures hierarchically organized from 8-10 nm primary units that assembled into 30-40 nm spherical aggregates, further associated into clusters with sizes from 200 nm to more than 10 µm. The $BSiO_2$ natural assemblies result in a self-similar architecture, FIGURE III.1a, experimentally confirmed in FIGURE III.1c. The specific surface areas (SSA) of unmodified, amino, and carboxyl-functionalized $BSiO_2$ particles, obtained by the Brunauer–Emmett–Teller multipoint model, were 325±2.5, 280±7.5 and 269±10.5 $m^2 \cdot g^{-1}$, respectively. Thus, the surface functionalization led to a marginal reduction in the SSA of $BSiO_2$, which is in agreement with previous reports on synthetically-modified mesoporous silica (JIAO et al., 2016; REHMAN et al., 2017; YI et al., 2015). Steric effects from larger moieties at silica surfaces are likely the main factor in the reduced SSA.

Amine and carboxyl groups on the surface of the biogenic silica were confirmed through XPS analyses (FIGURE S4). The electrostatic potential envelop of thymol at equilibrium conformation highlights a strongly polarized molecule with a shifted

quadrupolar moment, leading to delocalization of strong positive and negative areas. Thus, besides van der Walls and H-bonding, dipole-dipole and electrostatic interactions can take place between thymol with the native or modified silica (FIGURE III.1b).

FIGURE III.1 – SCHEMATICS (A) AND ELECTRON IMAGES (C) OF THE SELF-SIMILAR ARCHITECTURE OF BIOGENIC SILICA, AND THE EXPECTED INTERACTIONS BETWEEN SILICA AND THYMOL (B)

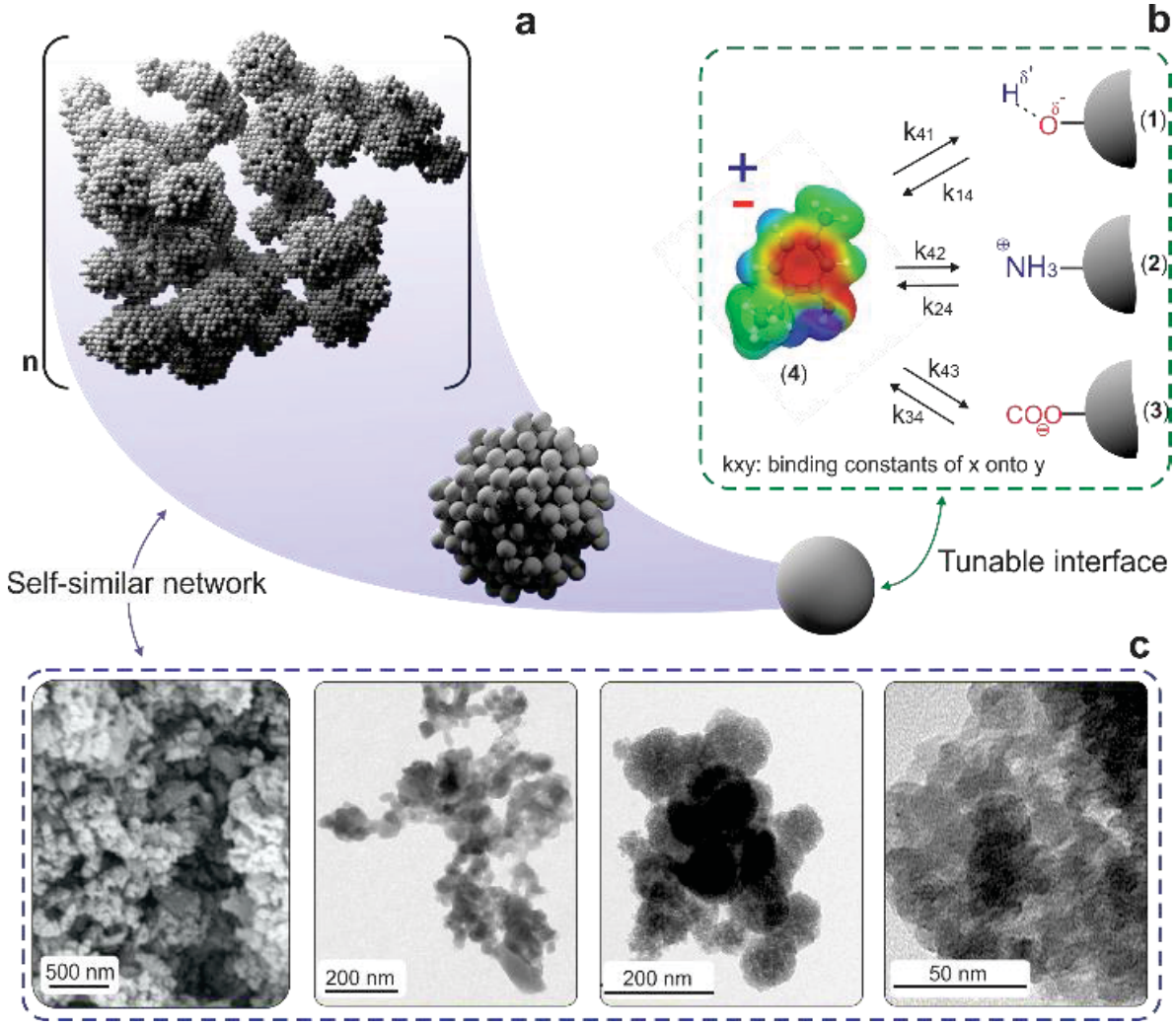

SOURCE: the author (2018).

The affinity of thymol with the various silica particles that were used as the stationary phase was first evaluated via thin layer chromatography (TLC). As a result of the poor water solubility of thymol, distilled water was not suitable to elute the oil (Rf = 0), regardless the type of silica stationary phase used. This emphasizes the need for loading

thymol in silica using an appropriate solvent, so that the cohesive crystal lattice energy that limits dissolution can be overcome and, thus, to obtain favorable release (ZHANG; CRESSWELL, 2016). Regarding organic solvents, the amino- and especially carboxyl-modified biogenic silica provided stronger interactions with thymol, as shown by the respective, comparatively lower thymol retention factors (FIGURE III.2a). In a typical TLC experiment, the eluting process is based on the competition between solvent and analyte for binding sites on the stationary phase, which occurs in terms of polarity similarity (REICH; SCHIBLI, 2006). A parallel can be directly drawn between TLC experiments and a system consisting of biogenic silica particles dispersed in thymol solution. The polarity of the solvent was fundamental for loading (FIGURE III.2b) or quantifying thymol on the different carriers. The strong affinity of thymol to polar solvents, in this case ethanol, allowed to effectively quantify its payload in the BDS. Indeed, a significant amount of thymol could be freed from the silica in ethanol. On the other hand, the non-polar n-hexane was able to dissolve thymol, but promoted spontaneous thymol loading on silica (FIGURE III.2b). The dynamic biocide loading capacity (maximum releasable payload) of the $BSiO_2$ particles varied from 70 to 50 $mg \cdot g^{-1}$, a similar range was reported for synthetic mesoporous silica nanoparticles with much higher surface area (up to 1000 $m^2 \cdot g^{-1}$) (POPAT et al., 2012a; WANYIKA, 2013; YI et al., 2015). Thus, the remarkably high loading capacity of biogenic silica is derived from its high-percolating fractal architecture.

Compared to the thymol loading in the unmodified $BSiO_2$ (SiOH@Thy), the dynamic biocide payload (extractable) was lower for the functionalized biogenic silica particles ($SiNH_2$@Thy and SiCOOH@Thy, FIGURE III.2b); however, the total payload was higher in these latter cases. The peak of thermal degradation of free thymol occurred at 160 °C (FIGURE III.2c and 2d) and thermal degradation of the functional groups on the biogenic silica (modified and unmodified) occurred above 200 °C (FIGURE S5). Therefore, the total thymol loading could be estimated by heating 100 mg of all three types of dried BDS at 200 °C for 24 h. All the mass loss in this procedure was attributed to thymol. By this method, the total amount of biocide loaded in the BDS was estimated to be 82.5, 99.5 and 119.0 $mg \cdot g^{-1}$ for SiOH@Thy, $SiNH_2$@Thy and SiCOOH@Thy, respectively. The extractable and the actual amount of thymol loaded in the unmodified carrier were similar (75 and 82.5 $mg \cdot g^{-1}$, respectively, 9.3% of non-released thymol in

EtOH); however, for the functionalized particles, the difference between the loaded and the releasable biocide increased by 63 and 83% for the amino- and carboxyl-modified $BSiO_2$ particles, respectively. The lower Rf of thymol on the SiCOOH carrier is indicative of strong interactions between the components.

FIGURE III.2 – RETENTION FACTOR (RF) OBTAINED FROM THIN LAYER CHROMATOGRAPHY EXPERIMENTS USING SIOH, $SINH_2$ AND SICOOH AS STATIONARY PHASES (A). ISOTHERMS FOR THYMOL ADSORPTION AT 25 °C ON THE BIOGENIC SILICA CARRIERS, SIOH, $SINH_2$ AND SICOOH (B). TG (C) AND DTA OF THYMOL ADSORBED ON $BSIO_2$

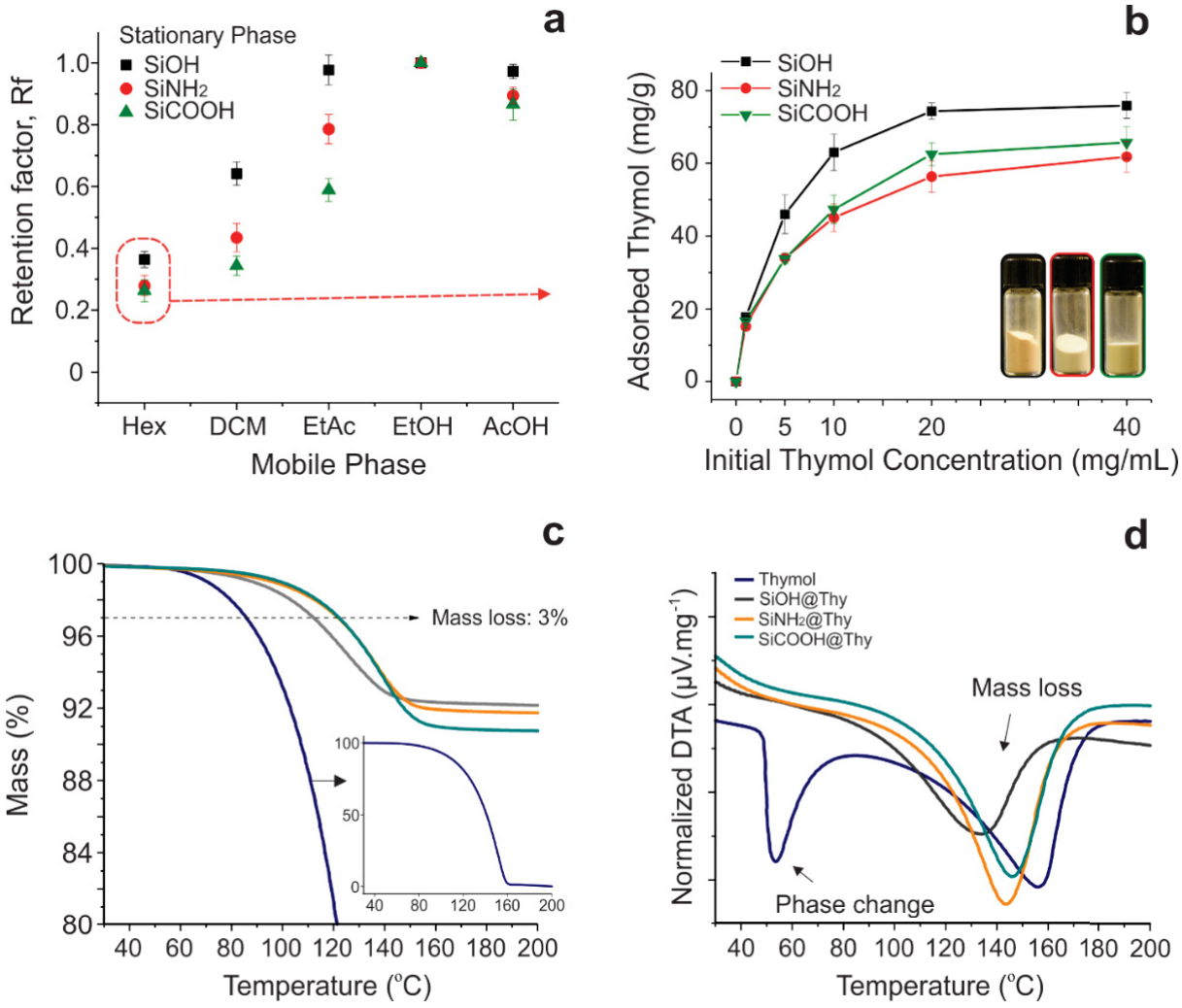

SOURCE: the author (2018).

Interestingly, the thermal stability of thymol significantly increased when it was loaded on silica. Compared to its free form, the temperature for the initial mass loss of

thymol loaded in unmodified $BSiO_2$ shifted from 85 to 110 °C (FIGURE III.2c). This temperature was even higher, 120 °C, when loaded in the functionalized particles. However, thymol absorbed on biogenic silica displayed a DTA peak corresponding to mass loss that shifted toward lower temperatures; meanwhile, the peak corresponding to phase change could not be observed (FIGURE III.2d). This indicates that thymol adsorption on all the carriers occurred with a strength that is beyond physical interactions. No phase change occurred as expected for the free oil molecules. Specifically, for free thymol, latent heat is required firstly to produce phase change from crystal to liquid (oil), then to break its cohesive energy and to promote volatilization/degradation. It is speculated that in a BDS, the thermal energy is only consumed to volatize/decompose the adsorbed thymol, which results in the shift toward lower temperatures. Moreover, the observed temperature shift was smaller in the case of the modified particles, indicating that a higher energy is required to overcome the silica-thymol interactions prior to degradation/volatilization. More specifically, the mass loss prior to volatilization of thymol adsorbed on silica (prior to the mass loss peak) occurred at lower temperature for unmodified silica, followed by higher temperatures in the case of amino- and carboxylic acid-functionalized silica. This further highlights that the strongest affinity of thymol is for carboxylic acids, followed by those with amine and with hydroxyl-surfaces.

III.3.2 CHARACTERIZATION OF THE $BSIO_2$-THYMOL BASED BDS

The FT-IR spectrum of the unmodified biogenic silica particles presented characteristic peaks at 1650 and 800 cm^{-1}, which are related to different vibration modes of the hydroxyl bonds in silica. The peaks at 1100 and 460 cm^{-1} correspond to the asymmetric stretching and bending vibration of Si-O-Si group, respectively (JIA et al., 2015). The region at *ca.* 2935 cm^{-1} (FIGURE S6) refers to the multiple arrangements of C-H stretching vibration in amine and carboxyl-functionalized silicas. Low intensity peaks appeared at 1705 and 1565 cm^{-1} for the SiCOOH carrier corresponding to the stretching vibration of the C=O from the carboxylic acid and amide groups, respectively. The mid-IR fingerprint for thymol comprises the wavenumber between 900 and 1400 cm^{-1}. In this region, characteristic, key peaks for thymol appear at 945, 1087 and 1290 cm^{-1} (SCHULZ;

QUILITZSCH; KRÜGER, 2003). In addition, characteristic peaks for aromatic rings corresponding to C-C=C symmetric and asymmetric stretch vibration at 1585 and 1460 cm^{-1}, respectively, were also useful to identify thymol in the BDS (PING et al., 2012).

The peaks related to thymol chemical structures are more defined in the SiCOOH@Thy spectrum. This result corroborates with data from thermal analyses (FIGURE III.2c and 2d) and the apparent surface chemical composition obtained via XPS FIGURE III.3d). These peaks are also observed for SiOH@Thy and SiNH2@Thy systems, but with a lower intensity (FIGURE III.3b). The spectrum of the SiCOOH@Thy sample also showed an increase in intensity of the peak at 1708 cm^{-1}, which is related to C=O stretching. Also, this peak was observed at a slightly more delocalized wavenumber than it observed from the carboxyl-based carrier. Hypothetically, ester bonds could have occurred between carboxylic acid termination of the silica surface and hydroxyl groups from thymol (HONG, 2015; MARTINI et al., 2014). The formation of this bond partially explains the higher stability of thymol on the SiCOOH carrier; however, it is important to emphasize that the amide groups present in SiCOOH could form strong H-bonds with thymol, which could also contribute to an enhanced thymol stability.

The proposed carbon-oxygen interactions between SiCOOH and thymol also appeared in the C1s high-resolution XPS spectra of the SiCOOH@Thy (FIGURE III.3c and 3d, FIGURE S7). The C1s XPS spectrum had a peak at 285 eV, corresponding to C-C and C-H moieties (BEAMSON; BRIGGS, 1993). Contributions at higher binding energies (increase by *ca.* 3.5 eV) usually appears as shoulders and are associated to carbon-oxygen interactions (BEAMSON; BRIGGS, 1993). The carboxyl groups originally presented on the modified silica carrier contributed to the C_{1s} spectra as an important component appearing as a shoulder at 288.5 eV. The C=O contribution in the carboxyl-based BDS appeared at different binding energy (287.5 eV), which indicate that the interaction between COOH termination and thymol can result in the formation of different carbon-oxygen interactions.

FIGURE III.3 – FTIR SPECTRA OF THE BIOGENIC SILICA CARRIERS (A) AND PREPARED BDS (B). C1S HIGH-RESOLUTION XPS SPECTRA OF THE UNMODIFIED AND MODIFIED PARTICLES (C) AND THE $BSIO_2$-THYMOL BASED BDS (D) WITH DETAIL OF THE APPARENT CARBON COMPOSITION AT THE BDS AND CARRIERS SURFACE. ZETA POTENTIAL OF THE SILICA SURFACE BEFORE (E) AND AFTER THYMOL LOADING (F) AS A FUNCTION OF PH

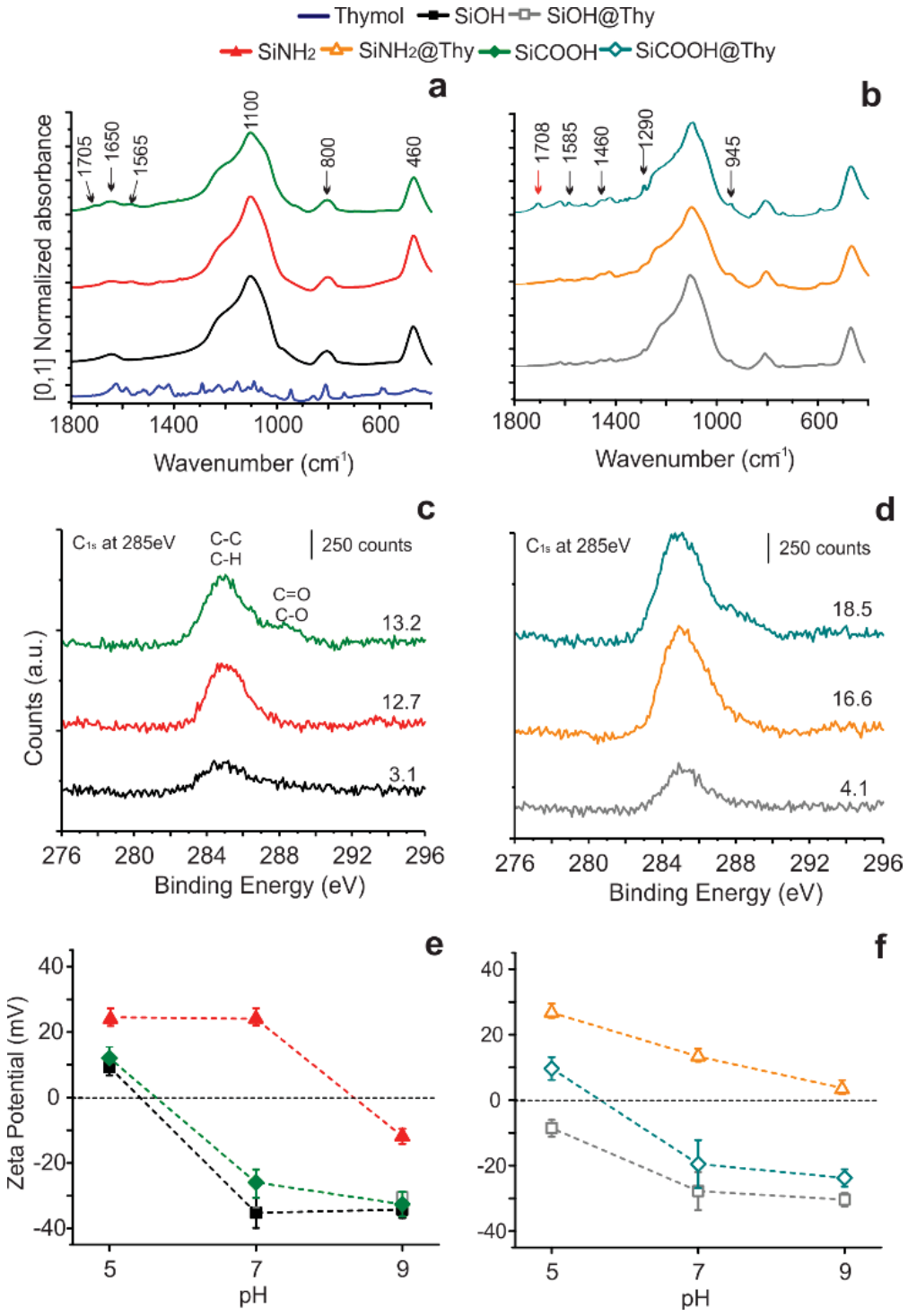

SOURCE: the author (2018).

The apparent carbon composition at the surface of the BDS, measured through XPS, corroborated the higher stability of thymol on BDS prepared with the functionalized particles (FIGURE III.3c and 3d). Nevertheless, thymol, as a phenolic monoterpene, is volatile (JANATOVA et al., 2015) and therefore the XPS quantification of thymol on the surface is compromised because the high vacuum needed for analysis. This can be expected to accelerate thymol volatilization, unless it strongly interacts with the surface. For instance, the disparity between the thymol content quantified in the SiOH carrier after its extraction (FIGURE III.2b) and XPS confirms this hypothesis. Thus, SiOH@Thy has a high thymol payload, but in this system the biocide is less stable than in the functionalized particles.

All carriers showed negative zeta potential at pH 9, while at acid and neutral pH the zeta potential varied according to the surface chemistry of the particles (FIGURE III.3e). Both SiOH and SiCOOH carriers presented an isoelectric point (IEP) between pH 5 and 6, while the $SiNH_2$ carrier had an IEP between pH 8 to 9. IEP and zeta potential as a function of pH results from the contributing charged groups on the silica surface. The differences observed for the IEP and zeta potential are attributed to the specific mechanisms of (de)protonation of the silanol, carboxyl and amino groups. Protonation of the amines seem to occur between pH 8 and 9 whereas deprotonation of the COOH groups would occur between pH 5 and 7.

After thymol loading, the zeta potential of the resultant BDS clearly shifted toward zero for all particulate systems. It means that both positive and negative charges at the silica surface were partially shielded by adsorption of the uncharged thymol. As it is shown, thymol presents both positive and negative electrostatic potential and is highly polar in nature (FIGURE III.1b). The zeta potential of the cargo and its carrier as well as the resultant BDS has significant implications to the responsiveness of the delivery, especially over pH changes (POPAT et al., 2012b).

III.3.3 BIOCIDE RELEASE PROFILES AND KINETICS CONSIDERATIONS

The prepared BDS were designed to control thymol dissolution in water by tailoring the carrier-biocide interactions. The release profiles behave similarly, regardless the size fractions of the carrier particles (from very large sedimenting particles to colloidally stable particles, FIGURE S8). This highlights that the self-similar nanostructure of the particles is a key feature of this biogenic silica-based BDS. In all release profiles, thymol releases from the carrier through two different stages: initial burst stage, observed in the first 24 h, followed by a slow-release stage, from 24 to 350 h (FIGURE III.4a). Equilibrium was not achieved for none of the BDS, at least during the observation time of 350 h, suggesting that controlled release may occur for even longer times. $SiNH_2$@Thy and SiCOOH@Thy systems released significantly lower amounts of thymol, which is a result of their stronger carrier-biocide interactions (FIGURE III.2 and FIGURE III.3). The initial burst release is attributed to the thymol sequential layers over its first layer on the silica surface. Considering thymol molecular size as well as the results observed from XPS analyses (FIGURE III.3c and 3d), the adsorbed amount of thymol was likely to result in multiple layers of thymol being adsorbed.

Several kinetic models often applied to describe cargo delivery (LIU; ZHANG; ZHANG, 2015; MATTOS et al., 2017d; MATTOS; MAGALHÃES, 2017; XU et al., 2017; YI et al., 2015) were assessed to fit experimental data from thymol release experiments (TABLE S3). The initial concentration of thymol in the release media was considered zero, and that only desorption occurred, thus simplifying the integrated form of the equations. The Elovich kinetic model fitted the thymol release profile very well (coefficient of determination over 0.96, TABLE S3). Elovich's fit highlights that thymol delivery follows a logarithmic, time-dependent, decay. This means that the differential amount delivered over time (determined by *k*) decreased proportionally to the amount released in previous stages. This mechanism is a result of the fractal network of the carrier that allows fast solvent (water) diffusion into and out of the carrier. In this condition, the thymol in the more exposed (outer) regions of the carrier is released promptly, while the thymol located in the inner regions of the carrier is released with more difficulty. It is speculated that over

the release time, the amount of thymol along the carrier cross-section became more homogeneous; thus, the release rate decreased due to a slower diffusion.

FIGURE III.4 – THYMOL RELEASE PROFILES UNDER REGULAR AQUEOUS MEDIA CONDITIONS (25 °C, pH 7, NaCl 0.5%) (A). RELEASE RATE COEFFICIENTS OF THE THYMOL OVER TEMPERATURE (B), pH (C) AND SALINITY (D) CHANGES

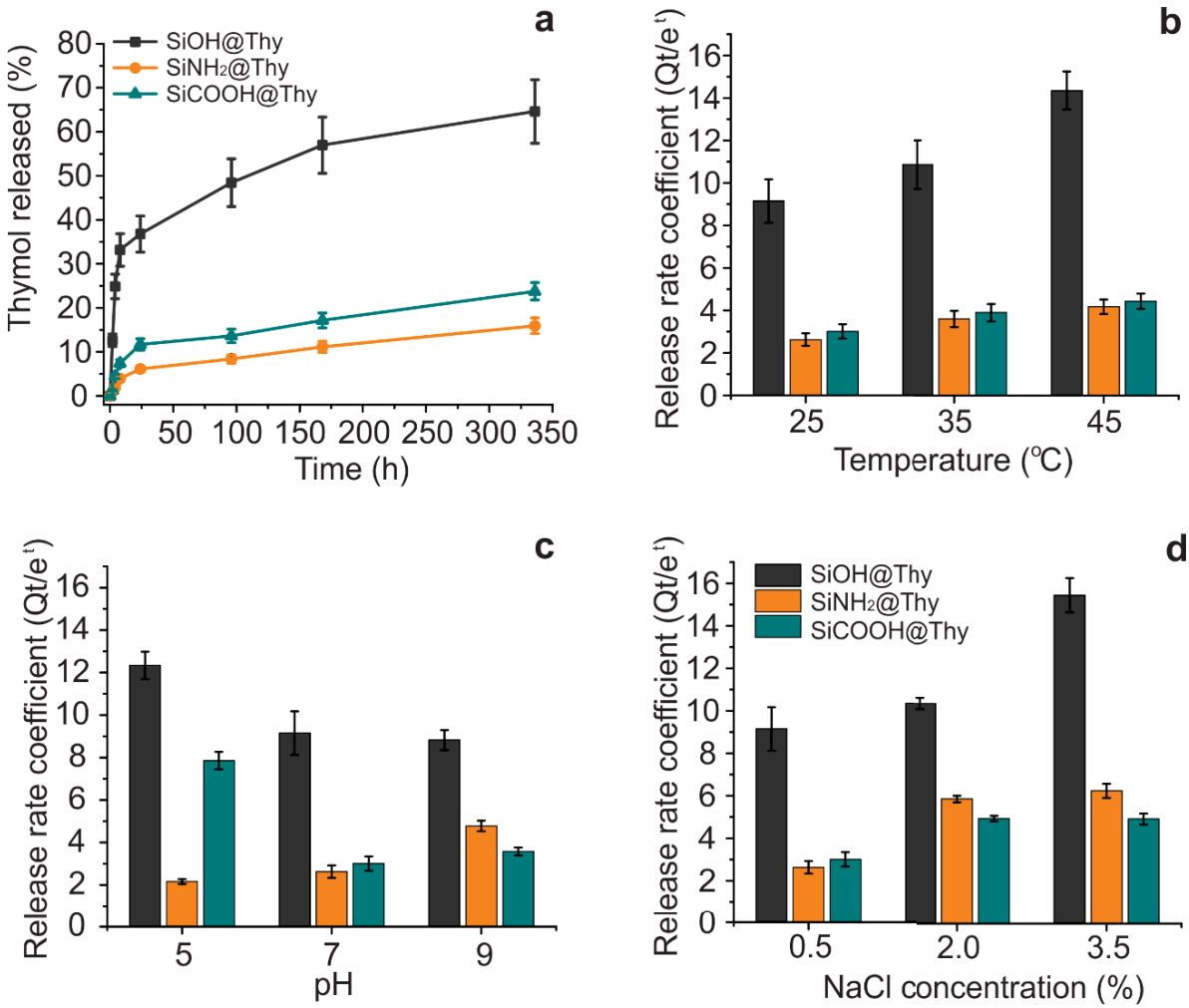

SOURCE: the author (2018).

The release rate coefficient, *k*, was determined from the slope of the Elovich linearized plot (FIGURE S9b). *k* was used to investigate the responsiveness of the BDS over pH, temperature and salinity (FIGURE III.4b, 4c, and 4d). Overall, at regular conditions (25ºC, pH 7, NaCl 0.5%), the release rate was three-fold higher in the SiOH@Thy system than in the BDS prepared with functionalized particles. By using

carrier mixtures, the delivery rate can be change and allow even finer tuning of the release dynamics. This is illustrated in FIGURE S9a for the theoretical release rate obtained from mixtures of SiOH@Thy and $SiNH_2$@Thy.

The release rate of thymol from all prepared BDS increased as the temperature increased (FIGURE III.4b). The effect of temperature, in terms of percentage variation, was higher for $SiNH_2$@Thy, followed by SiCOOH@Thy and SiOH@Thy. The $k_{45°C}/k_{15°C}$ ratio was 2.47, 1.86 and 1.55, respectively. An additional release profile at 15 °C was carried out in order to precisely obtain the activation energy, which was calculated to be 350, 235 and 125 $J \cdot mol^{-1}$ (FIGURE S9c).

The pH plays an important role in the release rate of thymol (FIGURE III.4c). When considering principally electrostatic interactions, the variations in the release rate observed at various values of pH can be understood considering that thymol is a phenolic molecule with an acid dissociation constant pKa of *ca.* 9. The release rate of the SiOH@Thy system became slower in a pH range where the particles presented a net negative charge (FIGURE III.3f), suggesting that the Si-OH surface, below pH 7, leads to faster release when compared with $Si\text{-}O^-$. In the BDS prepared with the amine-functionalized particles, the protonation of the NH_2 to NH_3^+, below pH 9, was essential to understand the behavior of *k* over pH changes. At pH 5 the NH_3^+ (carrier) and OH (biocide) did not interact, leading to the fastest release. Meanwhile, the NH_3^+ and O^- (pH 7) contributed to the slowest release because of the several interactions that can occur in these conditions (FIGURE III.1b). At pH 9 a weak interaction driven by NH_2 and O^- from the carrier (negative zeta-potential) occurred, resulting again in a faster release. Regarding the SiCOOH@Thy system, the release rate at pH 7 and 9 were similar, due to negative charge at the carrier surface and biocide. Looking only at electrostatic interactions, it was not expected much higher release rate at pH 5, since COOH and OH interaction is as weak as COO^- and O^-. However, acid media could act as a catalyst for hydrolysis of ester bonds, which hypothetically could have occurred between thymol and the SiCOOH carrier (HONG, 2015; MARTINI et al., 2014). Considering this to be true, it is proposed that the highest release rate of thymol from the SiCOOH@Thy system would be at pH 5, which was the experimental observation. In the discussion of the effect of pH

on release rate it is principally indicated the stronger, electrostatic interactions but other interactions such as van der Walls and H-bonding may play important role as well.

Salinity, like temperature, increased the release rate for all the carriers with the most significant effect being that of the release rate from $SiNH_2$@Thy (FIGURE III.4d). When the salinity is systematically increased, from 0.5 to 3.5% of NaCl, the release rate coefficient for $SiNH_2$@Thy increased by up to 2.5 times and up to *ca.* 1.6 times for the SiOH@Thy and SiCOOH@Thy systems. The strong effect of the ionic strength on the thymol release from the amine-based BDS, indicates that at the carrier-biocide interaction was strongly driven by electrostatic interactions. On the other hand, the less marked effect of ionic strength on the release rate in the SiOH@Thy and SiCOOH@Thy systems suggests that the carrier-biocide interactions were not only driven by electrostatic effects but also by van der Walls, short-range dipole-dipole (*e.g*. through quadrupole) and multiples H-bonding interactions.

III.3.4 BIOLOGICAL ACTIVITY OF BIOGENIC SILICA BASED BIOCIDE DELIVERY SYSTEM

The biocidal activity of the prepared BDS was assessed against *Escherichia coli* (gram negative) and *Staphylococcus aureus* (gram positive). The activity of free thymol against these organisms was previously reported (MARCHESE et al., 2016) and confirmed in this study (FIGURE III.5). The agar diffusion tests allowed us to qualitatively assess the bioactivity of the obtained BDS (FIGURE III.5a) and to highlight a higher activity than that of neat thymol.

Three well-defined zones of bacterial growth were observed in the agar diffusion plates for *S. aureus* (FIGURE III.5a) and *E.coli* (FIGURE S10). In order to provide more quantitative insights, it was measured the distance of the halo and calculated the ratio between the halo intensity of all three zones. The first zone corresponded to areas where the bacteria growth was not inhibited by the biocide, FIGURE III.5a(1). An intermediate region was identified for the SiNH2@Thy and SiCOOH@Thy pellets for both *S. aureus* and *E.coli* plates. The contrast in this zone was not strong, which corresponded to partially inhibited growth of bacteria FIGURE III.5a(2). The third region corresponded to complete

inhibition of bacterial growth, which could be easily identified for BDS specimens as no bacterial growth could be observed in this region, FIGURE III.5a(3). In contrast, free thymol oil or thymol physically mixed with silica presented a greater diameter of partial inhibition. Importantly, neither free thymol nor thymol mixed with silica completely inhibited bacterial growth. The same contrast in the partially inhibited zone (2) of BDSs were observed for both controls.

FIGURE III.5 – RESULTS OF TYPICAL AGAR DIFFUSION TESTS USING *Staphylococcus aureus* PLATES TREATED WITH THE BDS AND CONTROLS (A). LENGTH OF THE BACTERIA-FREE ZONE MEASURED IN PIXELS FOR BOTH *S. aureus* (GRAM +) AND *E. coli* (GRAM -) (B). RATIO BETWEEN HALO INTENSITY OF THE ZONE COLONIZED BY BACTERIA AND BACTERIA-FREE ZONE OF THE *S. aureus* (C) AND *E. coli* (D) PLATES

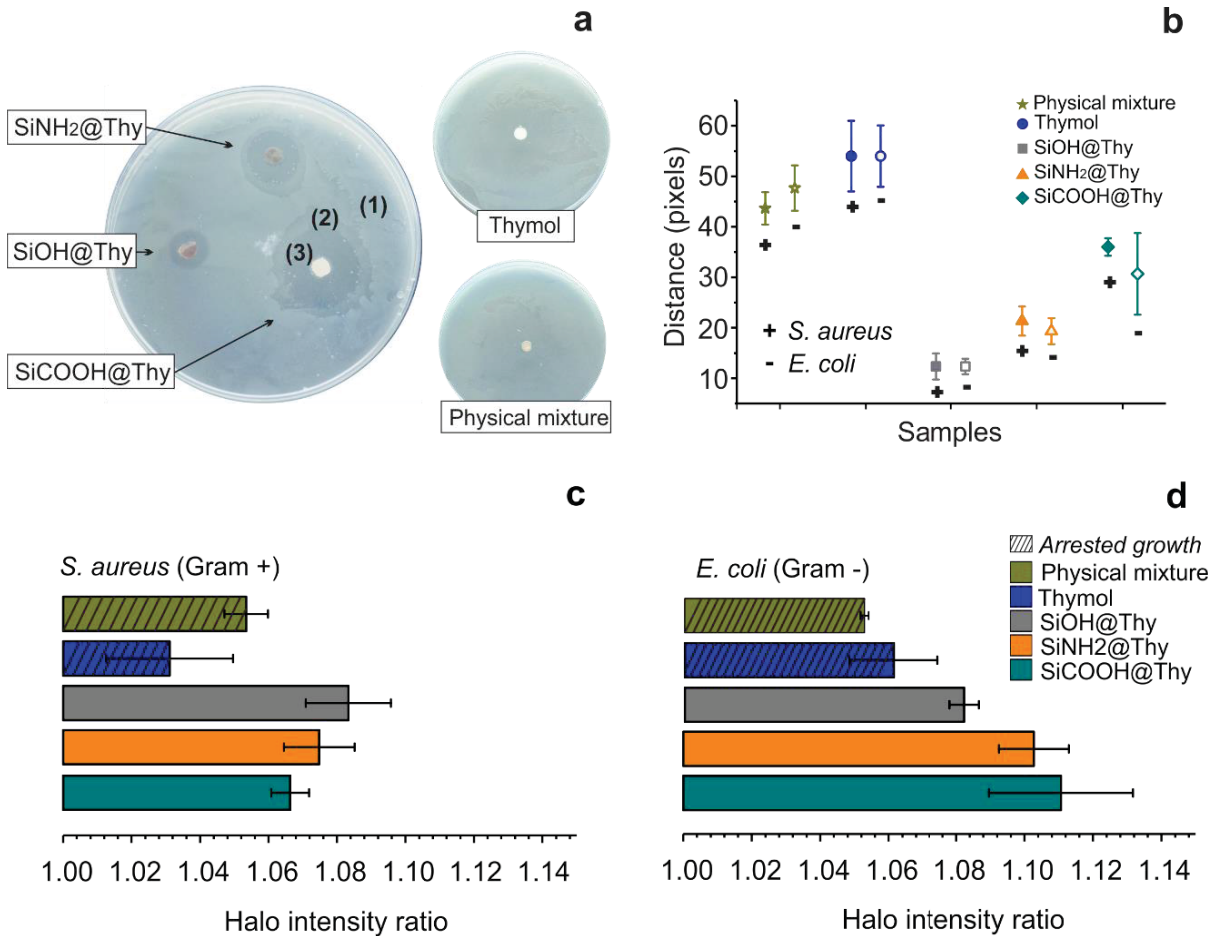

SOURCE: the author (2018).

The average halo intensity ratio for the control samples showed values ranging from 1.01 to 1.06 for the *S. aureus* plates and 1.05 to 1.075 for *E. coli* plates. As a

comparison, the same ratio for the various BDS achieved values ranging from 1.07 to 1.09 and 1.08 to1.11 for *S. aureus* and *E. coli* plates, respectively. Compared to its application in nanostructured BDS, thymol was less active in its free form. The physical mixture of thymol oil and unmodified silica further corroborated the improvement of thymol bioactivity through molecular adsorption on the nanostructured silica carrier. By doing so, the availability of the biocide was enhanced, thus improving a sustained biocidal activity. Among the BDS tested, a higher activity (higher ratio and distance) was noted, as expected for those with higher thymol loading, SiCOOH@Thy and $SiNH_2$@Thy. From this result, it was noticed that the biological activity of thymol may be also attributed to the molecules that were observed not to be delivered in the release conditions reported in FIGURE III.4, *i.e.,* the fraction of thymol strongly tethered on the carrier surface. Thus, even the BDS with a low biocide release performed best at controlling bacterial growth.

III.4 CONCLUSIONS

Biogenic silica carriers were used to support large thymol loadings that take advantage of a complex (fractal) structure, which afforded controlled and tailorable release. The biocide payload in the biogenic silica is comparable with mesoporous silica (*ca.* 100 mg per g of carrier), even considering specific surface areas twice higher for the last. The high accessibility of the surface area in such self-similar network was key to this achievement. Here, biocide delivery systems (BDS) that used thymol as model compound were shown as suitable and inexpensive platforms to obtain biocide dynamic loading and release. This was accomplished by tuning the surface charges on the biogenic silica upon functionalization with amine and carboxyl groups. Amine and carboxyl groups promoted stronger interactions between carrier and biocide, resulting in controllable and responsive release as well as higher thermal stability and localized antibacterial activity. Such systems are relevant for large-scale applications and show promise beyond the performance measured for neat or free biocide forms

CHAPTER IV

FORMATION OF SUPER-ROBUST SUPRAPARTICLES FROM BIOGENIC SILICA FOR CONTROLLED RELEASE, CARGO PROTECTION AND TOXIC HAZARDS PREVENTION

IV.1 INTRODUCTION

Biocides are crucial molecules for the protection of several biosystems; however, residual toxic molecules have been found in food, soil and ground water (AKTAR; SENGUPTA; CHOWDHURY, 2009). Looking for safer biosystems, on-demand release strategies have been investigated aiming at the replacement of the traditional biocides (MATTOS et al., 2017a). Nanotechnology offers new possibilities for delivering biocides in a controlled and responsive manner to combat pests in very specific conditions. Engineering biocides at the nanoscale is a promising approach to achieve sustainability, as their increased bioactive surface area promotes higher efficiency and more localized action (MATTOS et al., 2017a). The enhanced bioactivity in association with controlled delivery allow the use of reduced amounts of toxic molecules in those biosystems where biocides are mandatory. Whereas this approach can be used to reduce the concentration of toxins in food, soil and ground water, there is a concern about the bioaccumulation of nanomaterials (JUDY; BERTSCH, 2014; RICO et al., 2011) which limits their application for crop protection. The risks coming from the accumulation and fate of nanomaterials in the environment are not fully understood (COLVIN, 2003; SERVIN; WHITE, 2016), but institutions as the REACH (EU Regulation on Registration, Evaluation, Authorization and Restriction of Chemicals) and ECHA (European Chemical Agency) in Europe, as well as the FDA (U.S. Food and Drug Administration) and EPA (Environment Protection Agency) in North America, have started efforts to assess and manage potential risks, limits of exposure, best practices of handling and disposal, and regulatory actions of nanomaterials (PARISI; VIGANI; RODRÍGUEZ-CEREZO, 2014; RAUSCHER; RASMUSSEN; SOKULL-KLATTGEN, 2017).

The concerns on the use of nanomaterials for crop protection derive from the extensively discussion about the ability of plants to uptake nanoscaled structures (MA et al., 2010; RALIYA et al., 2016; TORNEY et al., 2007; ZHU et al., 2008). The major restrictions stand against the use of nanomaterials in edible plants or cereals once these internalized particles could be directly transferred to the processed food (RALIYA et al., 2016; ZHU et al., 2008). Even though, the internalization routes vary among plants the size of the nanostructure is a very important limiting factor (MA et al., 2010). For instance,

particles sizing up to 100 nm can be easily internalized and transported in plants directly through the stomatal opening (RALIYA et al., 2016). In addition, the vesicle's size during the plant endocytosis can reach 3 μm being able to internalize multiple nanoparticles (TORNEY et al., 2007) or even micrometric-scaled particle. In parallel, nanoparticles are a direct risk to workers as they can be easily inhaled (KREYLING et al., 2009; NEL, 2005; SUNG et al., 2008) or up taken through the skin (NEL et al., 2006; RANCAN et al., 2012), leading to serious health conditions.

For a less problematic and easier-to-handle delivery system to apply in agriculture, carriers with significantly larger sizes are desirable. The self-assembly of nanoparticles into superstructures is the best approach to combine in the same delivery system the intensified interface interactions and high loading capacity that come from the nanolevel (MATTOS et al., 2017a), with the reduced bioaccumulation capacity and non-targeted effects of macroscaled materials. Superstructuring has been recognized as an excellent tool to address current challenges in several fields of science, such as photonics (HAYWARD; SAVILLE; AKSAY, 2000), sensing (CECCHINI et al., 2013), energy storage (MAGASINSKI et al., 2010) and biomedicine (WANG et al., 2014). Nonetheless, superstructuring is the key to achieve sustainability in crop protection. Non-photostable biocides, *e.g.* emerging biopesticides (NURUZZAMAN et al., 2016), can be protected against light if loaded inside millimetric scaled carries. In parallel, millimetric particles have lower mobility when compared to nanoparticles and therefore reduced bioaccumulation capacity. Approaches using superstructured biocide delivery systems are win-win situations, where both environment and biocide would be protected.

Herein, it was introduced a versatile assembly of nanostructured bio-based materials into millimetric superstructures that are intended to be used as biocide delivery carriers aiming at more sustainable agriculture. Biogenic silica was used as building block and cellulose nanofibrils as a cohesive material of the superstructure (FIGURE IV.1). The high specific surface area of the biogenic silica particles (*ca.* 350 $m^2 \cdot g^{-1}$) (CARMONA et al., 2013; MATTOS et al., 2017c), as well as the high aspect ratio and branched features of the cellulose nanofibrils (ZHANG et al., 2013) make them the perfect combination to prepare highly porous and robust superstructures. It is shown how these two bio-based nanostructures can be versatile assembled into superstructures of tuned sizes and

shapes, tethering the biocide release rate and patterning the profiles. It is also shown alternative methodologies for pre- or in situ- loading cargo into superstructures, which has been limited to post loading steps (WANG et al., 2014). Thymol was used as a model biocide as it is a simple molecule that represents an easy and precise analytical characterization; however, the one can see that any cargo could be used. In addition, the low photostability of phenols (CHOWDHURY; NAG; RAY, 2017; NURUZZAMAN et al., 2016; TUREK; STINTZING, 2013) allowed us to experimentally investigate the existence of photodegradation considering its loading in nano or supraparticles. Light transmission measurements were used to theoretically approach the amount of thymol protected from photodegradation as a function of size of the superstructure. Lastly, the mobility of nano and supraparticles in soils were studied in order to show how supraparticles can be a safer carrier to delivery agrochemicals without deep penetration into soil and contamination of groundwater.

FIGURE IV. 1 – SUPRASTRUCTURING AS AN EFFICIENT STRATEGY TO REDUCE BIOACCUMULATION OF NANO- AND MICROPARTICLES IN SOIL AND GROUNDWATER

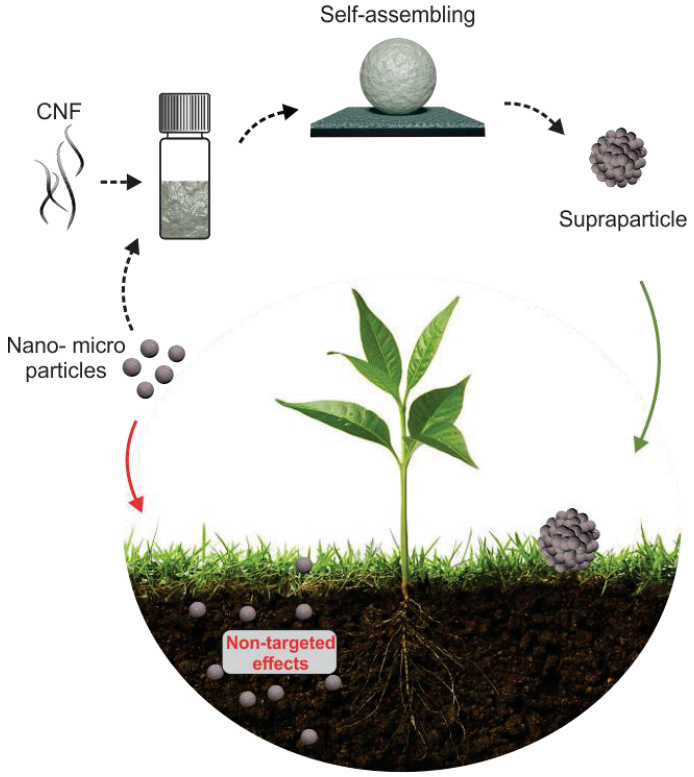

SOURCE: the author (2018).

IV.2 MATERIALS AND METHODS

IV.2.1 MATERIALS

The primary building blocks, biogenic silica particles ($BSiO_2$), were isolated from *Equisetum arvense* (horsetail) following the biorefining procedure previously described in CHAPTER II. Cellulose nanofibrils (CNF), used as the cohesion material for the superstructure assembly, were prepared by microfluidizing bleached sulfite hardwood (birch) fibers, as described in Guo et al. (2016). Thymol (CAS: 89-83-8) was purchase from Sigma-Aldrich and used as a model biocide.

IV.2.2 GENERAL ASSEMBLY OF THE $BSiO_2$-CNF SUPERSTRUCTURES

The $BSiO_2$ particles were dispersed in deionized water with a particle concentration of 20 wt.%, then tip ultrasonicated to form a suspension. The initial CNF suspension was prepared at 1.5 wt.% of solids. Both suspensions were diluted into another flask to achieve a fixed total solid content of 10% and different $BSiO_2$-to-CNF ratios. The $BSiO_2$-CNF dispersions were homogenized through vortex-ultrasound cycles. Aliquots, ranging from 5 to 20 µL, of the $BSiO_2$-CNF dispersions were cast in a flat, superhydrophobic substrate placed on a hot plate (60 ^{o}C). The droplets were left to dry for the assembly of the bio-based nanostructures into spherical superstructures.

IV.2.3 PREPARATION OF SUPERSTRUCTURES WITH DIFFERENT MACRO MORPHOLOGIES

Spheres, films and cylinders were prepared to investigate the effects of the "external" surface area on the release rate of the biocide. Three different substrates were prepared to simple assembly of differently-shaped superstructures (FIGURE S11). Spheres were obtained by casting the precursor dispersion on a flat superhydrophobic substrate, which was prepared by coating a cleaned glass slide with Teflon particles

(diameter *ca.* 30 µm) using a double-sided bonding tape (FIGURE S11a). The films were prepared by casting the precursor solution on a cleaned glass slide (FIGURE S11b). For the cylinders, a duct-like superhydrophobic template was prepared. First, a polymer template was prepared and then a superhydrophobic commercial formulation was sprayed on the template. The distance between the template walls was 1 mm (FIGURE S11c).

IV.2.4 METHODOLOGIES FOR THYMOL LOADING INTO THE SUPERSTRUCTURES

Three routes were used to load the thymol molecules in the superstructures: post, pre and in situ loading. Post-loading: supraparticles (50 mg) obtained as described in the general assembly were incubated for 24 h in 5 mL thymol solution in n-hexane (20 $mg \cdot mL^{-1}$). After, the thymol solution was removed and the supraparticles were dried at 80 ^{o}C for 4 h. Pre-loading: $BSiO_2$ building blocks were firstly loaded with thymol following the procedure described in the CHAPTER III. Briefly, 200 mg of particles were incubated for 24 h in 20 mL thymol solution in n-hexane (20 $mg \cdot mL^{-1}$), followed by centrifugation (2000 rpm for 2 min), and drying (80 ^{o}C for 4 h). The thymol-loaded building blocks were combined with CNF and used to assembly the SPs following the general assembly. In situ-loading: This procedure is slightly different from the general assembly. The same steps were followed, but 50 µL of water were replaced by 50 µL of a thymol ethanolic solution at 100 $mg \cdot mL^{-1}$ of concentration. The amount of thymol was calculated to be *ca.* 100 $mg \cdot g^{-1}$ (CHAPTER III), and the volume of ethanol was kept to a minimum.

IV.2.5 CHARACTERIZATION OF THE SUPERSTRUCTURED BIOCIDE DELIVERY SYSTEMS

The quantification of the thymol loaded in the superstructures was carried out by following the procedure described in the CHAPTER III. Briefly, 5-10 mg of SPs was extracted with 10 mL of absolute ethanol, then the concentration of the ethanolic thymol solution was measured at 275 nm using a UV calibration curve (FIGURE S1). The morphological features of the supraparticles were analyze in a field emission scanning

microscopy (SEM, Zeiss Sigma VP, Germany) using an acceleration voltage of 1.6 kV. The samples were firstly coated with 3 nm platinum layer. The compression strength of the SP was evaluated using a dynamic mechanical analysis instrument (Q800 from TA instruments). The compression rate was set to 4 $N \cdot min^{-1}$ and the acquisition rate was 1 s per point.

IV.2.6 BIOCIDE RELEASE PROFILES AND KINETIC CONSIDERATIONS

The thymol release profiles were obtained using deionized water at NaCl 0.5% $w \cdot v^{-1}$ of electrolyte concentration, pH 7 and 25 ^{o}C. Thymol-loaded superstructures (*ca.* 150 mg) obtained from different loading methods, CNF ratios, sizes and shapes were individually submerged in deionized water (1 L). Then, superstructures weighing *ca.* 10 mg were removed at fixed time intervals, from 0 to 160 h, and the amount of not-released thymol was extracted with absolute ethanol and quantified via UV calibration curve. The release profile data were acquired using triplicates.

Several kinetic models were applied in the experimental data looking for the best fitting. The Elovich kinetic model (CHIEN; CLAYTON, 1980) led to the highest coefficients of determination, allowing the evaluation of the release rate as a function of a single parameter (*k*).

IV.2.7 PHOTODEGRADATION STUDIES

$BSiO_2$-CNF films with different thicknesses, but CNF concentration fixed at 5%, were assembled on a quartz substrate. The thickness of the films was controlled by limiting the casting area, and using $BSiO_2$-CNF dispersions with different solid fractions (from 1 to 10% $w \cdot v^{-1}$). The thickness of the films was accessed using a digital caliper or an optical microscope. An UV-Vis spectrophotometer was used to systematically measure the fraction of light transmitted through the films. The photodegradation kinetics of unloaded thymol, and loaded in nano- or supraparticles was carried out under UV exposure. The unloaded and loaded systems were placed at 10 cm from the UV lamp

(λ_{max} at 356 nm), and samples were taken over time. The amount of remaining, non-degraded thymol was assessed using the same methodology applied for its quantification.

IV.2.8 EVALUATION OF THE MOBILITY OF NANO- AND SUPRAPARTICLES IN SOIL

The mobility of nano and supraparticles in soil were compared using column tests. Three different soils (TABLE S4) were used to investigate important variables such as pH, mineral content and texture on the diffusion of the particles through the column. The procedures were based on the work of Fang et al. (2009), but the columns were scaled down to 9 cm, and the nanoparticles suspension was concentrated to 1 $g \cdot L^{-1}$. Each experiment was carried out using individual columns. To evaluate the nanoparticles mobility, the columns were firstly washed with 50 mL of deionized water, and then 50 mL of the biogenic silica particles suspension was passed through. For the supraparticles evaluation, the soil was washed as before, then 50 mg of supraparticles were placed on the soil surface and 50 mL of water was passed through. As controls, the soil column was washed and then another 50 mL of deionized water was passed through. The liquid outflow of each experiment was taken in order to quantify the fraction of particles retained in the soil and the fraction leached to the outflow.

First, the outflow was evaluated in a UV-Vis spectrophotometer using measurements of the transmittance of the liquid in the visible range. The transmittance of the liquid outflow was compared with the transmittance of the initial nanoparticles suspension. Then, the solid content in the outflow was estimated using a gravimetric approach, by taking 25 mL of the outflow and drying it at 103 ^{o}C to obtain the solid fraction.

IV.3 RESULTS AND DISCUSSION

IV.3.1 GENERAL ASSEMBLY, LOADING METHODOLOGIES AND MECHANICAL CHARACTERIZATION

Low temperature (60 ºC) was necessary to accelerate the evaporation of the water from the $BSiO_2$-CNF suspension droplets. The free water volume inside the droplets reduces upon drying, increasing the solid fraction of the suspension until it self-assembles into a packed, but highly porous structure. Without acceleration of the drying process (*ca.* 10 min), the self-assembling takes significantly longer times (*ca.* 4 h depending on the droplet volume) resulting in flattened heterogenous supraparticles (SPs) as a result of the sedimentation of the bigger $BSiO_2$ particles. The formation of a physically entangled cellulose nanofibrils (CNF) net at extremely low solid concentrations (DE FRANCE; HOARE; CRANSTON, 2017) was key to stabilize the $BSiO_2$ particles suspension, and even without drying process, the assembled particles were not severely deformed as often reported (WANG et al., 2014). CNF display a highly branched morphology that undergoes multiple physically-driven orthogonal interactions upon drying (DE FRANCE; HOARE; CRANSTON, 2017; HENRIKSSON et al., 2008), thus resulting in a strong interlocked 3D net that was suitable to physically reinforce the assembled $BSiO_2$-based SPs. The use of CNF as the cohesion material allowed the rapid, low energy suprastructuring of $BSiO_2$ building blocks into versatile macroscaled materials (FIGURE IV.3b). Up to this point, annealing treatments at high temperature (*ca.* 600 ºC) were the only alternative to synthesize mechanically resistant silica-based SP (LEE et al., 2014; WANG et al., 2014).

Spheres or films were obtained by casting the $BSiO_2$/CNF dispersions on flat substrates with hydrophobic (fluorinated groups) or hydrophilic (silanol groups) surface chemistry; meanwhile hydrophobic molds were used for more complex architectures, here demonstrated through the assembling of cylinders. The size of the bio-based SPs, regardless their shape, is governed by the volume of the $BSiO_2$-CNF dispersion cast on the substrates. On the one hand, a 30 µL droplet cast on the hydrophobic substrate deforms as a result of the gravitational force, thus assembling a not-spherical, but still

functional SP. On the other hand, the volume was not a limitation in the assembling of films and cylinders.

As the annealing post step used to be essential for the assembling of robust silica-based supraparticles, the cargo loading used to be limited to post steps (WANG et al., 2014). Herein, it is shown that *in situ*- or pre-loading strategies can be explored once the cohesion of the supraparticles is driven by CNF-mediated physically particle interlocking. Pre-, *in situ*- and post-loading strategies resulted in different cargo payload (FIGURE IV2). The post-loading approach resulted in the highest cargo incorporation, which can be a result of the cargo accumulation not only on the building block pores and surface but also in the macropores of the assembled SP. The cargo capacity of the pre-loaded SP is limited by the loading capacity of the building blocks, in this case *ca.* 100 mg per g of biogenic silica (CHAPTER III). During the pre-loading strategy a small fraction of cargo is expected to desorb from the loaded-building block; however, this small fraction is probably re-entrapped in the outer layers of the SP. A stronger cargo-carrier interface interaction could be an efficient solution (CHAPTER III) to avoid desorption of the cargo during the (short-time) self-assembly. The *in situ* methodology resulted in the lowest dynamic payload. Even though, a certain amount of thymol was added to achieve a final payload of 90 $mg \cdot g^{-1}$, the payload was only *ca.* 12 $mg \cdot g^{-1}$. The best hypotheses are that, or thymol was partially volatilized during the drying or it is extremely entrapped at the CNF-$BSiO_2$ interface that could not be extracted.

The cargo payload was not significantly affected by the CNF fraction, casting volume and morphology of the superstructures (FIGURE IV.2b, 2c, and 2d). The homogeneity in the payload states the expressively high pore access of the superstructure. The same payload was achieved even when the diameter of the SPs increased from 500 µm to 2 mm. The use of naturally hierarchical organized biogenic silica as building blocks provided a porous architecture spanning length scales from the micro- (silica smallest units), going through the meso (silica smallest units assembling into silica microstructures) to the macro- (resultant silica-CNF superstructure) levels, leading to an excellent pore access for both load and release cargo. From the payload results, the one can see that the CNF fraction at 5% (the highest applied) did not limit the access to the pores at micro and mesoscales, neither to the macroscale (FIGURE IV.3a).

The macropores of the superstructures are resultant from the self-limiting packing of the chosen building blocks. The packing constrictions of the irregular-shaped biogenic silica is compensated by the branched 3D net, formed from the self-assembly of the cellulose nanofibrils, to form a super-robust superstructure.

FIGURE IV.2 – VERSATILE SELF-ASSEMBLY OF THE BIO-BASED SUPERSTRUCTURES (A), AND RESULTANT THYMOL PAYLOAD AS A FUNCTION OF CNF FRACTION (B), SIZE (C) AND MORPHOLOGY (D)

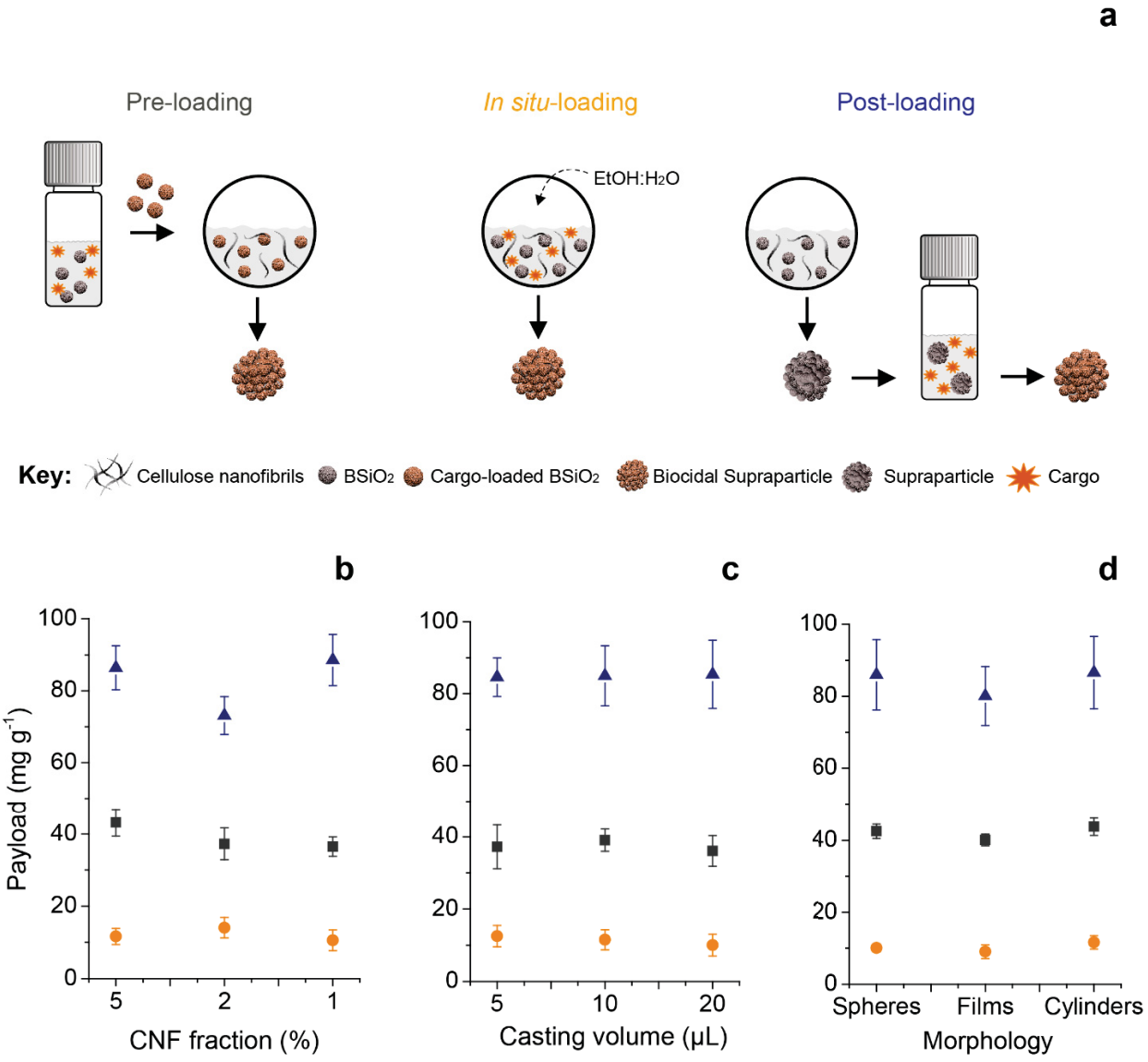

SOURCE: the author (2018).

To evaluate the robustness of the SPs, uniaxial compression tests were performed. The resulting curves (FIGURE IV.3c) were similar to those reported for perfectly inelastic aggregates (ANTONYUK et al., 2005) where no Hertzian elastic deformation occurs in the small strain regime. With CNF addition, the biogenic silica SPs became more cohesive due to higher adhesion forces between introduced by the fibers, as indicated by the increasing slopes from 1 to 5% CNF (FIGURE IV.3c). Differently from usual compression of particle aggregates, no abrupt breakage was observed. Instead, starting at about 10% strain, plateau zones with increased slopes as a function of CNF ratio indicated further reinforcement during crack generation and propagation. This behavior is in accordance to what has been previously reported for fiber-reinforced composites, where fiber debonding and sliding assist in the energy dissipation during crack propagation (HE et al., 1994). Fractured SPs, however, should be avoided as they might behave differently during application and can also further generate fragments. Therefore, the comparison carried further herein concerns the critical point for the transition to the plateau region in the load-displacement curve (FIGURE IV.3d to 3f).

By changing the fundamental building block of the SPs from the colloidal fraction of biogenic silica, a near two-fold increase from 1.5 to 2.9 N in the critical load was observed (FIGURE S12a). This was possibly caused by the better packing of the colloidal fraction. It is possible to infer that the stiffness of the SP assembled using the colloidal fraction is higher than the SP from raw particles, once the resulting slope from the displacement x force curve is higher.

The incorporation of cargo in the pre and post step did not change the mechanical integrity of the supraparticles; however, the biocidal supraparticles assembled using the *in situ*-loading strategy presented reduced mechanical robustness (FIGURE IV.3d). The high pore access of the SPs, and their integrity in polar solvent (FIGURE IV.3b2), allowed the post incorporation of cargo without structural modifications. *In situ*-loading has led to the lowest mechanical robustness. Hypothetically, the dissolved thymol at the particle-CNF interface hindered physical interactions between the hydrophilic surfaces of cellulose and silica, reducing their adhesion. Similar behavior was observed when the pre-loaded building blocks were used, but it occurred not as intense as the *in situ* approach. In the pre-load approach, a deeper penetration of the cargo in the building

block occurs and thus the concentration of cargo at the silica outer units is reduced, increasing the density of interactions (mostly via H-bonding) between cellulose and silica. Even though, all prepared SPs presented considered mechanical robustness (FIGURE IV.3d).

FIGURE IV. 3 – MORPHOLOGICAL FEATURES OF THE ASSEMBLED SUPERSTRUCTURES (A,B), STATIC FORCE X STRAIN CURVES (C) AND MECHANICAL KEY VALUES TO EVALUATE THE ROBUSTNESS OF THE SUPRAPARTICLES (D,E AND F)

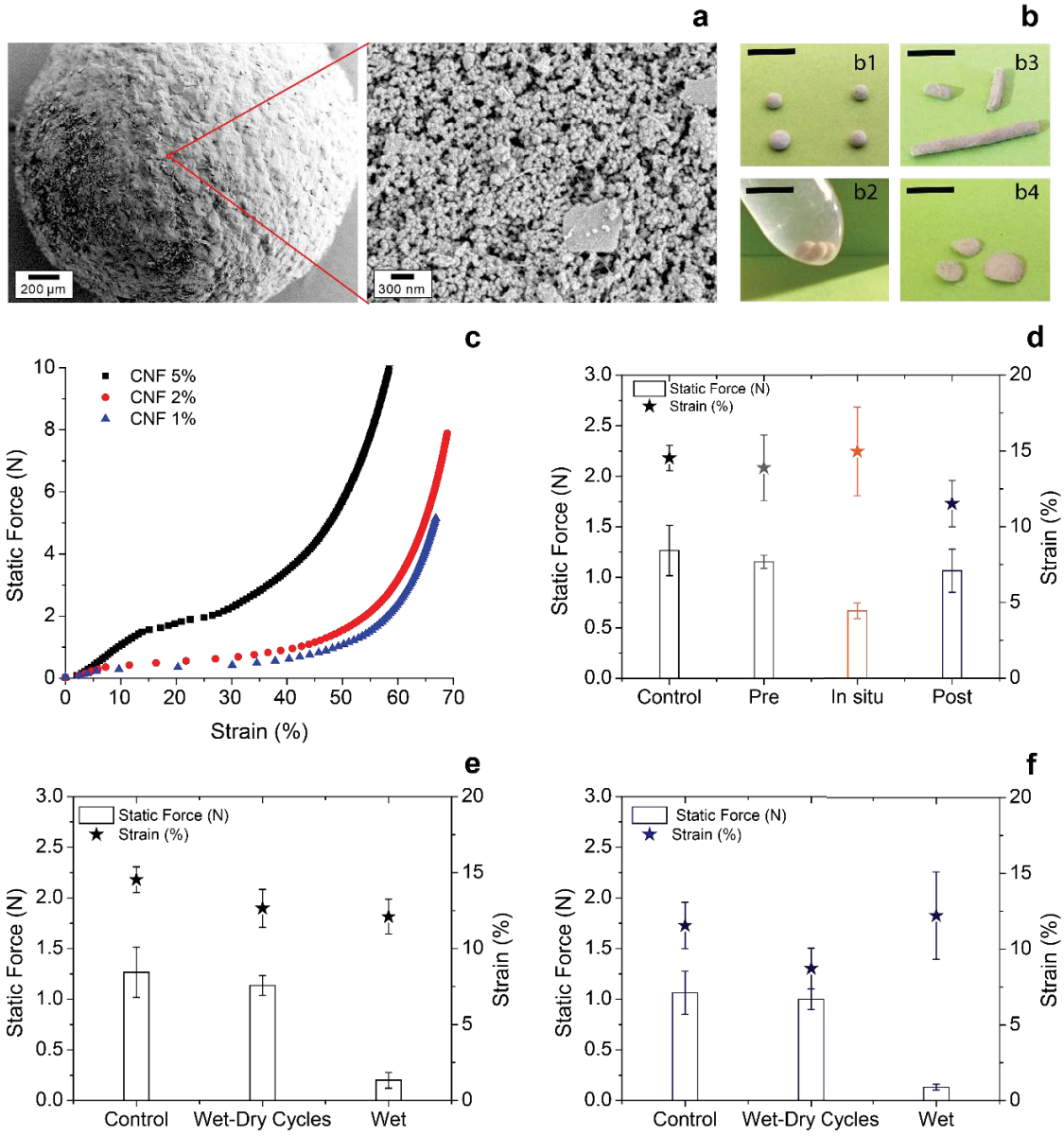

SOURCE: the author (2018).

The 5% CNF/spherical supraparticles were submitted to several integrity tests in order to simulate severe environments (FIGURE IV.3e-3f and FIGURE S12b-S12e). The supraparticles kept their mechanical properties after 5 wet-dry cycles (each cycle has 5h soaking and 5h drying at 103 ºC). Both SP and loaded-SP showed resistance against compression in wet state; however, the robustness was severely reduced (FIGURE IV.3e-3f). Cellulose nanofibrils hydrate and swell over 6 times upon water soaking (UETANI; YANO, 2012), leading to an increase in their deformability. In addition, the H-bonds between silica and cellulose are likely overcome by those with water, reducing the cohesion of the SPs. However, even at the most severe wetting condition the supraparticles with diameter of 2 mm were still able to hold 0.75 N of mechanical load.

In addition, treatment in aqueous media at pH 4 and 9 (controlled through the addition of HCl or NaOH) did not significantly change the mechanical properties of the loaded-supraparticles (FIGURE S12c). On the other hand, a slightly increment was observed for the raw supraparticles (FIGURE S12b), which possibly came from the leaching of not-well-packed silica units, and then further drying into a stronger packed SP. At these pH values the surface charges in both silica (MATTOS; ROJAS; MAGALHÃES, 2016) and cellulose (SEHAQUI et al., 2015) do not drastically change. Besides, the concentration of acid or alkali are not high enough to trigger structural changes in the cellulose or silica that can be driven or by dissolution or degradation. On the other hand, treatments with 1M H_2SO_4 and 1M NaOH solutions promoted drastic changes in the mechanical integrity of the control and loaded SPs (FIGURE S12c and S12d). Depolymerization of cellulose is likely to happen at this acid concentration (RINALDI; SCHÜTH, 2009), weakening the cohesion of the SP. Concentrated NaOH might promote silica dissolution (FERTANI-GMATI; JEMAL, 2011), and also changes in the crystallinity of cellulose (MITTAL et al., 2011). Both changes could induce loss in mechanical resistance. Short-term thermal aging (100 ºC for 1 week) and soaking in boiling water for 1h did not result in structural changes in the $BSiO_2$-CNF based supraparticles (FIGURE S12d and S12e).

IV. 3.2 RELEASE PROFILES AND KINETIC CONSIDERATIONS

The different strategies applied for biocide loading resulted in similar release profiles (FIGURE IV.4b); however, the amount of the biocide delivered upon soaking varied according to the loading approach (FIGURE IV.4a). The thymol release from the SPs behave similarly of the observed for the nanoparticles chosen as building blocks (FIGURE S12). This highlights that the cellulose nanofibrils did not hinder the pore access of the assembled silica particles. Overall, thymol releases from the SPs through two weel-defined stages: initial burst stage, observed in the first 12 h, followed by a slow-release stage, from 12 to 170 h (FIGURE IV.4b). Equilibrium stage was not achieved for none of the superstructured carriers along 170h, suggesting an even longer-term sustained release. The initial burst release is associated to a higher concentration of cargo on the outer layers of the SPs, whereas the fraction of thymol released at this point is attributed to the amount of thymol initially loaded.

Mechanisms of cargo delivering are often identified through the fitting of kinetic models on the experimental release data (LIU; ZHANG; ZHANG, 2015; MATTOS et al., 2017d; MATTOS; MAGALHÃES, 2017; XU et al., 2017; YI et al., 2015). The Elovich kinetic model fitted the cargo release from the SPs with the best coefficients of determination (over 0.95, TABLE S5). Korsmeyer-Peppas model approached linearity on the experimental data (TABLE S5), suggesting that there was a combination of diffusion and swelling mechanisms during thymol release. The Elovich's fit indicates that the cargo fraction delivered over time (which rate is determined by k) decreased proportionally to the fractions recently released, characterizing a logarithmically time-dependency behavior (CHIEN; CLAYTON, 1980). It is hypothesized that this mechanism is a result of the highly porous architecture of the SPs that allows spontaneous water flow into and out of the SP. Those molecules loaded in the outer, more exposed, regions are released promptly. Simultaneously, the molecules deeply incorporated in the particle diffuse to the outer regions for subsequent release. The Korsmeyer-Peppas model was firstly described when evaluating drug delivery from hydrophilic polymers (KORSMEYER et al., 1983). Its fit indicates an anomalous release driven by a complex combination of diffusion and swelling followed by relaxation of the carrier. This release mechanism is a result of the

cellulose nanofibrils swelling when in contact with water (AHOLA et al., 2008) that can result in fibrils with 6-fold higher volume (UETANI; YANO, 2012), making the whole SP swells. From the kinetic approaches it is possible to affirm that diffusion and polymer relaxation are the driven mechanisms for thymol release from the assembled SPs.

FIGURE IV.4 – BIOCIDE RELEASE PROFILES CONSIDERING CONCENTRATION (A) AND RELATIVE AMOUNT (B). RELEASE RATE COEFFICIENTS AS A FUNCTION OF CNF SOLID FRACTION (C), CASTING VOLUME (D) AND MORPHOLOGY (E)

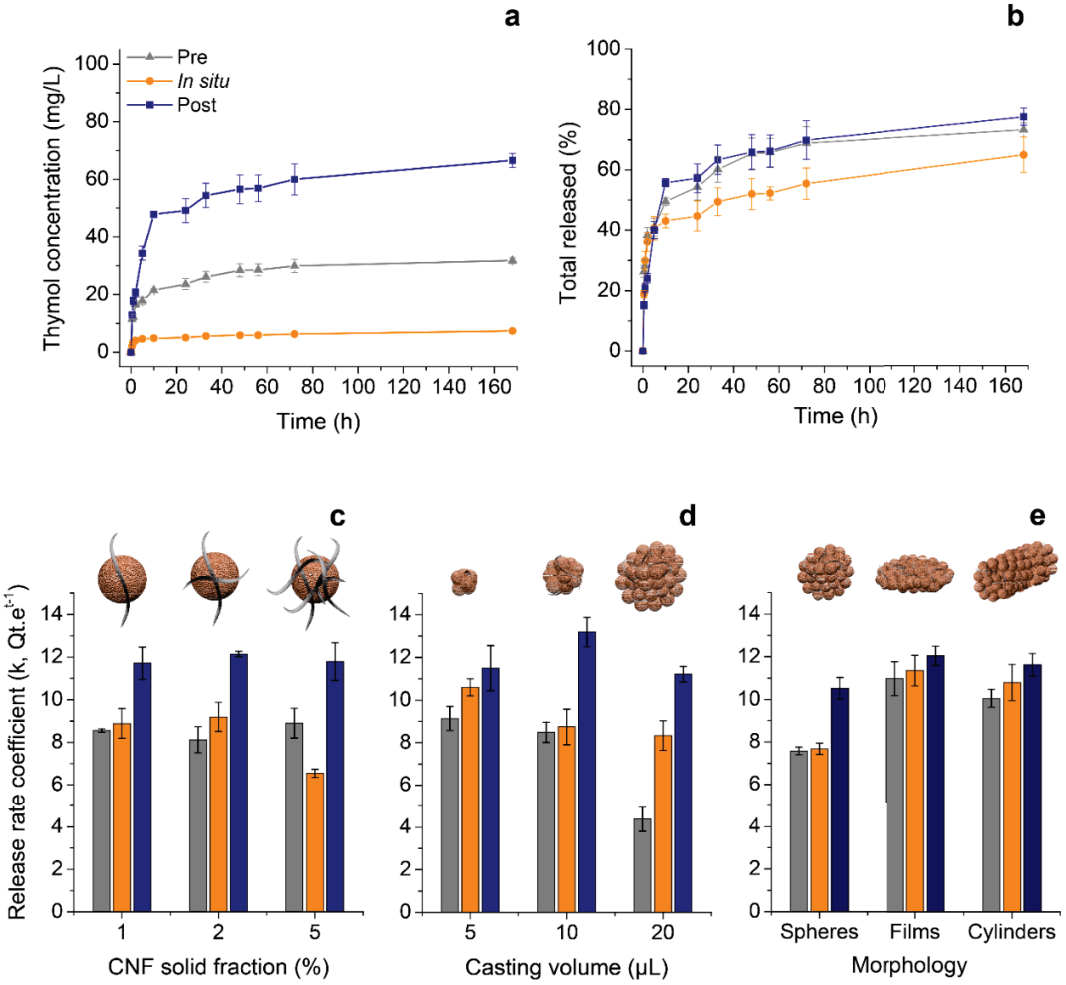

SOURCE: the author (2018).

The release rate coefficient, *k*, was obtained from the slope of the Elovich linearized plot (FIGURE S14). *k* was used to investigate the delivery performance of the assembled SPs as a function of CNF fraction, size and morphology (FIGURE IV.4c, 4d,

and 4e). When the CNF fraction was systematically increased the release rate coefficient did not change for the SPs loaded via pre- and post-loading. A significant decrease in *k* was observed for the *in situ*-loaded SPs with 5% of CNF fraction. It is hypothesized that, during the *in situ*-loading, the high CNF content provided an intensified entrapment of the cargo at the silica-cellulose interface. In addition, the low cargo fraction in the SPs prepared via *in situ*-loading could be a factor leading to better entrapment (FIGURE IV.4c).

There was a marked effect of the casting volume on the biocide release rate from the pre-loaded SPs (FIGURE IV.4d). The casting volume is strictly related to the SP size (FIGURE IV.3b). The use of pre-loaded building blocks resulted in a more homogenous distribution of biocide across the SP. Thus, the bigger the SP, the longer the center-entrapped biocide diffusion path until reaching the external area. The less marked effect of size on the *k* calculated for *in situ*- and post-loaded SPs suggests a higher concentration of biocide at the outer regions. Even though, there was a tendency in *k* decreasing when reducing the size of the SP (FIGURE IV.4c). The size of the delivery system is not as marked as observed for polymeric/drug monolithic dispersion (SIEPMANN; SIEPMANN, 2008) because of the highly porous character of $BSiO_2$-based SPs (FIGURE IV.3a). The surface area-to-volume ratio of bulk delivery systems (*i.e.* non-porous) is key for controlling the release rate of the cargo (SIEPMANN; SIEPMANN, 2008). Herein, *k* follows the same pattern for all loading methodologies as far as the morphology of the assembled superstructure (FIGURE IV.4e).

The highest *k* was calculated for the films, while the lowest for the spheres. Considering the same volume, the “external” surface area ratio of the assembled superstructured systems is *ca.* 1:1.2:5.4 for sphere:cylinder:films. The release rate coefficient follows the pattern but not the magnitude. For instance, *k* is only 1.4 times higher in the pre-loaded films when compared to the pre-loaded spheres. Thus, it is possible to affirm that the release performance is not strongly influenced by size, CNF fraction or morphology, making it a quite versatile approach to assemble SP with well-controlled, homogenous release properties.

IV. 3.3 BIOCIDE PROTECTION AGAINST PHOTODEGRADATION

The UV-shielding properties of amorphous silica has been widely used in many fields of science, such as optoelectronics (CORREA-DUARTE; GIERSIG; LIZ-MARZÁN, 1998) and textile engineering (ABIDI et al., 2007). Nonetheless, UV-shielding is of great interest to prevent the photodegradation of pesticides thus increasing their long-term action. Herein, millimetric supraparticles were designed and applied to decrease the "external" surface area-to-bulk ratio and consequently to protect cargo against light (FIGURE IV.5a).

FIGURE IV. 5 – REPRESENTATION OF THE SUPRAPARTICLE'S ZONES AFFECTED BY LIGHT (A) AS ESTIMATED BY LIGHT TRANSMITTANCE (B). PHOTODEGRADATION KINETICS OF UNLOADED AND LOAD THYMOL UNDER UV EXPOSURE (λmax 356 NM) AS A FUNCTION OF TIME (C)

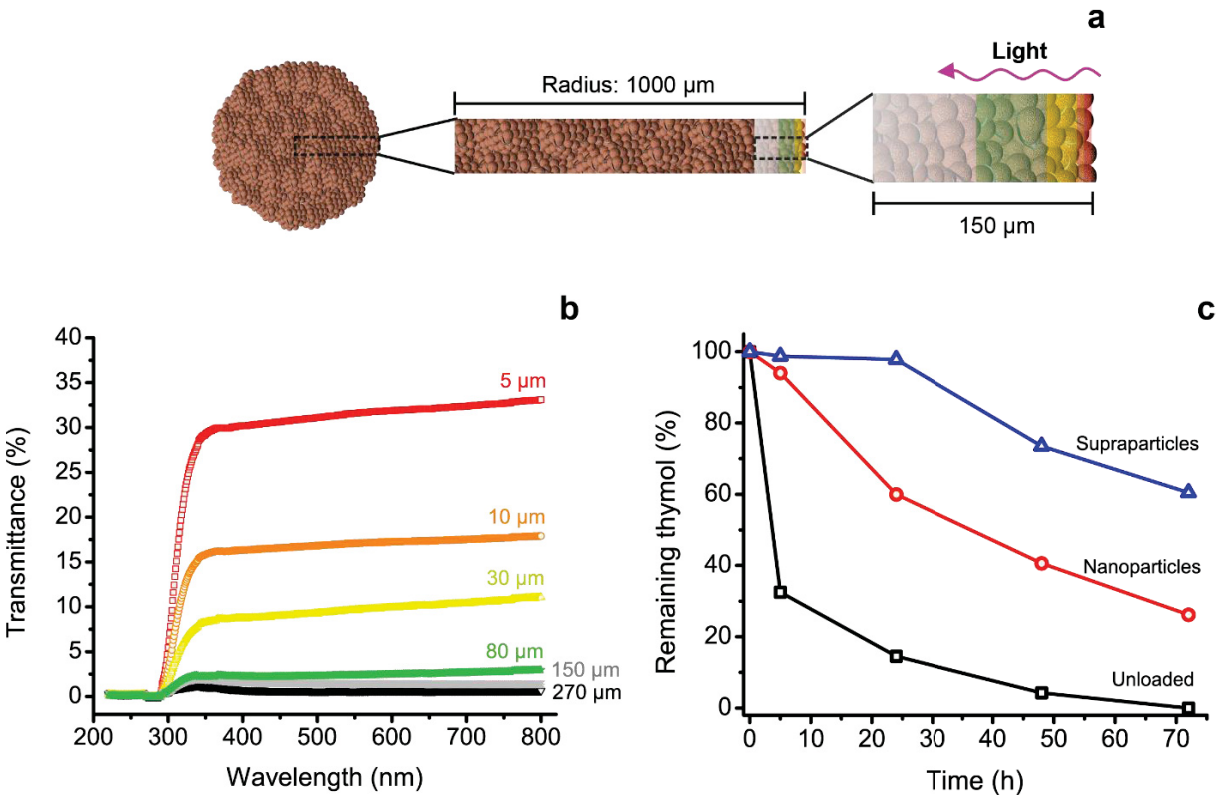

SOURCE: the author (2018)

The fraction of light transmitted through $BSiO_2$-CNF films (CNF fraction: 5%) prepared with gradually increased thickness was first systematically investigated

(FIGURE IV.5b). Overall, the light transmission in the UV zone was null already in the lower thickness (5 μm). In this case, the UV irradiation is absorbed, or even scattered, diffracted or reflected by the silica particles. In the visible range, the transmittance is *ca.* 35% for the films with 5 μm and it gradually decreases until near zero for the films with 150 μm (FIGURE IV.5b). A parallel can be drawn from films to spheres. Considering supraparticles with diameter *ca.* 2 mm, and that light penetrates only the outer 150 μm of the whole sphere (FIGURE IV.5a and 5b), it is possible to infer that theoretically *ca.* 85% of the cargo is protected against light. Clearly, the protection increases in directly relationship with the size of the SP. An experimental procedure was carried out in order to validate the theoretical value for cargo protection (FIGURE IV.5c). $BSiO_2$ nano- and supraparticles loaded with thymol, as well as dissolved thymol as control, were submitted to UV irradiation at room temperature (25 ºC). The remaining thymol was extracted and measured over time (FIGURE IV.5c). Significantly higher fraction of thymol remained in the SPs after 24 h of exposure when compared to the nanoparticles and the solution. Whereas *ca.* 100% of thymol remained in the SPs, only 60% was not lost in the nanoparticles. In the same time interval only 15% of the dissolved thymol was not degraded. At the end of the experiment (72 h), it was observed that 65% of the thymol remained in the SPs, and that the cargo protection was at least twice higher in the supraparticles when compared to the nanoparticles.

The experimental (65%) and theoretical (85%) values were different, but close. Several factors could be contributing for this discrepancy, such as differences in the light intensity in both studies and parallel degradation of thymol triggered by environmental effects (temperature, humidity, ozone and oxygen). In addition, a higher concentration of thymol in the outer regions of the post-loaded SP could be expected, thus leading to a higher degradation than the theoretical value. Even though, the value achieved for cargo protection using the SP assembling strategy is impressive when compared with previously works that, for instance, used silica nanocapsules aiming at the same purposes (LI et al., 2006).

IV. 3.4 STUDY OF NANO- AND SUPRAPARTICLES MOBILITY IN SOIL COLUMNS

The high mobility of nanoparticles in soil (SCHRICK et al., 2004) has limited the application of nanoscaled delivery systems for crop protection. In parallel with the bioaccumulation of nanomaterials, nanoparticles can also act as a carrier for the pesticides to contaminate groundwater. Herein, the mobility of nanoparticles and supraparticles in soil using column tests was compared (FIGURE IV.6a). Three soils with different characteristics were selected to investigate factors such as pH, mineral content, density and texture (TABLE S4) on the particles diffusivity. Transmittance measurements of the water outflow were acquired to assess the fraction of particles accumulated along the soil column and the leached fraction (FIGURE IV.6b). The transmittance of the outflow is inversely related to the solid content in suspension. Aliquots of the outflow were dried to get an approximation of their solid content (FIGURE IV.6c). Comparing the outflow samples with controls it was possible to reach conclusive values.

The nanoparticles behave mainly in two manners: they partially accumulated in the soil or completely diffused through the column until reach the outflow (FIGURE IV.6a). Their behavior is linked with the specific characteristics of the soils (FIGURE IV.6, FIGURE S14 and TABLE S4). It was observed a very high permeability of the nanoparticles in the Soil A. This soil has very low mineral content and organic matter, at the same time that it is composed mostly by sand (TABLE S4). Soil B retained the highest fraction of the nanoparticles, while Soil C presented intermediary retention capacity. Soil B is rich in charged positive ions, such as Mg^{+2} and Ca^{+2} (TABLE S4). This condition was key to promote the highest retention of silica nanoparticles, which at acid conditions are negatively charged (MATTOS; ROJAS; MAGALHÃES, 2016). Besides the electrostatic interactions taking place between silica nanoparticles and the positive ions contained in the soil, there was the texture factor. Clay-rich soils have higher nanoparticles sticking capacity than sandy soils (FANG et al., 2009; SCHRICK et al., 2004).

In addition, the organic matter displays an important role in the formation of nanoclusters in the soil (AIKEN; HSU-KIM; RYAN, 2011; GRILLO; ROSA; FRACETO, 2015), being also responsible to promote lower diffusion. Lastly, Soil C has characteristics of Soil A and B, thus behaving intermediary as far as retention capacity. However, either

retention in the soil or leaching into the groundwater are non-target effects when considering the utilization of particles for crop protection

FIGURE IV.6 – SCHEMATIC REPRESENTATION OF THE BEHAVIOR OF NANO AND SUPRAPARTICLES IN THE SOIL COLUMN TESTS (A). LIGHT TRANSMITTANCE OF THE OUTFLOW (B). AND A GRAVIMETRIC APPROACH (C) WERE USED TO ESTIMATE THE AMOUNT OF LEACHED PARTICLES

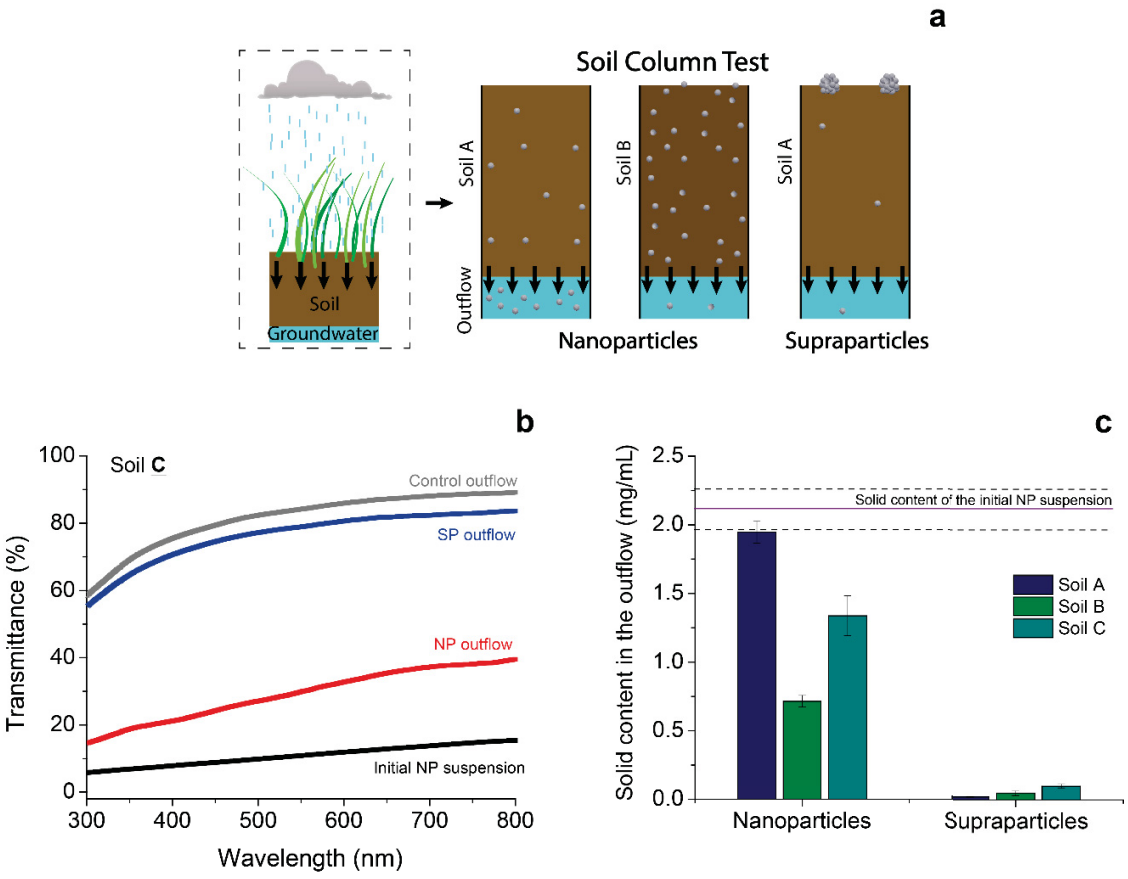

SOURCE: the author (2018)

The levels of each non-targeted effect (soil accumulation or leaching to ground water) depend on the soil sites and their characteristics, but both will happen if nanoparticles were used directly in contact with soil. On the other hand, it was shown that regardless the soil, the prepared biocidal SPs presented very limited mobility in soil, being restricted to penetration only few millimeters on the soil surface (FIGURE S14). This behavior is associated with the size of the SPs that significantly reduced their mobility.

IV.4 CONCLUSIONS

Highly porous, robust superstructures with well-controlled size and different morphologies could be assemble by using biogenic silica particles as building blocks and cellulose nanofibrils as a cohesive component. Versatile loading strategies were proposed to load thymol into the superstructures. Specifically, pre- and in situ-loading can now be explored as the robustness of the particles derives from the strong CNF-silica physically entanglement, and not from annealing processes. Considering these two significant advances it is possible to visualize applications outside of drug delivery, such as 3D printing, catalyst, sensor and synthetic biology.

The biocide release profiles are similar to those acquired for the biogenic silica nanoparticles. The robustness of the supraparticles is impressive, as they went through several wet-dry cycles, acid treatments, and thermal stresses without any significant decrement of their compression strength. Quite interesting, CNF acts as a fracture holder of the supraparticle giving to it an extra mechanical resistance after the elastic deformation regime.

Supraparticles for biocide delivery is a win-win situation as far as biocide and environment protection. Once loaded in the supraparticles the biocide is significantly protected against photodegradation, thus increasing its long-term activity. In parallel, using supraparticles it is possible to avoid non-targeted effects such as deep penetration in soil and contamination of groundwater which is often caused by nanoparticles.

REFERENCES

ABBASZADEH, S. et al. Antifungal efficacy of thymol, carvacrol, eugenol and menthol as alternative agents to control the growth of food-relevant fungi. **Journal de Mycologie Medicale**, v. 24, n. 2, 2014.

ABDULLAYEV, E. et al. Halloysite tubes as nanocontainers for anticorrosion coating with benzotriazole. **ACS Applied Materials and Interfaces**, v. 1, n. 7, p. 1437–1443, 2009.

ABIDI, N. et al. Cotton fabric surface modification for improved UV radiation protection using sol–gel process. **Journal of Applied Polymer Science**, v. 104, n. 1, p. 111–117, 2007.

AGO, M. et al. Supramolecular assemblies of lignin into nano- and microparticles. **MRS Bulletin**, v. 42, n. 5, p. 371–378, 2017.

AHOLA, S. et al. Model Films from Native Cellulose Nanofibrils. Preparation, Swelling, and Surface Interactions. **Biomacromolecules**, v. 9, n. 4, p. 1273–1282, 2008.

AIKEN, G. R.; HSU-KIM, H.; RYAN, J. N. Influence of Dissolved Organic Matter on the Environmental Fate of Metals, Nanoparticles, and Colloids. **Environmental Science & Technology**, v. 45, n. 8, p. 3196–3201, 2011.

AKELAH, A.; REHAB, A.; EL-GAMAL, M. M. Preparation and applications of controlled release systems based on intercalated atrazine salt and polymeric atrazine salt onto montmorillonite clay. **Materials Science and Engineering: C**, v. 28, n. 7, p. 1123–1131, 2008.

AKTAR, M. W.; SENGUPTA, D.; CHOWDHURY, A. Impact of pesticides use in agriculture: their benefits and hazards. **Interdisciplinary Toxicology**, v. 2, n. 1, p. 1–12, 20 mar. 2009.

ALI, S. W.; RAJENDRAN, S.; JOSHI, M. Synthesis and characterization of chitosan and silver loaded chitosan nanoparticles for bioactive polyester. **Carbohydrate Polymers**, v. 83, n. 2, p. 438–446, 2011.

AN, Y. et al. Preparation and self-assembly of carboxylic acid-functionalized silica. **Journal of Colloid and Interface Science**, v. 311, n. 2, p. 507–513, 2007.

ANDERSSON, J. et al. Influences of Material Characteristics on Ibuprofen Drug Loading and Release Profiles from Ordered Micro- and Mesoporous Silica Matrices. **Chemistry of Materials**, v. 16, n. 21, p. 4160–4167, 2004.

ANDERSSON TROJER, M. et al. Use of microcapsules as controlled release devices for coatings. **Advances in colloid and interface science**, v. 222, p. 18–43, 2015.

ANTONYUK, S. et al. Breakage behaviour of spherical granulates by compression. **Chemical Engineering Science**, v. 60, n. 14, p. 4031–4044, 2005.

AOUADA, F. A. et al. Polyacrylamide and methylcellulose hydrogel as delivery vehicle for the controlled release of paraquat pesticide. **Journal of Materials Science**, v. 45, n. 18, p. 4977–4985, 2010.

APPELL, M.; JACKSON, M. A. **Applications of Nanoporous Materials**. Advances in Applied Nanotechnology for Agriculture. **Anais**...American Chemical Society, 2013

ARMATAS, G. S. Determination of the effects of the pore size distribution and pore connectivity distribution on the pore tortuosity and diffusive transport in model porous networks. **Chemical Engineering Science**, v. 61, n. 14, p. 4662–4675, 2006.

ASRAR, J. et al. Controlled release of tebuconazole from a polymer matrix microparticle: Release kinetics and length of efficacy. **Journal of Agricultural and Food Chemistry**, v. 52, n. 15, p. 4814–4820, 2004.

ATHINARAYANAN, J. et al. Synthesis of biogenic silica nanoparticles from rice husks for biomedical applications. **Ceramics International**, v. 41, n. 1, p. 275–281, 2014.

AZEEM, B. et al. Review on materials & methods to produce controlled release coated urea fertilizer. **Journal of Controlled Release**, v. 181, p. 11–21, 2014.

BAI, C. et al. Starch-based hydrogel loading with carbendazim for controlled-release and water absorption. **Carbohydrate Polymers**, v. 125, p. 376–383, 2015.

BAMUFLEH, H. S.; ALHAMED, Y. A.; DAOUS, M. A. Furfural from midribs of date-palm trees by sulfuric acid hydrolysis. **Industrial Crops and Products**, v. 42, n. 1, p. 421–428, 2013.

BEAMSON, G.; BRIGGS, D. High Resolution XPS of Organic Polymers: The Scienta ESCA300 Database. **Journal of Chemical Education**, v. 70, n. 1, p. A25, 1993.

BERGEK, J. et al. Controlled release of microencapsulated 2-n-octyl-4-isothiazolin-3-one from coatings: Effect of microscopic and macroscopic pores. **Colloids and Surfaces A: Physicochemical and Engineering Aspects**, v. 458, n. 1, p. 155–167, 2014.

BÖTTCHER, H. et al. Sol-gel composite films with controlled release of biocides. **Journal of controlled release : official journal of the Controlled Release Society**, v. 60, p. 57–65, 1999.

BOYANDIN, A. N. et al. Constructing Slow-Release Formulations of Metribuzin Based on Degradable Poly(3-hydroxybutyrate). **Journal of Agricultural and Food Chemistry**, v. 64, n. 28, p. 5625–5632, 2016.

BRUNNER, T. J. et al. In Vitro Cytotoxicity of Oxide Nanoparticles : Comparison to Asbestos , Silica , and the Effect of Particle Solubility In Vitro Cytotoxicity of Oxide Nanoparticles : Comparison to Asbestos , Silica , and the Effect of Particle Solubility †. **Environmental Science & Technology**, v. 40, n. 14, p. 4374–4381, 2006.

BURROWS, H. D. et al. Reaction pathways and mechanisms of photodegradation of pesticides. **Journal of Photochemistry and Photobiology B: Biology**, v. 67, n. 2, p. 71–108, 2002.

CABRAL, H.; KATAOKA, K. Progress of drug-loaded polymeric micelles into clinical studies. **Journal of Controlled Release**, v. 190, p. 465–476, 2014.

CAMPOS, E. V. R. et al. **Polysaccharides as safer release systems for agrochemicalsAgronomy for Sustainable Development**, 2014.

CAO, J.; JIANG, X. Preservation of wood and other sustainable biomaterials in China. **ACS Symposium Series**, v. 1158, p. 363–383, 2014.

CARMONA, V. B. et al. Nanosilica from rice husk: Extraction and characterization. **Industrial Crops and Products**, v. 43, n. 1, p. 291–296, 2013.

CECCHINI, M. P. et al. Self-assembled nanoparticle arrays for multiphase trace analyte detection. **Nature Materials**, v. 12, n. 2, p. 165–171, 2013.

CHANG, B. et al. Surface functionalization of magnetic mesoporous silica nanoparticles for controlled drug release. **Journal of Materials Chemistry**, v. 20, n. 44, p. 9941, 2010.

CHANG, J. et al. Bioaccumulation and enantioselectivity of type I and type II pyrethroid pesticides in earthworm. **Chemosphere**, v. 144, p. 1351–1357, 2016.

CHAUHAN, N. et al. Development of Chitosan Nanocapsules for the Controlled Release of Hexaconazole. **International Journal of Biological Macromolecules**, v. 97, p. 616–624, 2016.

CHAVAN, P. S.; TUPE, S. G. Antifungal activity and mechanism of action of carvacrol and thymol against vineyard and wine spoilage yeasts. **Food Control**, v. 46, p. 115–120, 2014.

CHEN, H. et al. Extraction of lignocellulose and synthesis of porous silica nanoparticles from rice husks: A comprehensive utilization of rice husk biomass. **ACS Sustainable Chemistry and Engineering**, v. 1, n. 2, p. 254–259, 2013.

CHEN, J. et al. Slow-release formulation of a new biological pesticide, pyoluteorin, with mesoporous silica. **Journal of Agricultural and Food Chemistry**, v. 59, n. 1, p. 307–311, 2011.

CHEN, X.; MAO, S. S. Titanium Dioxide Nanomaterials: Synthesis, Properties, Modifications, and Applications. **Chemical Reviews**, v. 107, n. 7, p. 2891–2959, 2007.

CHIEN, S. H.; CLAYTON, W. R. Application of Elovich Equation to the Kinetics of Phosphate Release and Sorption in Soils. **Soil Science Society of America Journal**, v. 44, n. 2, p. 265, 1980.

CHOWDHURY, P.; NAG, S.; RAY, A. K. Degradation of Phenolic Compounds Through UV and Visible- Light-Driven Photocatalysis: Technical and Economic Aspects. In: SOTO-HERNANDEZ, M.; PALMA-TENANGO, M.; GARCIA-MATEOS, M. DEL R. (Eds.). . **Phenolic Compounds - Natural Sources, Importance and Applications**. Rijeka: InTech, 2017.

CIOLACU, D. et al. New cellulose-lignin hydrogels and their application in controlled release of polyphenols. **Materials Science and Engineering C**, v. 32, n. 3, p. 452–463, 2012.

COLVIN, V. L. **The potential environmental impact of engineered nanomaterialsNature Biotechnology**, 2003.

CORREA-DUARTE, M. A.; GIERSIG, M.; LIZ-MARZÁN, L. M. Stabilization of CdS semiconductor nanoparticles against photodegradation by a silica coating procedure. **Chemical Physics Letters**, v. 286, n. 5, p. 497–501, 1998.

COTTERILL, J. V; WILKINS, R. M. Controlled Release of Phenylurea Herbicides from a Lignin Matrix : Release Kinetics and Modification with Urea. **J. Agric. Food Chem**, v. 44, n. 25 mL, p. 2908–2912, 1996.

CRUTE, I. Chapter 6 Balancing the Environmental Consequences of Agriculture with the Need for Food Security. In: **Environmental Impacts of Modern Agriculture**. [s.l.] The Royal Society of Chemistry, 2012. p. 129–149.

DAS, S. K. et al. Effects of surface acidity and pore size of mesoporous alumina on degree of loading and controlled release of ibuprofen. **Microporous and Mesoporous Materials**, v. 118, n. 1–3, p. 267–272, 2009.

DE FRANCE, K. J.; HOARE, T.; CRANSTON, E. D. Review of Hydrogels and Aerogels Containing Nanocellulose. **Chemistry of Materials**, v. 29, n. 11, p. 4609–4631, 13 jun. 2017.

DELLICOLLI, H. T.; CHARLESTON, N. Controlled Release of Pesticides from Kraft Lignin Carriers. **ACS Symposium Series; American Chemical Society**, p. 84–93, 1977.

DING, G. et al. Preparation and characterization of kasuga-silica-conjugated nanospheres for sustained antimicrobial activity. **Journal of Nanoparticle Research**, v.

16, n. 11, p. 1–10, 2014.

DING, X. et al. Efficient one-pot synthesis and loading of self-assembled amphiphilic chitosan nanoparticles for low-leaching wood preservation. **Carbohydrate Polymers**, v. 86, n. 1, p. 58–64, 2011.

DO MONTE, F. H. M. et al. Antinociceptive and anti-inflammatory properties of the hydroalcoholic extract of stems from Equisetum arvense L. in mice. **Pharmacological Research**, v. 49, n. 3, p. 239–243, 2004.

DOS SANTOS, J. G. et al. Sedative and anticonvulsant effects of hydroalcoholic extract of Equisetum arvense. **Fitoterapia**, v. 76, n. 6, p. 508–513, 2005.

EVERSDIJK, J. et al. Development and evaluation of a biocide release system for prolonged antifungal activity in finishing materials. **Progress in Organic Coatings**, v. 74, n. 4, p. 640–644, 2012.

FANG, J. et al. Stability of titania nanoparticles in soil suspensions and transport in saturated homogeneous soil columns. **Environmental Pollution**, v. 157, n. 4, p. 1101–1109, 2009.

FERNÁNDEZ-PÉREZ, M. et al. Controlled release of diuron from an alginate-bentonite formulation: Water release kinetics and soil mobility study. **Journal of Agricultural and Food Chemistry**, v. 47, n. 2, p. 791–798, 1999.

FERNÁNDEZ-PÉREZ, M. et al. Ethylcellulose and lignin as bearer polymers in controlled release formulations of chloridazon. **Carbohydrate Polymers**, v. 83, n. 4, p. 1672–1679, 2011.

FERNANDEZ-PEREZ, M.; GONZALEZ-PRADAS, E.; URENA-AMATE, M. D. Controlled Release of Imidacloprid from a Lignin Matrix : Water Release Kinetics and Soil Mobility Study. **Journal of agricultural and food chemistry**, v. 46, n. 98, p. 3828–3834, 1998.

FERTANI-GMATI, M.; JEMAL, M. Thermochemistry and kinetics of silica dissolution in NaOH aqueous solution. **Thermochimica Acta**, v. 513, n. 1, p. 43–48, 2011.

FLORES-CÉSPEDES, F. et al. Preparation and Characterization of Azadirachtin Alginate-Biosorbent Based Formulations: Water Release Kinetics and Photodegradation Study. **Journal of Agricultural and Food Chemistry**, v. 63, n. 38, p. 8391–8398, 2015.

FOLEY, J. A. et al. Solutions for a cultivated planet. **Nature**, v. 478, n. 7369, p. 337–42, 2011.

GANDINI, A.; LACERDA, T. M. From monomers to polymers from renewable resources: Recent advances. **Progress in Polymer Science**, v. 48, p. 1–39, 2015.

GE, X. et al. Complexation of carbendazim with hydroxypropyl-β-cyclodextrin to improve solubility and fungicidal activity. **Carbohydrate Polymers**, v. 89, n. 1, p. 208–212, 2012.

GESZKE-MORITZ, M.; MORITZ, M. APTES-modified mesoporous silicas as the carriers for poorly water-soluble drug. Modeling of diflunisal adsorption and release. **Applied Surface Science**, v. 368, p. 348–359, 2016.

GHOSH, S.; JIJIL, C. P.; DEVI, R. N. In situ encapsulation of ultra small ceria nanoparticles stable at high temperatures in the channels of mesoporous silica. **Microporous and Mesoporous Materials**, v. 155, p. 215–219, 2012.

GODIN, B. et al. Chemical characteristics and biofuel potential of several vegetal biomasses grown under a wide range of environmental conditions. **Industrial Crops and Products**, v. 48, p. 1–12, 2013.

GREAVES, H. et al. **Protocols for assessment of wood preservatives**. [s.l: s.n.].

GRILLO, R. et al. Chitosan/tripolyphosphate nanoparticles loaded with paraquat herbicide: An environmentally safer alternative for weed control. **Journal of Hazardous Materials**, v. 278, p. 163–171, 2014.

GRILLO, R. et al. Chitosan nanoparticles loaded the herbicide paraquat: The influence of the aquatic humic substances on the colloidal stability and toxicity. **Journal of Hazardous Materials**, v. 286, p. 562–572, 2015.

GRILLO, R.; ROSA, A. H.; FRACETO, L. F. Engineered nanoparticles and organic matter: A review of the state-of-the-art. **Chemosphere**, v. 119, p. 608–619, 2015.

GU, S. et al. A detailed study of the effects of pyrolysis temperature and feedstock particle size on the preparation of nanosilica from rice husk. **Industrial Crops and Products**, v. 50, p. 540–549, 2013.

GUO, J. et al. Attachment of gold nanoparticles on cellulose nanofibrils via click reactions and electrostatic interactions. **Cellulose**, v. 23, n. 5, p. 3065–3075, out. 2016.

GUO, Y.-G.; HU, J.-S.; WAN, L.-J. Nanostructured Materials for Electrochemical Energy Conversion and Storage Devices. **Advanced Materials**, v. 20, n. 15, p. 2878–2887, 2008.

HALL, K. E. et al. Pesticide sorption and leaching potential on three Hawaiian soils. **Journal of Environmental Management**, v. 159, p. 227–234, 2015.

HAMES, B. et al. **Preparation of Samples for Compositional AnalysisBiomass Analysis Technology Team Laboratory Analytical Procedure**. [s.l: s.n.].

HANDA, P.; FANT, C.; NYDÉN, M. Antifouling agent release from marine coatings-ion pair formation/dissolution for controlled release. **Progress in Organic Coatings**, v. 57, n. 4, p. 376–382, 2006.

HANSEN, C. **The three dimensional solubility parameter and solvent diffusion coefficient and their importance in surface coating formulation.** Copenhagen: Danish Technical Press, 1967.

HARTMANN, M. Hierarchical Zeolites: A Proven Strategy to Combine Shape Selectivity with Efficient Mass Transport. **Angewandte Chemie International Edition**, v. 43, n. 44, p. 5880–5882, 2004.

HAYWARD, R. C.; SAVILLE, D. A.; AKSAY, I. A. Electrophoretic assembly of colloidal crystals with optically tunable micropatterns. **Nature**, v. 404, n. 6773, p. 56–59, 2000.

HE, M. Y. et al. Inelastic strains due to matrix cracking in unidirectional fiber-reinforced composites. **Mechanics of Materials**, v. 18, n. 3, p. 213–229, 1994.

HENRIKSSON, M. et al. Cellulose Nanopaper Structures of High Toughness. **Biomacromolecules**, v. 9, n. 6, p. 1579–1585, 2008.

HILDEBRAND, J. H.; SCOTT, R. L. **The Solubility of Nonelectrolytes**. 3rd. ed. New York, NY, NY: Dover Publications, 1964.

HOBBESLAND, A; KJUUS, H.; THELLE, D. S. Study of cancer incidence among 8530 male workers in eight Norwegian plants producing ferrosilicon and silicon metal. **Occupational and environmental medicine**, v. 56, n. 9, p. 625–31, 1999.

HOLZHUTER, G.; NARAYANAN, K.; GERBER, T. **Structure of silica in Equisetum arvense**. Analytical and Bioanalytical Chemistry. **Anais**...2003

HONG, K. H. Preparation and properties of phenolic compound/BTCA treated cotton fabrics for functional textile applications. **Cellulose**, v. 22, n. 3, p. 2129–2136, jun. 2015.

HONGMIN, M. et al. A Novel Controlled Release Immunosensor based on Benzimidazole Functionalized SiO2 and Cyclodextrin Functionalized Gold. **Scientific Reports**, v. 6, 2016.

HORNIG, S. et al. Synthetic polymeric nanoparticles by nanoprecipitation. **Journal of Materials Chemistry**, v. 19, n. 23, p. 3838, 2009.

HU, Q. DA; TANG, G. P.; CHU, P. K. Cyclodextrin-based host-guest supramolecular nanoparticles for delivery: From design to applications. **Accounts of Chemical Research**, v. 47, n. 7, p. 2017–2025, 2014.

HUDZICKI, J. Kirby-Bauer Disk Diffusion Susceptibility Test Protocol. **American**

Society for Microbiology, n. December 2009, p. 1–23, 2009.

ICONOMOPOULOU, S. M. et al. Incorporation of low molecular weight biocides into polystyrene-divinyl benzene beads with controlled release characteristics. **Journal of Controlled Release**, v. 102, n. 1, p. 223–233, 2005.

INDUSTRIES, E. **GPS Safety Summary: Silicon tetrachlorideTechnical Information**. [s.l: s.n.].

JAMSA, S. et al. Slow release of a biocidal agent from polymeric microcapsules for preventing biodeterioration. **Progress in Organic Coatings**, v. 76, n. 1, p. 269–276, 2013.

JANATOVA, A. et al. Long-term antifungal activity of volatile essential oil components released from mesoporous silica materials. **Industrial Crops and Products**, v. 67, p. 216–220, 2015.

JEROBIN, J. et al. Biodegradable polymer based encapsulation of neem oil nanoemulsion for controlled release of Aza-A. **Carbohydrate Polymers**, v. 90, n. 4, p. 1750–1756, 2012.

JIA, C. et al. Controlled-release drug carriers based hierarchical silica microtubes templated from cellulose acetate nanofibers. **Journal of Applied Polymer Science**, v. 132, n. 38, p. n/a-n/a, 10 out. 2015.

JIAO, J. et al. Improvement of adsorbent materials for {CO2} capture by amine functionalized mesoporous silica with worm-hole framework structure. **Chemical Engineering Journal**, v. 306, p. 9–16, 2016.

JOSHI, G. V. et al. Mesoporous synthetic hectorites: A versatile layered host with drug delivery application. **Microporous and Mesoporous Materials**, v. 142, n. 2–3, p. 542–548, 2011.

JUDY, J. D.; BERTSCH, P. M. Chapter One - Bioavailability, Toxicity, and Fate of Manufactured Nanomaterials in Terrestrial Ecosystems. In: SPARKS, D. L. (Ed.). . Advances in Agronomy. [s.l.] Academic Press, 2014. v. 123p. 1–64.

KAPOOR, S.; HEGDE, R.; BHATTACHARYYA, A. J. Influence of surface chemistry of mesoporous alumina with wide pore distribution on controlled drug release. **Journal of Controlled Release**, v. 140, n. 1, p. 34–39, 2009.

KATAGI, T. Photodegradation of Pesticides on Plant and Soil Surfaces. In: WARE, G. W. (Ed.). . **Reviews of Environmental Contamination and Toxicology: Continuation of Residue Reviews**. New York, NY, NY: Springer New York, 2004. p. 1–78.

KATAGI, T. **Soil column leaching of pesticidesReviews of Environmental**

Contamination and Toxicology, 2013.

KIMOTO, N.; TAKAHASHI, A.; INUBUSHI, K. **Design and release profile of timed-release coated granules of systemic insecticideJournal of Pesticide Science**, 2007.

KITAMURA, M.; FUJIMOTO, M. Release control of industrial biocide (CMI) using clathrate crystal with TEP. **Journal of Crystal Growth**, v. 256, n. 3–4, p. 393–400, 2003.

KOBLER, J.; MÖLLER, K.; BEIN, T. Colloidal Suspensions of Functionalized Mesoporous Silica Nanoparticles. **ACS Nano**, v. 2, n. 4, p. 791–799, 2008.

KORDALI, S. et al. Antifungal, phytotoxic and insecticidal properties of essential oil isolated from Turkish Origanum acutidens and its three components, carvacrol, thymol and p-cymene. **Bioresource Technology**, v. 99, n. 18, p. 8788–8795, 2008.

KORSMEYER, R. W. et al. Mechanisms of solute release from porous hydrophilic polymers. **International Journal of Pharmaceutics**, v. 15, n. 1, p. 25–35, 1983.

KREYLING, W. G. et al. Size dependence of the translocation of inhaled iridium and carbon nanoparticle aggregates from the lung of rats to the blood and secondary target organs. **Inhalation Toxicology**, v. 21, n. sup1, p. 55–60, 2009.

KREYLING, W. G.; SEMMLER-BEHNKE, M.; CHAUDHRY, Q. **A complementary definition of nanomaterialNano Today**, 2010.

KUANG, D.; BREZESINSKI, T.; SMARSLY, B. Hierarchical Porous Silica Materials with a Trimodal Pore System Using Surfactant Templates. **Journal of the American Chemical Society**, v. 126, n. 34, p. 10534–10535, 2004.

KUMAR, S. et al. Synthesis, characterization and on field evaluation of pesticide loaded sodium alginate nanoparticles. **Carbohydrate Polymers**, v. 101, n. 1, p. 1061–1067, 2014.

KUMAR, S. et al. Development and evaluation of alginate-chitosan nanocapsules for controlled release of acetamiprid. **International Journal of Biological Macromolecules**, v. 81, p. 631–637, 2015.

LAMBERTH, C. et al. Current challenges and trends in the discovery of agrochemicals. **Science (New York, N.Y.)**, v. 341, n. 6147, p. 742–6, 2013.

LAMICHHANE, J. R. et al. Challenges and opportunities for integrated pest management in Europe: A telling example of minor uses. . 2015, p. 42–47.

LANGÅRD, S.; ANDERSEN, A; RAVNESTAD, J. Incidence of cancer among

ferrochromium and ferrosilicon workers: an extended observation period. **British journal of industrial medicine**, v. 47, n. 1, p. 14–19, 1990.

LAW, C.; EXLEY, C. New insight into silica deposition in horsetail (Equisetum arvense). **BMC plant biology**, v. 11, n. 1, p. 112, 2011.

LAZZARI, S. et al. Fractal-like structures in colloid science. **Advances in Colloid and Interface Science**, v. 235, p. 1–13, 2016.

LEE, D.-W. et al. Facile synthesis of mesoporous silica and titania supraparticles by a meniscus templating route on a superhydrophobic surface and their application to adsorbents. **Nanoscale**, v. 6, n. 7, p. 3483, 2014.

LI, Z.-Z. et al. Controlled release of avermectin from porous hollow silica nanoparticles: Influence of shell thickness on loading efficiency, UV-shielding property and release. **Journal of Controlled Release**, v. 111, n. 1, p. 81–88, 2006.

LIANG, X. et al. Influence of anti-solvents on lignin fractionation of eucalyptus globulus via green solvent system pretreatment. **Separation and Purification Technology**, v. 163, p. 258–266, 2016.

LIAO, I. C. et al. Controlled release from fibers of polyelectrolyte complexes. **Journal of Controlled Release**, v. 104, n. 2, p. 347–358, 2005.

LIU, J.; ZHANG, X.; ZHANG, Y. Preparation and Release Behavior of Chlorpyrifos Adsolubilized into Layered Zinc Hydroxide Nitrate Intercalated with Dodecylbenzenesulfonate. **ACS Applied Materials & Interfaces**, v. 7, n. 21, p. 11180–11188, 2015.

LIU, L. et al. Robust Self-Standing Chitin Nanofiber/Nanowhisker Hydrogels with Designed Surface Charges and Ultralow Mass Content via Gas Phase Coagulation. **Biomacromolecules**, v. 17, n. 11, p. 3773–3781, 2016.

LIU, N. et al. Rice husks as a sustainable source of nanostructured silicon for high performance Li-ion battery anodes. **Scientific Reports**, v. 3, n. 1, p. 1919, 2013.

LIU, P.; HEINSON, W. R.; CHAKRABARTY, R. K. Fractal scaling of soot packing density across five size decades. **Aerosol Science and Technology**, v. 51, n. 7, p. 879–886, 2017.

LIU, Y. et al. Simultaneous preparation of silica and activated carbon from rice husk ash. **Journal of Cleaner Production**, v. 32, p. 204–209, 2012.

LIU, Y.; LAKS, P.; HEIDEN, P. Controlled release of biocides in solid wood. III. Preparation and characterization of surfactant-free nanoparticles. **Journal of Applied Polymer Science**, v. 86, n. 3, p. 615–621, 2002a.

LIU, Y.; LAKS, P.; HEIDEN, P. Controlled release of biocides in solid wood. II. Efficacy against Trametes versicolor and Gloeophyllum trabeum wood decay fungi. **Journal of Applied Polymer Science**, v. 86, n. 3, p. 608–614, 2002b.

LIU, Y.; LAKS, P.; HEIDEN, P. Controlled release of biocides in solid wood. I. Efficacy against brown rot wood decay fungus (Gloeophyllum trabeum). **Journal of Applied Polymer Science**, v. 86, n. 3, p. 596–607, 2002c.

LÓPEZ, F. et al. Optimization of furfural production by acid hydrolysis of Eucalyptus globulus in two stages. **Chemical Engineering Journal**, v. 240, p. 195–201, 2014.

LOURENÇON, T. V. et al. Hardwood and softwood kraft lignins fractionation by simple sequential acid precipitation. **Separation and Purification Technology**, v. 154, p. 82–88, 2015.

LU, J. et al. Biocompatibility, biodistribution, and drug-delivery efficiency of mesoporous silica nanoparticles for cancer therapy in animals. **Small**, v. 6, n. 16, p. 1794–1805, 2010.

LUONG-VAN, E. et al. Controlled release of heparin from poly(??-caprolactone) electrospun fibers. **Biomaterials**, v. 27, n. 9, p. 2042–2050, 2006.

LVOV, Y.; ABDULLAYEV, E. Functional polymer-clay nanotube composites with sustained release of chemical agents. **Progress in Polymer Science**, v. 38, n. 10–11, p. 1690–1719, 2013.

LVOV, Y. M. et al. Halloysite clay nanotubes for controlled release of protective agents. **ACS Nano**, v. 2, n. 5, p. 814–820, 2008.

LVOV, Y. M.; PRICE, R. R. Halloysite Nanotubules, a Novel Substrate for the Controlled Delivery of Bioactive Molecules. In: RUIZ-HITZKY, E.; ARIGA, K.; LVOV, Y. (Eds.). . **Bio-Inorganic Hybrid Nanomaterials**. London: Wiley, 2007. p. 419–441.

MA, J. F.; YAMAJI, N. **Silicon uptake and accumulation in higher plantsTrends in Plant Science**, 2006.

MA, X. et al. Interactions between engineered nanoparticles (ENPs) and plants : Phytotoxicity , uptake and accumulation. **Science of the Total Environment**, v. 408, n. 16, p. 3053–3061, 2010.

MAGALHÃES, W. L. E.; CAO, X.; LUCIA, L. A. Cellulose Nanocrystals/Cellulose Core-in-Shell Nanocomposite Assemblies. **Langmuir**, v. 25, n. 22, p. 13250–13257, 2009.

MAGALHÃES, W. L. E.; MATTOS, B. D.; MISSIO, A. L. Field testing of CCA-treated Brazilian spotted gum. **International Biodeterioration and Biodegradation**, v. 74, p. 124–128, 2012.

MAGASINSKI, A. et al. High-performance lithium-ion anodes using a hierarchical bottom-up approach. **Nature Materials**, v. 9, n. 4, p. 461–461, 2010.

MAIA, F. et al. Incorporation of biocides in nanocapsules for protective coatings used in maritime applications. **Chemical Engineering Journal**, v. 270, p. 150–157, 2015.

MALEKI, A. et al. Mesoporous silica materials: From physico-chemical properties to enhanced dissolution of poorly water-soluble drugs. **Journal of Controlled Release**, v. 262, n. Supplement C, p. 329–347, 28 set. 2017.

MANDELBROT, B. B. **The Fractal Geometry of Nature**. [s.l: s.n.]. v. 51

MARCHESE, A. et al. Antibacterial and antifungal activities of thymol: a brief review of the literature. **Food Chemistry**, v. 210, p. 402–414, 2016.

MARTENS, J. A. et al. Catalytic and molecular separation properties of Zeogrids and Zeotiles. **Catalysis Today**, v. 168, n. 1, p. 17–27, 2011.

MARTINI, R. et al. Antifungal cellulose by capsaicin grafting. **Cellulose**, v. 21, n. 3, p. 1909–1919, 2014.

MAS, N. et al. Enhanced antifungal efficacy of tebuconazole using gated pH-driven mesoporous nanoparticles. **International Journal of Nanomedicine**, v. 9, n. 1, p. 2597–2606, 2014.

MATTOS, B. D. et al. Controlled release for crop and wood protection: Recent progress toward sustainable and safe nanostructured biocidal systems. **Journal of Controlled Release**, v. 262, 2017a.

MATTOS, B. D. et al. Consecutive Production of Hydroalcoholic Extracts, Carbohydrates Derivatives and Silica Nanoparticles from Equisetum arvense. **Waste and Biomass Valorization**, v. 0, n. 0, p. 0, 2017b.

MATTOS, B. D. et al. Consecutive Production of Hydroalcoholic Extracts, Carbohydrates Derivatives and Silica Nanoparticles from Equisetum arvense. **Waste and Biomass Valorization**, 2017c.

MATTOS, B. D. B. D. et al. Biogenic silica nanoparticles loaded with neem bark extract as green, slow-release biocide. **Journal of Cleaner Production**, v. 142, p. 4206–4213, 2017d.

MATTOS, B. D.; MAGALHÃES, W. L. E. Biogenic nanosilica blended by nanofibrillated cellulose as support for slow-release of tebuconazole. **Journal of Nanoparticle Research**, v. 18, n. 9, p. 1–10, 2016.

MATTOS, B. D.; MAGALHÃES, W. L. E. Design and preparation of carbendazim-loaded

alumina nanoparticles as a controlled-release biocide for wood protection. **International Biodeterioration & Biodegradation**, v. 123, p. 174–181, 2017.

MATTOS, B. D.; ROJAS, O. J.; MAGALH?ES, W. L. E. Biogenic SiO<inf>2</inf> in colloidal dispersions via ball milling and ultrasonication. **Powder Technology**, v. 301, 2016.

MATTOS, B. D.; ROJAS, O. J.; MAGALHÃES, W. L. E. Biogenic SiO2 in colloidal dispersions via ball milling and ultrasonication. **Powder Technology**, v. 301, p. 58–64, 2016.

MAXMEN, A. Crop pests: Under attack. **Nature**, v. 501, n. 7468, p. S15–S17, 2013.

MEAKIN, P. Fractal aggregates. **Advances in Colloid and Interface Science**, v. 28, n. Supplement C, p. 249–331, 1987.

MEDEIROS, F. C. M. DE et al. Fungicidal activity of essential oils from Brazilian Cerrado species against wood decay fungi. **International Biodeterioration & Biodegradation**, v. 114, p. 87–93, 2016.

MERCER, T. G.; FROSTICK, L. E. Evaluating the potential for environmental pollution from chromated copper arsenate (CCA)-treated wood waste: A new mass balance approach. **Journal of Hazardous Materials**, v. 276, p. 10–18, 2014.

MERRILL, A.; WATT, B. Energy value of foods - basis and derivation. **USDA Agricultural Research Service Human Nutrition Research Branch**, v. 74, p. 109, 1973.

MEYER, W. L. et al. Functional nano-dispensers (FNDs) for delivery of insecticides against phytopathogen vectors. **Green Chem.**, v. 17, n. 8, p. 4173–4177, 2015.

MILOVANOVIC, S. et al. Application of cellulose acetate for controlled release of thymol. **Carbohydrate Polymers**, v. 147, p. 344–353, 2016.

MITTAL, A. et al. Effects of alkaline or liquid-ammonia treatment on crystalline cellulose: changes in crystalline structure and effects on enzymatic digestibility. **Biotechnology for Biofuels**, v. 4, p. 41, 19 out. 2011.

MUKHOPADHYAY, S. S. **Nanotechnology in agriculture: Prospects and constraintsNanotechnology, Science and Applications**, 2014.

NAZ, M. Y.; SULAIMAN, S. A. Slow release coating remedy for nitrogen loss from conventional urea: a review. **Journal of Controlled Release**, v. 225, p. 109–120, 2016.

NEL, A. Air Pollution-Related Illness: Effects of Particles. **Science**, v. 308, n. 5723, p. 804–806, 2005.

NEL, A. et al. Toxic Potential of Materials at the Nanolevel. **Science**, v. 311, n. 5761, p. 622–627, 2006.

NICOLÁS-CARLOCK, J. R.; CARRILLO-ESTRADA, J. L.; DOSSETTI, V. Universal fractality of morphological transitions in stochastic growth processes. **Scientific Reports**, v. 7, n. 1, p. 3523, 2017.

NURUZZAMAN, M. et al. Nanoencapsulation, Nano-guard for Pesticides: A New Window for Safe Application. **Journal of Agricultural and Food Chemistry**, v. 64, n. 7, p. 1447–1483, 2016.

OERKE, E.-C. Crop losses to pests. **The Journal of Agricultural Science**, v. 144, n. 1, p. 31, 2006.

OH, H. et al. Hepatoprotective and free radical scavenging activities of phenolic petrosins and flavonoids isolated from Equisetum arvense. **Journal of Ethnopharmacology**, v. 95, n. 2–3, p. 421–424, 2004.

ONISZCZUK, A. et al. Extraction methods for the determination of phenolic compounds from Equisetum arvense L. herb. **Industrial Crops and Products**, v. 61, p. 377–381, 2014.

OSBORN, D. Chapter 5 Pesticides in Modern Agriculture. In: **Environmental Impacts of Modern Agriculture**. [s.l.] The Royal Society of Chemistry, 2012. p. 111–128.

PANG, L. et al. Preparation and anti-UV property of modified cellulose membranes for biopesticides controlled release. **Industrial Crops and Products**, v. 89, p. 176–181, 2016.

PARAK, W. J.; NEL, A. E.; WEISS, P. S. Grand Challenges for Nanoscience and Nanotechnology. **ACS Nano**, v. 9, n. 7, p. 6637–6640, 2015.

PARISI, C.; VIGANI, M.; RODRÍGUEZ-CEREZO, E. Agricultural Nanotechnologies: What are the current possibilities? **Nano Today**, 2014.

PARK, K. Drug delivery of the future: Chasing the invisible gorilla. **Journal of Controlled Release**, v. 240, p. 2–8, 2016.

PASETA, L. et al. Encapsulation of essential oils in porous silica and MOFs for trichloroisocyanuric acid tablets used for water treatment in swimming pools. **Chemical Engineering Journal**, v. 292, p. 28–34, 2016.

PELTO, J. M. et al. Encapsulation of 3-iodo-2-propynyl *N* -butylcarbamate (IPBC) in polystyrene-polycaprolactone (PS/PCL) blends. **Journal of Microencapsulation**, v. 31, n. 5, p. 415–421, 2014.

PERLATTI, B. et al. Polymeric Nanoparticle-Based Insecticides: A Controlled Release Purpose for Agrochemicals. **Insecticides - Development of Safer and More Effective Technologies**, p. 523–550, 2013.

PING, L. et al. Condensed tannins from grape pomace: Characterization by FTIR and MALDI TOF and production of environment friendly wood adhesive. **Industrial Crops and Products**, v. 40, p. 13–20, 2012.

PODE, R. **Potential applications of rice husk ash waste from rice husk biomass power plantRenewable and Sustainable Energy Reviews**, 2016.

POPAT, A. et al. Adsorption and release of biocides with mesoporous silica nanoparticles. **Nanoscale**, v. 4, n. 3, p. 970, 2012a.

POPAT, A. et al. A pH-responsive drug delivery system based on chitosan coated mesoporous silica nanoparticles. **Journal of Materials Chemistry**, v. 22, n. 22, p. 11173, 2012b.

PRADO, A. G. S.; MOURA, A. O.; NUNES, A. R. Nanosized Silica Modified with Carboxylic Acid as Support for Controlled Release of Herbicides. **Journal of Agricultural and Food Chemistry**, v. 59, n. 16, p. 8847–8852, 2011.

PYTLAKOWSKA, K. et al. Multi-element analysis of mineral and trace elements in medicinal herbs and their infusions. **Food Chemistry**, v. 135, n. 2, p. 494–501, 2012.

QIAN, K. et al. Release kinetics of tebuconazole from porous hollow silica nanospheres prepared by miniemulsion method. **Microporous and Mesoporous Materials**, v. 169, p. 1–6, 2013.

QU, F. et al. A controlled release of ibuprofen by systematically tailoring the morphology of mesoporous silica materials. **Journal of Solid State Chemistry**, v. 179, n. 7, p. 2027–2035, 2006.

RAI, M.; YADAV, A.; GADE, A. Silver nanoparticles as a new generation of antimicrobials. **Biotechnology Advances**, v. 27, n. 1, p. 76–83, 2009.

RALIYA, R. et al. Quantitative Understanding of Nanoparticle Uptake in Watermelon Plants. **Frontiers in Plant Science**, v. 7, 2016.

RANCAN, F. et al. Skin Penetration and Cellular Uptake of Amorphous Silica Nanoparticles with Variable Size, Surface Functionalization, and Colloidal Stability. **ACS Nano**, v. 6, n. 8, p. 6829–6842, 2012.

RAUSCHER, H.; RASMUSSEN, K.; SOKULL-KL??TTGEN, B. Regulatory Aspects of Nanomaterials in the EU. **Chemie-Ingenieur-Technik**, v. 89, n. 3, p. 224–231, 2017.

REHMAN, F. et al. Amine bridges grafted mesoporous silica, as a prolonged/controlled drug release system for the enhanced therapeutic effect of short life drugs. **Materials Science and Engineering: C**, v. 72, p. 34–41, 2017.

REICH, E.; SCHIBLI, A. **High-Performance Thin-Layer Chromatography for the Analysis of Medicinal Plants**. 1. ed. [s.l.] Thieme, 2006.

RICHTER, A. P. et al. Synthesis and characterization of biodegradable lignin nanoparticles with tunable surface properties. **Langmuir**, v. 32, n. 25, p. 6468–6477, 2016.

RICO, C. M. et al. Interaction of Nanoparticles with Edible Plants and Their Possible Implications in the Food Chain. **Journal of Agricultural and Food Chemistry**, v. 59, n. 8, p. 3485–3498, 2011.

RIDGWAY, C. J.; GANE, P. A. C.; SCHOELKOPF, J. Modified calcium carbonate coatings with rapid absorption and extensive liquid uptake capacity. **Colloids and Surfaces A: Physicochemical and Engineering Aspects**, v. 236, n. 1–3, p. 91–102, 2004.

RINALDI, R.; SCHÜTH, F. Acid Hydrolysis of Cellulose as the Entry Point into Biorefinery Schemes. **ChemSusChem**, v. 2, n. 12, p. 1096–1107, 2009.

ROBERTS, M. T.; LEIBOVITCH, E. H. Chapter 2 Comparison of EU and US Law on Sustainable Food Processing. In: **Alternatives to Conventional Food Processing**. [s.l.] The Royal Society of Chemistry, 2011. p. 11–92.

ROY, A. et al. Controlled pesticide release from biodegradable polymers. **Central European Journal of Chemistry**, v. 12, n. 4, p. 453–469, 2014.

SCARFATO, P. et al. Development and evaluation of halloysite nanotube-based carrier for biocide activity in construction materials protection. **Applied Clay Science**, 2016.

SCHRICK, B. et al. Delivery Vehicles for Zerovalent Metal Nanoparticles in Soil and Groundwater. **Chemistry of Materials**, v. 16, n. 11, p. 2187–2193, 1 jun. 2004.

SCHULZ, H.; QUILITZSCH, R.; KRÜGER, H. Rapid evaluation and quantitative analysis of thyme, origano and chamomile essential oils by ATR-IR and NIR spectroscopy. **Journal of Molecular Structure**, v. 661, p. 299–306, 2003.

SEGVIĆ KLARIĆ, M. et al. Antifungal activity of thyme (Thymus vulgaris L.) essential oil and thymol against moulds from damp dwellings. **Letters in applied microbiology**, v. 44, n. 1, p. 36–42, jan. 2007.

SEHAQUI, H. et al. Humic acid adsorption onto cationic cellulose nanofibers for bioinspired removal of copper(ii) and a positively charged dye. **Soft Matter**, v. 11, n. 26,

p. 5294–5300, 2015.

SERVIN, A. D.; WHITE, J. C. Nanotechnology in agriculture: Next steps for understanding engineered nanoparticle exposure and risk. **NanoImpact**, v. 1, p. 9–12, 2016.

SHCHUKIN, D. G. et al. Active anticorrosion coatings with halloysite nanocontainers. **Journal of Physical Chemistry C**, v. 112, n. 4, p. 958–964, 2008.

SHERMA, J.; FRIED, B. **Handbook of thin-layer chromatography**. [s.l: s.n.]. v. 331

SIDDIQUE, R. Utilization of silica fume in concrete: Review of hardened properties. **Resources, Conservation and Recycling**, v. 55, n. 11, p. 923–932, 2011.

SIEPMANN, J.; SIEPMANN, F. Mathematical modeling of drug delivery. **International journal of pharmaceutics**, v. 364, n. 2, p. 328–43, 2008.

SIEPMANN, J.; SIEPMANN, F. Modeling of diffusion controlled drug delivery. **Journal of controlled release : official journal of the Controlled Release Society**, v. 161, n. 2, p. 351–62, 2012.

SILVA, M. DOS S. et al. Paraquat-loaded alginate/chitosan nanoparticles: Preparation, characterization and soil sorption studies. **Journal of Hazardous Materials**, 2011.

SINGH, B. et al. Controlled release of the fungicide thiram from starch–alginate–clay based formulation. **Applied Clay Science**, v. 45, n. 1–2, p. 76–82, 2009.

SINGH, B.; SHARMA, D. K.; GUPTA, A. The controlled and sustained release of a fungicide from starch and alginate beads. **Journal of environmental science and health. Part. B, Pesticides, food contaminants, and agricultural wastes**, v. 44, n. 2, p. 113–122, 2009.

SLOWING, I. I. et al. Mesoporous silica nanoparticles as controlled release drug delivery and gene transfection carriers. **Advanced Drug Delivery Reviews**, v. 60, n. 11, p. 1278–1288, 2008.

SLUITER, A. et al. Determination of Extractives in Biomass. **Biomass Analysis Technology Team Laboratory Analytical Procedure**, n. January, p. 1–8, 2004.

SLUITER, A. et al. **Determination of structural carbohydrates and lignin in biomass determination of structural carbohydrates and lignin in biomassNational Renewable Energy Laboratory (NREL)**. [s.l: s.n.].

SLUITER, A. et al. **NREL/TP-510-42618 analytical procedure - Determination of structural carbohydrates and lignin in BiomassNREL/TP-510-42618**, 2012. Disponível em: <http://www.nrel.gov/docs/gen/fy13/42618.pdf>

SORENSEN, G. et al. Controlled release of biocide from silica microparticles in wood paint. **Progress in Organic Coatings**, v. 68, n. 4, p. 299–306, 2010.

STRØMME, M. et al. Mesoporous silica-based nanomaterials for drug delivery: evaluation of structural properties associated with release rate. **Wiley Interdisciplinary Reviews: Nanomedicine and Nanobiotechnology**, v. 1, n. 1, p. 140–148, 2009.

SUN, Z. et al. A controlled release strategy of antifouling agent in coating based on intercalated layered double hydroxides. **Materials Letters**, v. 172, p. 105–108, 2016.

SUNG, J. H. et al. Lung Function Changes in Sprague-Dawley Rats After Prolonged Inhalation Exposure to Silver Nanoparticles. **Inhalation Toxicology**, v. 20, n. 6, p. 567–574, 2008.

TANG, L. et al. Sustained Antifungal Activity from a Ketoconazole-Loaded Nanostructured Mesoporous Silicon Platform. **Silicon**, v. 5, n. 3, p. 213–217, 2013.

TARDY, B. L. et al. Nanocellulose–surfactant interactions. **Current Opinion in Colloid & Interface Science**, v. 29, p. 57–67, 2017.

THOMIDIS, T.; FILOTHEOU, A. Evaluation of five essential oils as bio-fungicides on the control of Pilidiella granati rot in pomegranate. **Crop Protection**, v. 89, p. 66–71, 2016.

TORNEY, F. et al. Mesoporous silica nanoparticles deliver DNA and chemicals into plants. **Nature Nanotechnology**, v. 2, n. 5, p. 295–300, 2007.

TSABOULA, A. et al. Environmental and human risk hierarchy of pesticides: A prioritization method, based on monitoring, hazard assessment and environmental fate. **Environment international**, v. 91, p. 78–93, 2016.

TURCOTTE, D. L. **Fractals and Chaos in Geology and Geophysics**. 2. ed. Cambridge: Cambridge University Press, 1997.

TUREK, C.; STINTZING, F. C. Stability of Essential Oils: A Review. **Comprehensive Reviews in Food Science and Food Safety**, v. 12, n. 1, p. 40–53, 2013.

UETANI, K.; YANO, H. Zeta Potential Time Dependence Reveals the Swelling Dynamics of Wood Cellulose Nanofibrils. **Langmuir**, v. 28, n. 1, p. 818–827, 2012.

UMEDA, J.; KONDOH, K.; MICHIURA, Y. Process Parameters Optimization in Preparing High-Purity Amorphous Silica Originated from Rice Husks. **Materials Transactions**, v. 48, n. 12, p. 3095–3100, 2007.

UNITED STATES ENVIRONMENTAL PROTECTION AGENCY. **Test Guidelines for Pesticide Data Requirements**. Disponível em: <https://www.epa.gov/pesticide-science-and-assessing-pesticide-risks/test-guidelines-pesticide-data-

requirements#finding-test>. Acesso em: 13 jul. 2017.

VANTOMME, A. et al. Self-formation of hierarchical micro-meso-macroporous structures: Generation of the new concept “Hierarchical Catalysis”. **Colloids and Surfaces A: Physicochemical and Engineering Aspects**, v. 300, n. 1, p. 70–78, 2007.

WANG, Q. et al. Chitosan/starch fibers and their properties for drug controlled release. **European Journal of Pharmaceutics and Biopharmaceutics**, v. 66, n. 3, p. 398–404, 2007.

WANG, Y. et al. Encapsulation of Water-Insoluble Drugs in Polymer Capsules Prepared Using Mesoporous Silica Templates for Intracellular Drug Delivery. **Advanced Materials**, v. 22, n. 38, p. 4293–4297, 2010.

WANG, Y. et al. Mesoporous silica supraparticles for sustained inner-ear drug delivery. **Small**, v. 10, n. 21, p. 4244–4248, 2014.

WANG, Y. et al. Facile Fabrication of Flowerlike Natural Nanotube/Layered Double Hydroxide Composites as Effective Carrier for Lysozyme Immobilization. **ACS Sustainable Chemistry & Engineering**, v. 3, n. 6, p. 1183–1189, 2015.

WANI, A. et al. Surface functionalization of mesoporous silica nanoparticles controls loading and release behavior of mitoxantrone. **Pharmaceutical Research**, v. 29, n. 9, p. 2407–2418, 2012.

WANYIKA, H. Sustained release of fungicide metalaxyl by mesoporous silica nanospheres. **Journal of Nanoparticle Research**, v. 15, n. 8, p. 1–9, 2013.

WEINWURM, F. et al. Lignin concentration and fractionation from ethanol organosolv liquors by ultra- and nanofiltration. **Journal of Cleaner Production**, v. 136, p. 62–71, 2016.

WIBOWO, D. et al. Sustained release of fipronil insecticide in Vitro and in Vivo from biocompatible silica nanocapsules. **Journal of Agricultural and Food Chemistry**, v. 62, n. 52, p. 12504–12511, 2014.

WU, S.-H.; MOU, C.-Y.; LIN, H.-P. Synthesis of mesoporous silica nanoparticles. **Chemical Society Reviews**, v. 42, n. 9, p. 3862, 2013.

XU, X. et al. A Near-Infrared and Temperature-Responsive Pesticide Release Platform through Core–Shell Polydopamine@PNIPAm Nanocomposites. **ACS Applied Materials & Interfaces**, v. 9, n. 7, p. 6424–6432, 2017.

YANG, F. L. et al. Structural characterization of nanoparticles loaded with garlic essential oil and their insecticidal activity against Tribolium castaneum (Herbst)

(Coleoptera: Tenebrionidae). **Journal of Agricultural and Food Chemistry**, v. 57, n. 21, p. 10156–10162, 2009.

YANG, H. et al. Supramolecular chemistry at interfaces: Host-guest interactions for fabricating multifunctional biointerfaces. **Accounts of Chemical Research**, v. 47, n. 7, p. 2106–2115, 2014.

YEARLA, S. R.; PADMASREE, K. Exploitation of subabul stem lignin as a matrix in controlled release agrochemical nanoformulations: a case study with herbicide diuron. **Environmental Science and Pollution Research**, v. 23, n. 18, p. 18085–18098, 2016.

YEMIS, O.; MAZZA, G. Acid-catalyzed conversion of xylose, xylan and straw into furfural by microwave-assisted reaction. **Bioresource Technology**, v. 102, n. 15, p. 7371–7378, 2011.

YI, Z. et al. Functionalized Mesoporous Silica Nanoparticles with Redox-Responsive Short-Chain Gatekeepers for Agrochemical Delivery. **ACS Applied Materials & Interfaces**, v. 7, n. 18, p. 9937–9946, 2015.

YUN, Y. H.; LEE, B. K.; PARK, K. Controlled Drug Delivery: Historical perspective for the next generation. **Journal of Controlled Release**, v. 219, p. 2–7, 2015.

ZENG, S. et al. Nanomaterials enhanced surface plasmon resonance for biological and chemical sensing applications. **Chem. Soc. Rev.**, v. 43, n. 10, p. 3426–3452, 2014.

ZHANG, H. et al. A study on the consecutive preparation of d-xylose and pure superfine silica from rice husk. **Bioresource Technology**, v. 101, n. 4, p. 1263–1267, 2010.

ZHANG, H. et al. A new method of utilizing rice husk: Consecutively preparing d-xylose, organosolv lignin, ethanol and amorphous superfine silica. **Journal of Hazardous Materials**, v. 291, p. 65–73, 2015.

ZHANG, X.; CRESSWELL, M. **Inorganic Controlled Release Technology**. [s.l: s.n.].

ZHANG, Y. et al. Cellulose Nanofibrils: from strong materials to bioactive surfaces. **Journal of Renewable Materials**, v. 1, n. 3, p. 195–211, 2013.

ZHAO, J.; WILKINS, R. M.; ILKINS, R. I. M. W. Controlled release of the herbicide, fluometuron, from matrix granules based on fractionated organosolv lignins. **Journal of Agricultural and Food Chemistry**, v. 51, n. 14, p. 4023–4028, 2003.

ZHENG, Q. et al. A pH-responsive controlled release system using layered double hydroxide (LDH)-capped mesoporous silica nanoparticles. **Journal of Materials Chemistry B**, v. 1, n. 11, p. 1644–1648, 2013.

ZHU, C. L. et al. **Cell microenvironment stimuli-responsive controlled-release**

delivery systems based on mesoporous silica nanoparticlesJournal of Food and Drug Analysis, 2014.

ZHU, H. et al. Uptake, translocation, and accumulation of manufactured iron oxide nanoparticles by pumpkin plants. **Journal of Environmental Monitoring**, v. 10, n. 6, p. 713, 2008.

SUPPLEMENTARY MATERIAL

TABLE S1 – ANALYSIS OF VARIANCE OF FACTORS AFFECTING THE RESPONSES FROM THE BIOREFINING OF E. ARVENSE *(SUM OF SQUARES TYPE III)*

Response	Factor	Sum of Squares	dF	Mean square	F-test	P-value
Hydrolysis yield	HT	371.24	1	371.24	12.34	0.0019
	t	77.3998	1	77.3998	2.57	0.1223
	$[H^+]$	4460.07	1	4460.07	148.31	0.0001
	Error	691.666	23	30.0724		
Total sugars	HT	62.7601	1	62.7601	6.97	0.0146
	t	9.62878	1	9.62878	1.07	0.3117
	$[H^+]$	345.94	1	345.94	38.44	0.0001
	Error	206.997	23	8.99989		
Total furan compounds	HT	0.182658	1	0.182658	3.18	0.0876
	t	0.0211665	1	0.0211665	0.37	0.5495
	$[H^+]$	1.38107	1	1.38107	24.07	0.0001
	Error	1.31953	23	0.0573709		
High heating value	HT	0.0700627	1	0.0700627	1.58	0.2213
	t	0.00011756	1	0.000117556	0	0.9594
	$[H^+]$	2.13349	1	2.13349	48.14	0.0001
	Error	1.01934	23	0.0443191		
Ash content	HT	77.9007	1	77.9007	25.36	0.0001
	t	18.8548	1	18.8548	6.14	0.0214
	$[H^+]$	92.7059	1	92.7059	30.18	0.0001
	CT	16.7068	1	16.7068	5.44	0.0293
	Error	67.5841	22	3.072		
Whiteness index	HT	280.056	1	280.056	1.34	0.2592
	t	9.97556	1	9.97556	0.05	0.829
	$[H^+]$	4930.25	1	4930.25	23.61	0.0001
	CT	373.556	1	373.556	1.79	0.1947
	Error	4593.34	22	208.788		
Specific surface area	HT	31970.8	1	31970.8	7.26	0.0132
	t	3589.87	1	3589.87	0.82	0.3763
	$[H^+]$	71770	1	71770	16.3	0.0006
	CT	5509	1	5509	1.25	0.2754
	Error	96873.1	22	4403.32		
Purity	HT	0.119235	1	0.119235	0.01	0.9364
	t	19.4168	1	19.4168	1.06	0.3143
	$[H^+]$	930.846	1	930.846	50.85	0.0001
	CT	0.991232	1	0.991232	0.05	0.8182
	Error	402.76	22	18.3073		

TABLE S2 – STATISTIC PARAMETERS OF THE MULTIPLE LINEAR MODELS CREATED FOR THE RESPONSES *OF THE BIOREFINING OF* E. ARVENSE

Response	Source	Sum of Squares	dF	Mean square	F	P-value
Hydrolysis yield	Model	4943.77	3	1647.92	54.58	<0.0001
	Error	694.44	23	30.19		
Total sugars	Model	418.32	3	139.443	15.49	<0.0001
	Error	206.99	23	8.99		
Total furan	Model	1.58	3	0.52	9.21	0.0003
	Error	1.31	23	0.06		
Ash content	Model	206.16	4	51.54	16.78	<0.0001
	Error	67.58	22	3.07		
High heating value	Model	2.20	3	0.73	16.57	<0.0001
	Error	1.01	23	0.04		
Whiteness index	Model	5593.83	4	1398.46	6.7	0.0011
	Error	4593.34	22	208.78		
Surface Area	Model	112840.00	4	28209.9	6.41	0.0014
	Error	96873.1	22	4403.32		
Purity	Model	951.373	4	237.84	12.99	<0.0001
	Error	402.76	22	18.30		

TABLE S3 – COEFFICIENT OF DETERMINATION OF THE KINETIC MODELS APPLIED AS A TENTATIVE TO EXPLAIN THE RELEASE OF THYMOL OUT FROM BIOGENIC SILICA

Model	Equation	SiOH@Thy	$SiNH_2$@Thy	SiCOOH@Thy
Zero Order	$Qt = kt$	0.78	0.67	0.86
First Order	$Qt = e^{-kt}$	0.57	0.43	0.60
Second Order	$1/Qt = kt$	0.37	0.23	0.34
Parabolic-diffusion	$Qt = kt^{1/2}$	0.88	0.81	0.94
Korsmeyer-Peppas	$\log Qt = \log k + n \log t$	0.78	0.85	0.91
Elovich	$Qt = k\ln t$	0.96	0.96	0.98

Qt = amount released at time *t*; *t* = time; *k* = release rate constant; *n* = kinetic exponent of the Korsmeyer-Peppas model.

* The equations were presented in their integrated forms and considering an initial 0 concentration of the biocide in the release microenvironment.

TABLE S4 – OVERALL CHEMICAL COMPOSITION, AND TEXTURE OF THE SOILS SELECTED TO INVESTIGATE THE MOBILITY OF NANOPARTICLES VERSUS SUPRAPARTICLES

Soil	pH ($CaCl_2$)	Ca[a]	Mg[a]	K[a]	P[b]	C (%)	Clay[c]	Sand[c]
A	4.35	0.94	0.03	0.09	44.3	0.61	122	875
B	5.20	9.20	2.80	0.64	3.7	4.77	>600	
C	3.70	0.20	0.10	0.15	2.5	3.51	334	433

Key: [a] $cmol \cdot dm^{-3}$; [b] $mg \cdot kg^{-1}$; [c] $g \cdot kg^{-1}$

TABLE S5 – COEFFICIENT OF DETERMINATION OF THE KINETIC MODELS APPLIED AS A TENTATIVE TO EXPLAIN THE RELEASE OF THYMOL FROM THE SUPRAPARTICLES (SPHERES PREPARED USING CNF 5% AND 10 µL)

Model	Equation	Loading approach		
		Pre	In situ	Post
Zero Order	$Qt = kt$	0.61	0.66	0.54
First Order	$Qt = e^{-kt}$	0.51	0.48	0.41
Second Order	$1/Qt = kt$	0.41	0.32	0.3
Parabolic-diffusion	$Qt = kt^{1/2}$	0.86	0.85	0.8
Korsmeyer-Peppas	$\log Qt = \log k + n \log t$	0.97	0.89	0.97
Elovich	$Qt = k\ln t$	**0.98**	**0.95**	**0.97**

Qt = amount released at time t; t = time; *k* = release rate constant; n = kinetic exponent of the Korsmeyer-Peppas model;

* The equations were presented in their integrated state, considering only desorption and that the initial concentration of the biocide in the release microenvironment as equal to zero.

FIGURE S1 - UV SPECTRA OBTAINED FOR ETHANOLIC THYMOL SOLUTIONS (a) IN ORDER TO BUILD A CALIBRATION CURVE (b)

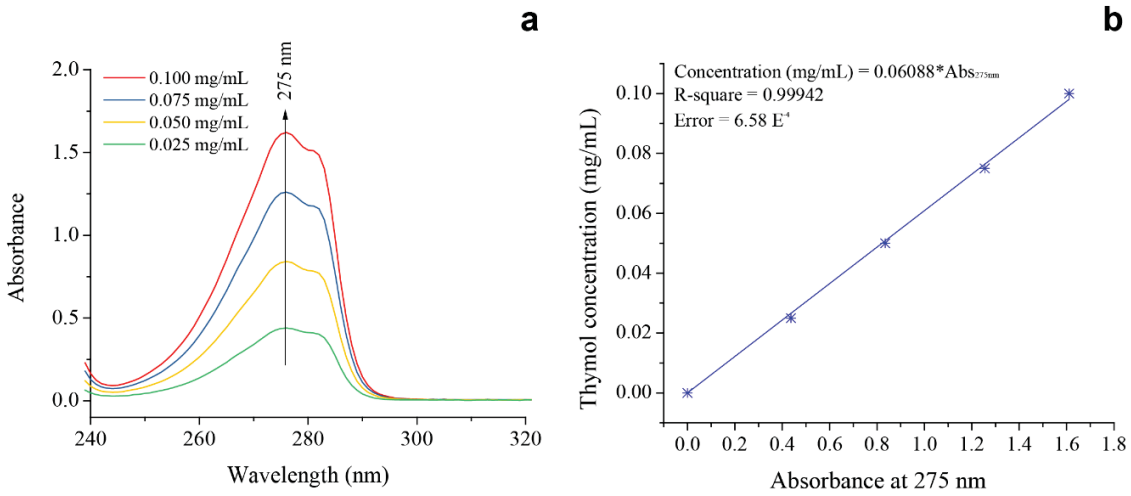

SOURCE: the author (2018).

FIGURE S2 – EXPERIMENTAL PROCEDURE TO CALCULATE THE QUANTITATIVE BIOACTIVITY OF THE PREPARED BDS

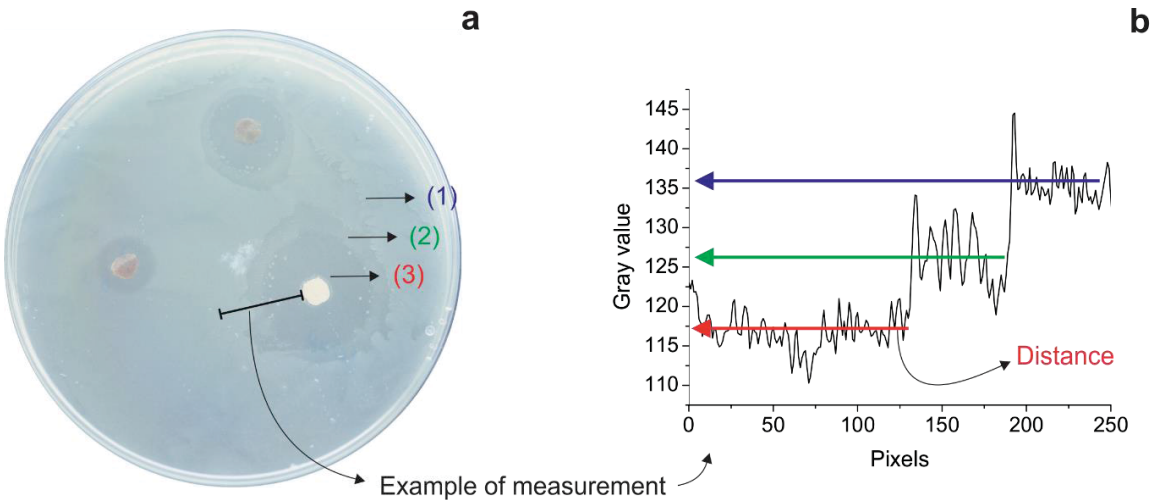

SOURCE: the author (2018).

Detailed information on the zones of interest (a) and halo intensity profiles (b), in order to exemplify the systematic procedure. 1: no inhibition zone; 2: partially inhibition zone; 3: complete inhibition zone. The software ImageJ was used to create grayscale profiles of neighboring area of the discs observed in the biocidal assay. To avoid external influence from the light reflection of the images, the results were presented as the ratio between the intensity of region where bacteria colonies were unaffected by the BDS and the region next to the BDS pellets. Also, the diameter of the pellets was measured in pixels as an internal comparison for bactericidal assessment of the BDS. Three-line measurements were made spaced by 120°. The referred gray value was taken as an average of the entire zone in reference.

FIGURE S3 – PROCEDURE ADOPTED FOR SIZE FRACTIONATION OF BIOGENIC SILICA

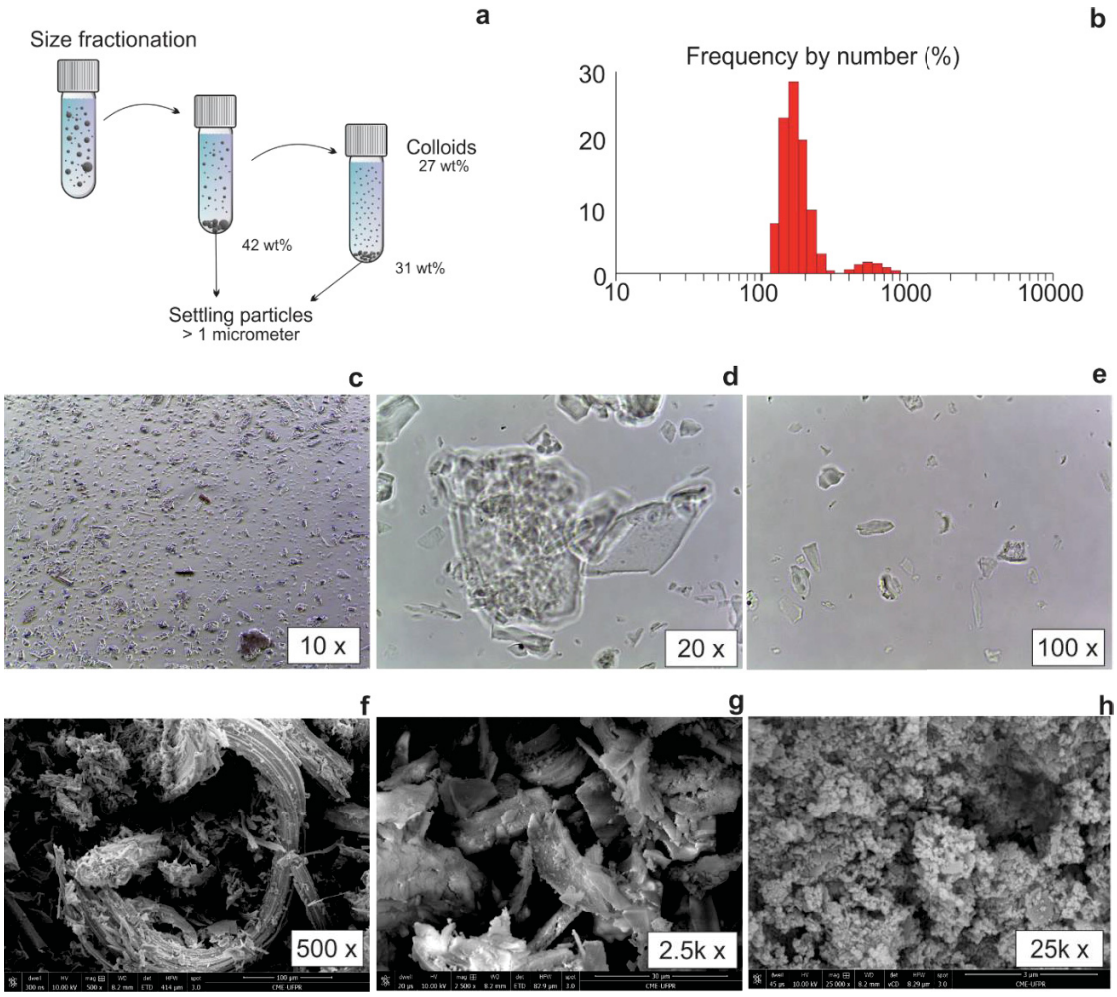

SOURCE: the author (2018).

Sequential sedimentation procedures were carried out in order to separate size fraction of the biogenic silica aiming at a better understanding of the effect of particles size on the biocide release rate (FIGURE S3a). DLS results for the obtained colloidal fraction (b). Optical images of settling biogenic silica particles at 10 (FIGURE S3c) and 20 (FIGURE S3d) times of magnification showing their irregular shapes derived from cell wall plant. Optical image of the colloidal fraction of biogenic silica (FIGURE S3c). Scanning electron microscopy images at 25k times of magnification (FIGURE S3h) stating their high porosity even being not colloidally stable fractal-like particles (FIGURE S3g).

FIGURE S4 – SURFACE CHARACTERIZATION OF $BSiO_2$ NANOPARTICLES THROUGH XPS ANALYSIS

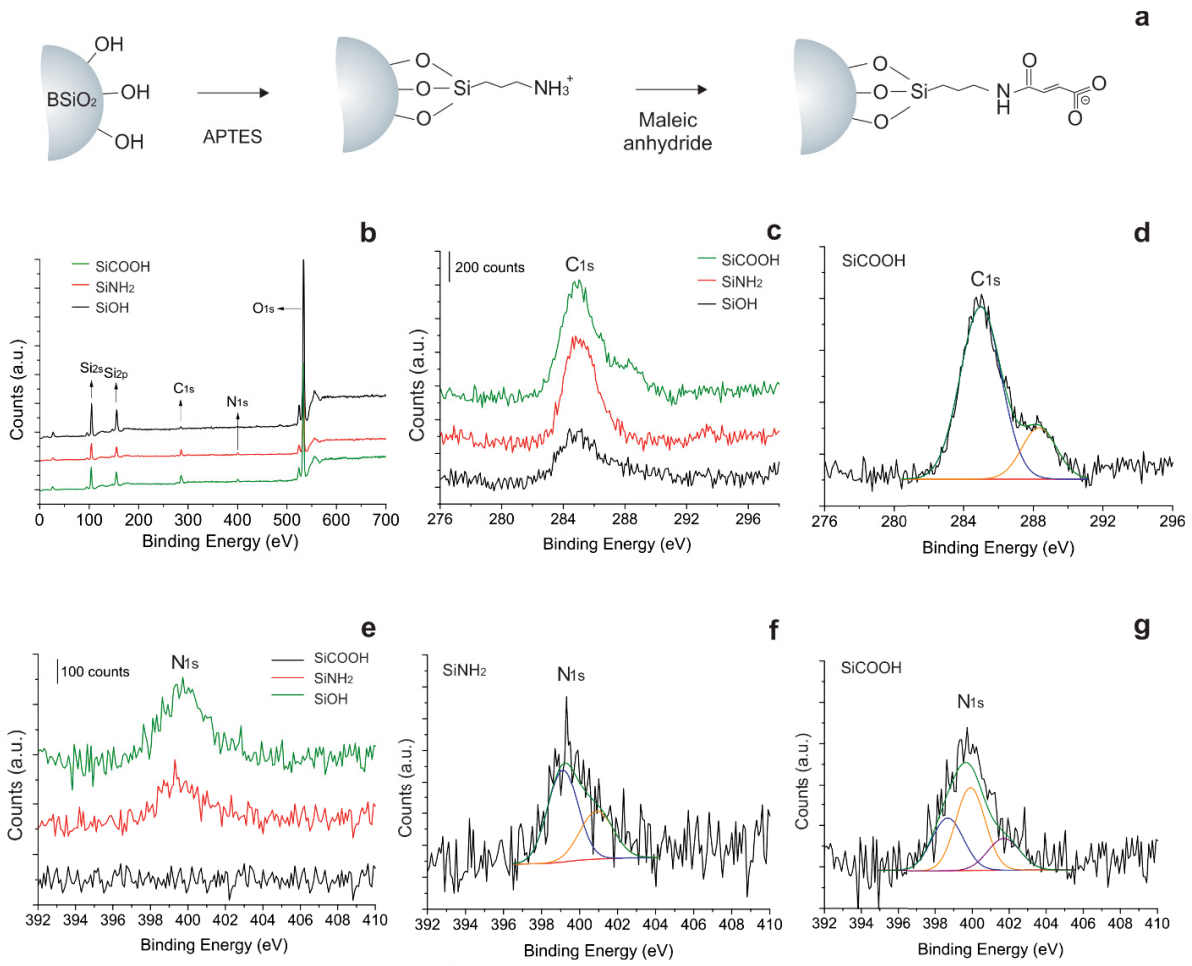

SOURCE: the author (2018).

The XPS analysis stating the surface functionalization is presented in the FIGURE S4. The same characteristic carbon peak related to the C-H and C-C chemical structures was observed at 285 eV for the SiOH and $SiNH_2$ particles (FIGURE S4c); however, a new carbon moiety with peak at 288.5 eV was verified after deconvolution of the high-resolution carbon spectra of the SiCOOH particles (FIGURE S4d). The high-resolution XPS spectra of N_{1s} for the SiCOOH (FIGURE S4g) particles shows notable differences when compared to the $SiNH_2$ (FIGURE S4f). Free amino groups appear at 399.1 eV for both $SiNH_2$ and SiCOOH particles; however, the contribution of these groups to the total nitrogen response decreased from 63.7 to 32.6% after carboxyl-functionalization because

part was converted into amide groups via ring opening linker elongation reaction with maleic anhydride. The interactions between neighboring amino groups undergo H-bonding or between amino groups and unreacted silica hydroxyl groups appeared at around 401.5 eV. Again, this peak had lower contribution (20.0%) in the N_{1s} main peak for the SiCOOH particles when compared to the $SiNH_2$ (36.3%). A small shift was observed for this component, and it may be attributed to the interaction of the amino groups with OH moieties from carboxyl termination instead with those from silanol groups. After deconvolution, a new nitrogen component related to the amide group appeared at 399.9 eV and it contributed to 47.5% of the total N_{1s} spectrum of the SiCOOH particles. From these results, it is possible to say that the free amino groups were partially converted into amide groups via chemical reaction with maleic anhydride resulting in the carboxyl termination.

FIGURE S5 – THERMOGRAVIMETRIC (A) AND THERMAL DIFFERENTIAL (B) CURVES OF THE AS-PREPARED AND FUNCTIONALIZED BIOGENIC SILICA PARTICLES

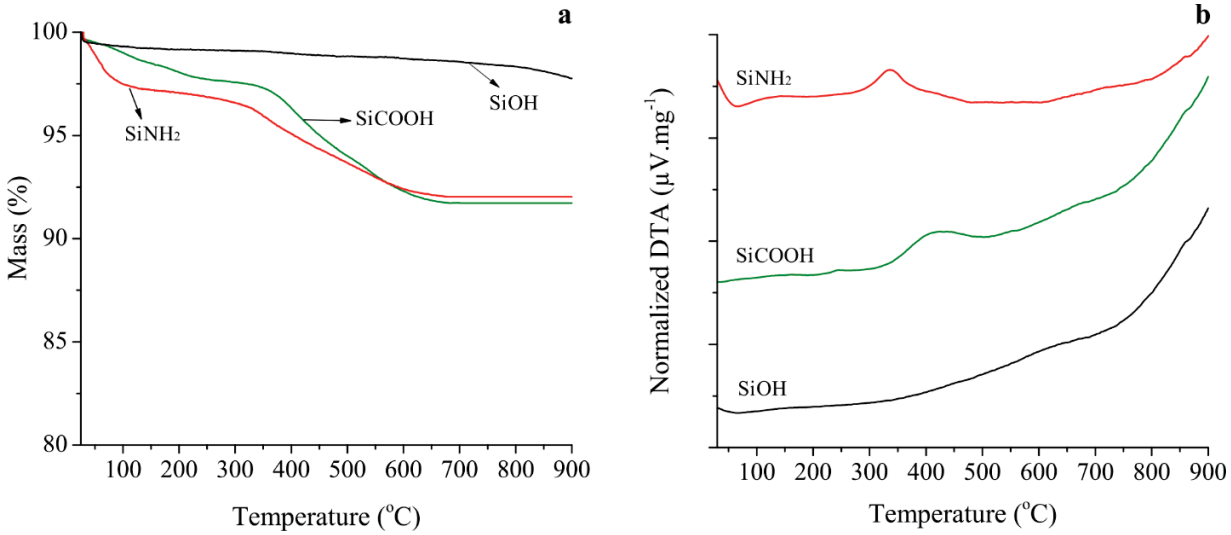

SOURCE: the author (2018).

FIGURE S6 – FTIR SPECTRA OF THE UNMODIFIED AND MODIFIED BIOGENIC SILICA PARTICLES DETAILING THE ASSIGNMENTS FOR EACH IDENTIFIED PEAK

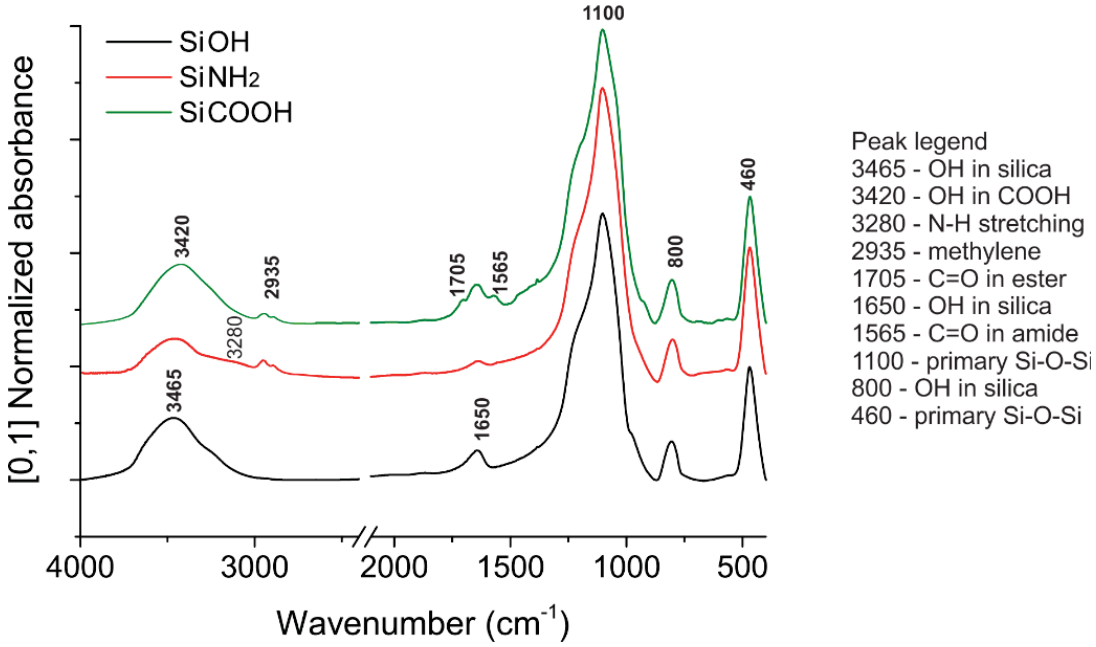

SOURCE: the author (2018).

FIGURE S7 – DECONVOLUTION OF THE C_{1S} HIGH-RESOLUTION SPECTRA OF THE SIOH@THY (A) $SIONH_2$@THY (C) SICOOH@THY (D)

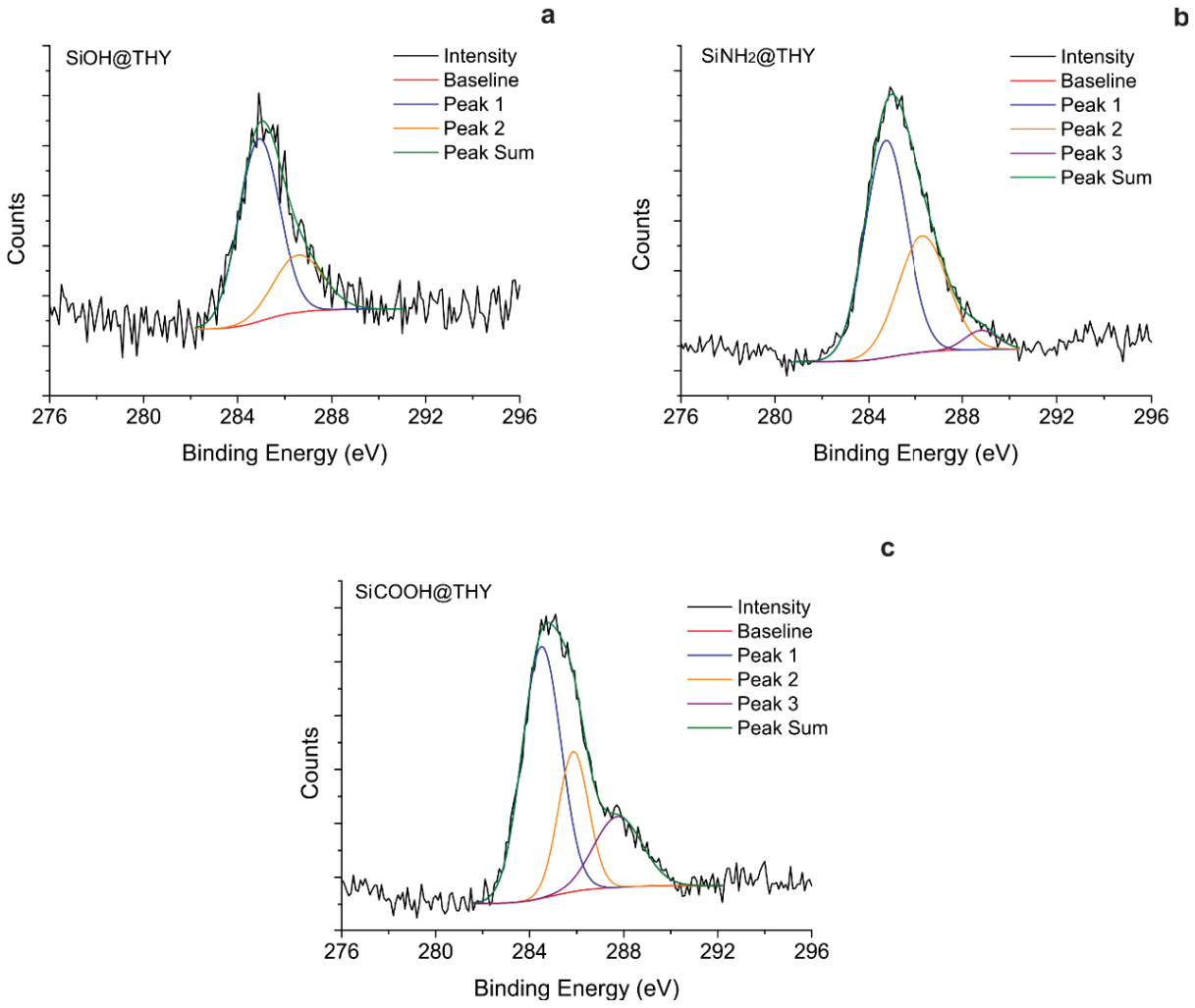

SOURCE: the author (2018).

FIGURE S8 – THYMOL RELEASE RATE FROM SiOH@THY PREPARED WITH THE DIFFERENT SILICA PARTICLE SIZES

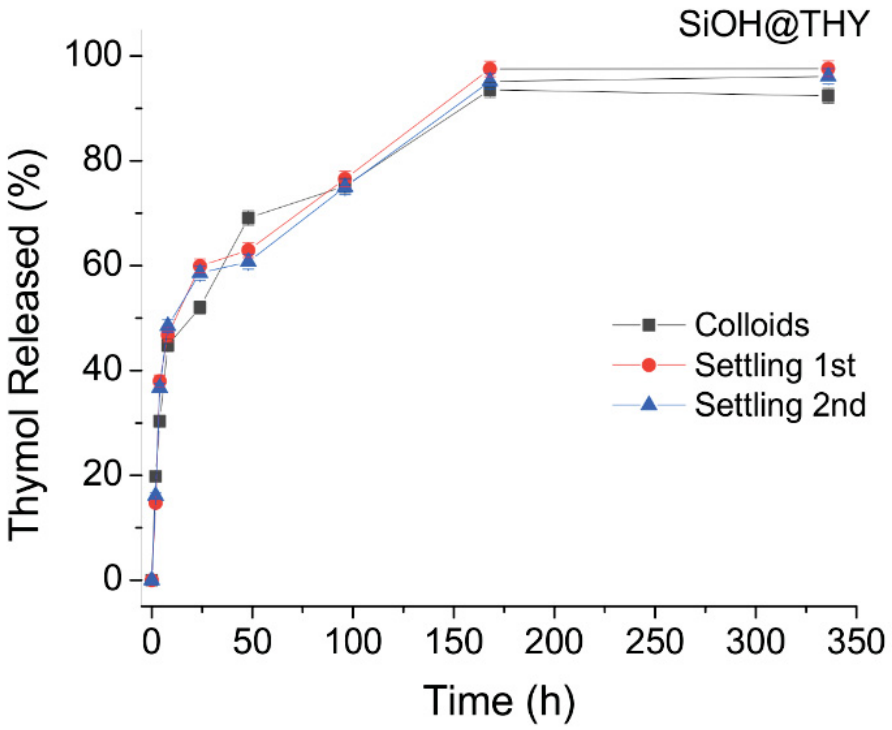

SOURCE: the author (2018).

FIGURE S9 – SUPPLEMENTARY KINETIC AND THERMODYNAMIC CONSIDERATIONS OF THE BIOCIDE DELIVERY FROM BIOGENIC SILICA PARTICLES

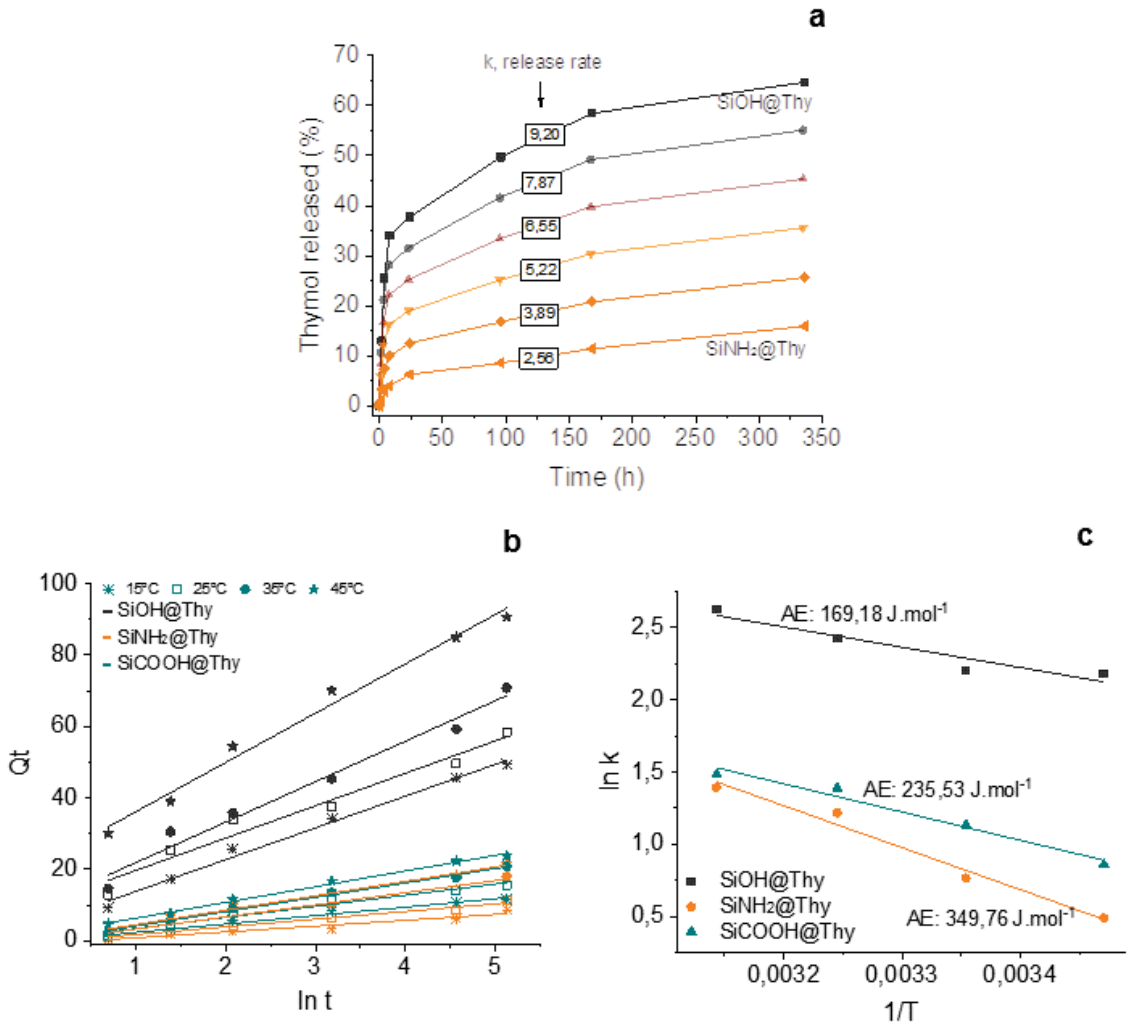

SOURCE: the author (2018).

Theoretical thymol profiles with tethered release rate through fraction compositions between the BDS with the fastest and slowest release rate (a). Elovich linearization of the thymol release out profiles at different temperatures for all obtained BDS (b) in order to calculate the activation energy of their release using the Arrhenius plot (c). An additional release profile at 15 ºC was carried out in order to precisely obtain the activation energy.

FIGURE S10 – CONTROL PLATES OF THE AGAR DIFFUSION ASSAY (TOP ROW), AND TEST RESULTS ON *Escherichia coli* (A) AND *Staphylococcus aureus* (B) *Escherichia coli* PLATES TREATED WITH UNDISSOLVED THYMOL (C) AND MIXED THYMOL/SILICA DISCS (E). *Staphylococcus aureus* PLATES TREATED WITH UNDISSOLVED THYMOL (D) AND MIXED THYMOL/SILICA DISCS (F)

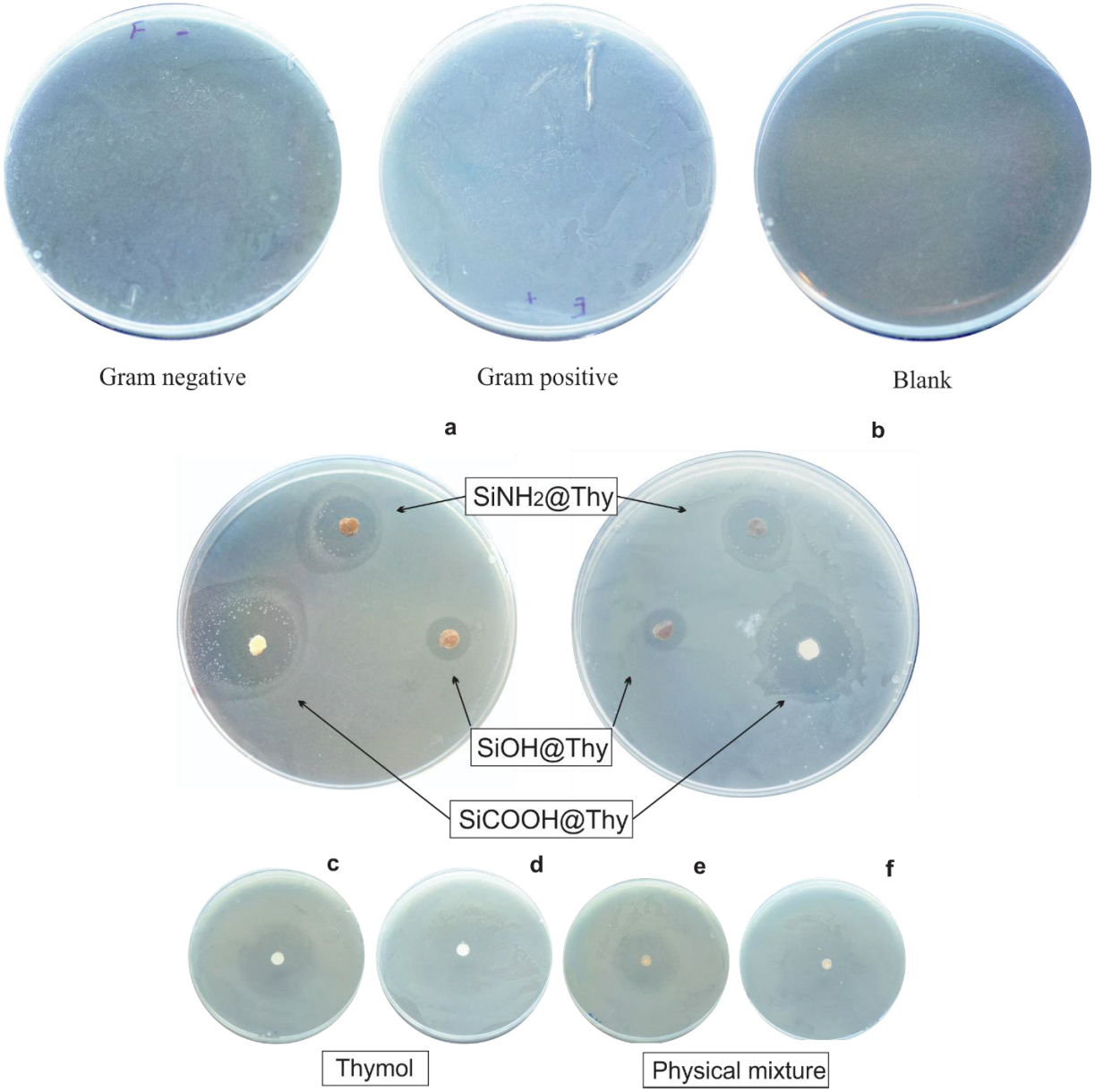

SOURCE: the author (2018).

FIGURE S 11 - SCHEMATIC REPRESENTATION OF THE DIFFERENT SUBSTRATES USED TO PREPARE SUPERSTRUCTURES WITH DIFFERENT SHAPES

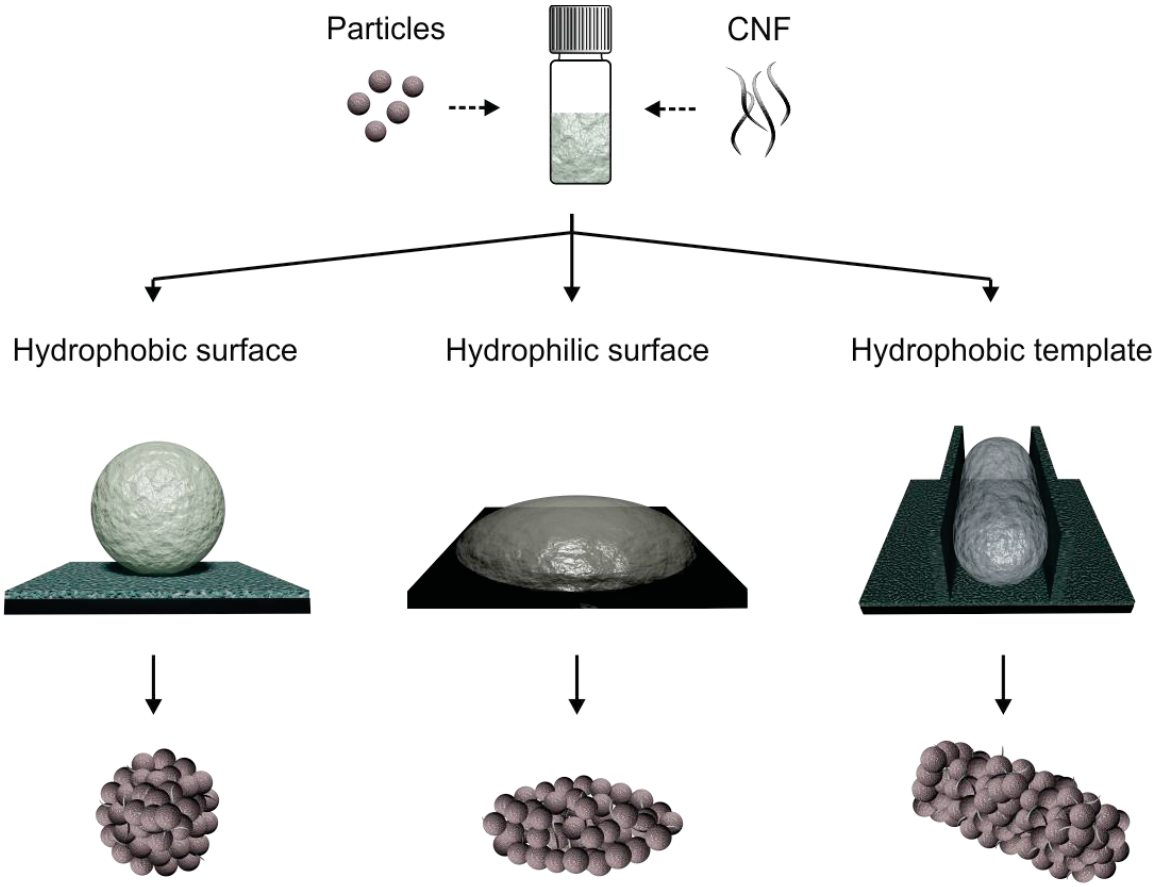

SOURCE: the author (2018).

FIGURE S12 – COMPRESSION RESULTS OF SUPRAPARTICLES ASSEMBLED USING THE COLLOIDS VERSUS RAW PARTICLES (A) AND INTEGRITY TESTS AS A FUNCTION OF pH (B,C) AND THERMAL TREATMENTS (D,E)

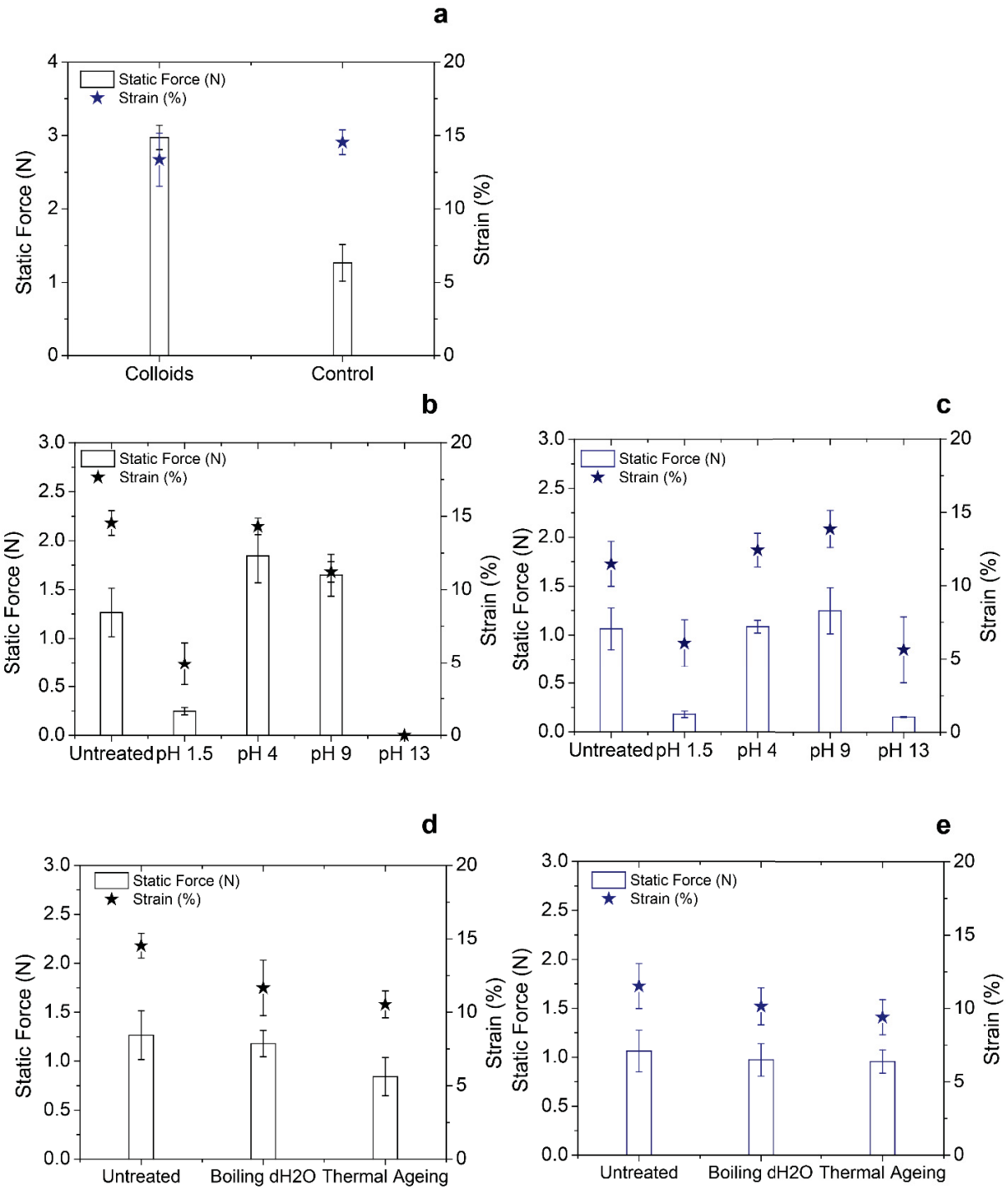

SOURCE: the author (2018).

FIGURE S13 – COMPARISON OF THE BIOCIDE RELEASE PROFILES ACQUIRED FOR THE SUPRAPARTICLES AND THE COLLOIDALLY-STABLE BSiO2 NANOPARTICLES

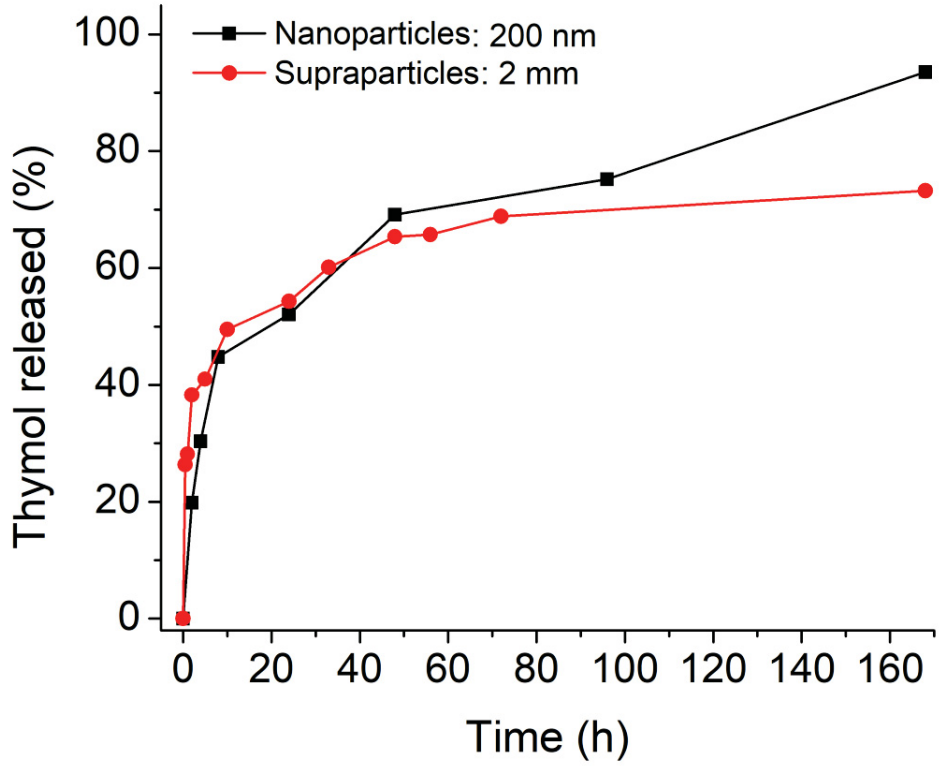

SOURCE: the author (2018).

FIGURE S14 – LINEARIZATION OF THE RELEASE EXPERIMENTAL DATA USING THE ZERO-ORDER (A) PSEUDO-FIRST-ORDER (B), PSEUDO-SECOND-ORDER (C), PARABOLIC DIFFUSION (D), KORSMEYER-PEPPAS (E) AND ELOVICH (F) KINETIC MODELS

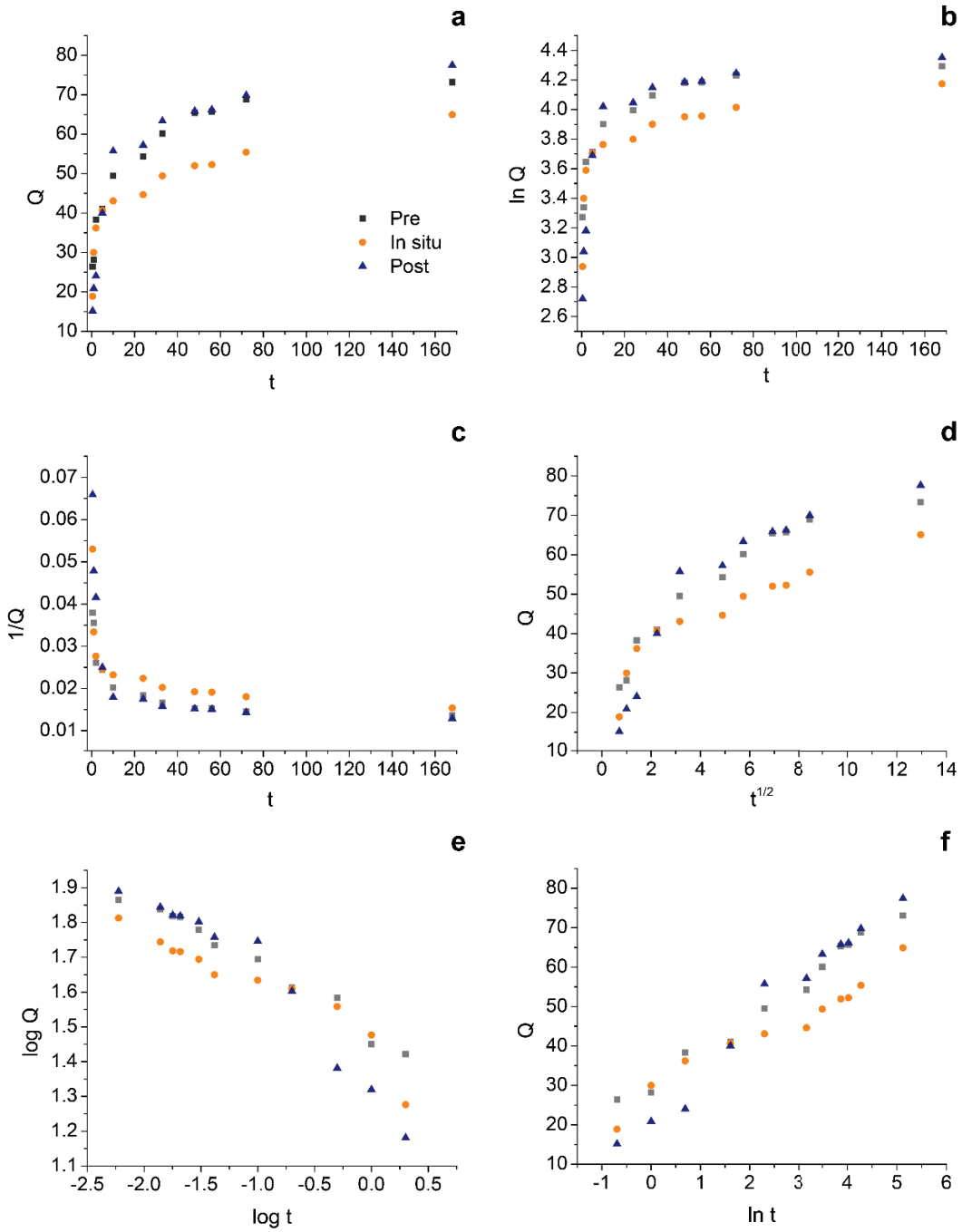

SOURCE: the author (2018).

FIGURE S15 – INVESTIGATION OF THE MOBILITY OF PARTICLES IN SOIL (A). TRANSMITTANCE SPECTRA ACQUIRED IN THE RANGE FROM 300 TO 800 NM IN ORDER TO INVESTIGATE THE PRESENCE OF SUSPENDED SOLIDS IN THE OUTFLOW (B,C)

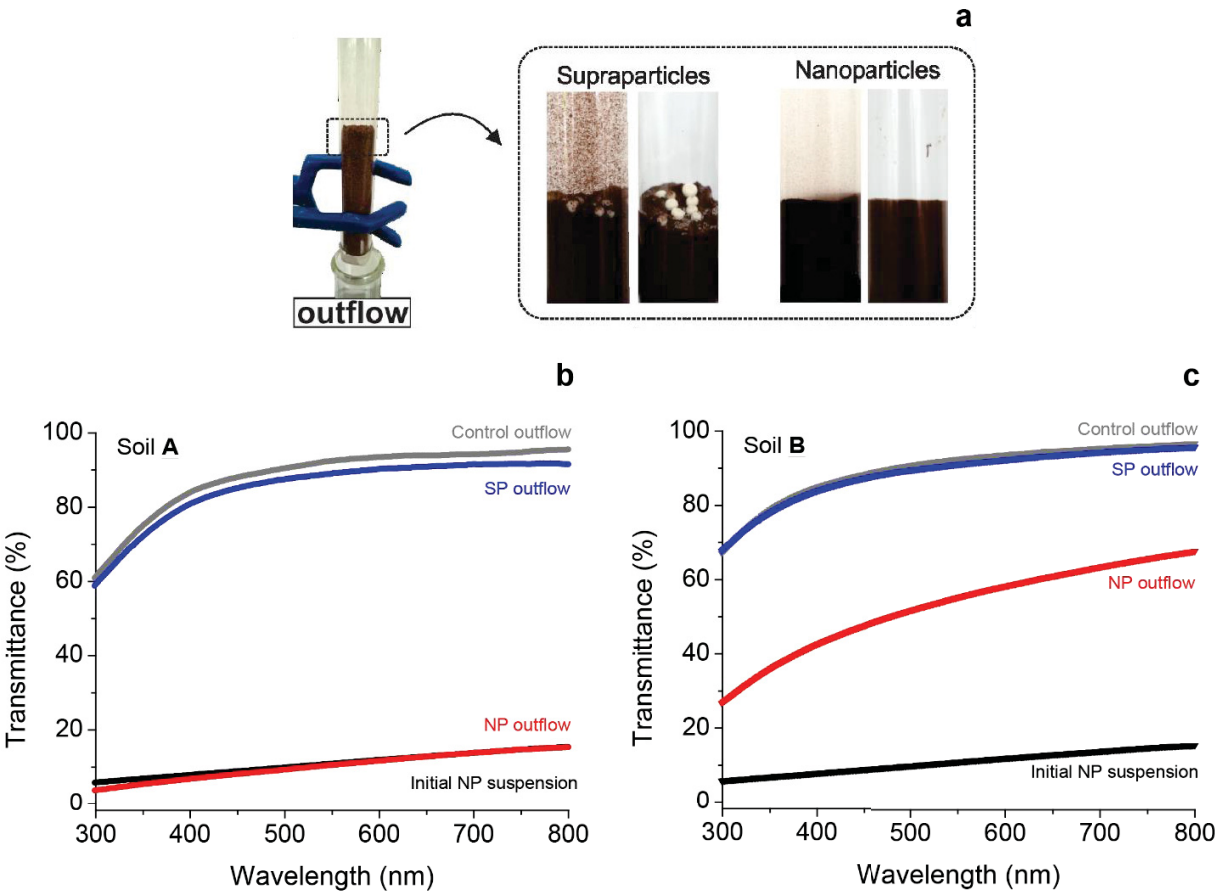

SOURCE: the author (2018).